AUBURN

SAMUEL GINN
COLLEGE OF ENGINEERING

Research Report for ALDOT Project 930-645

EVALUATION OF CRACKING OF THE US 331 BRIDGE DECK

Submitted to

The Alabama Department of Transportation

Prepared by

Anton K. Schindler, Mary L. Hughes,
Robert W. Barnes, and Benjamin E. Byard

AUGUST 2010

Highway Research Center
Harbert Engineering Center
Auburn, Alabama 36849

www.eng.auburn.edu/research/centers/hrc.html

1. Report No. FHWA/ALDOT 930-645	**2. Government Accession No.**	**3. Recipient Catalog No.**	
4. Title and Subtitle Evaluation of cracking of the US 331 bridge deck		**5. Report Date** August 2010	
		6. Performing Organization Code	
7. Author(s) Anton K. Schindler, Mary L. Hughes, Robert W. Barnes, and Benjamin E. Byard		**8. Performing Organization Report No.** FHWA/ALDOT 930-645	
9. Performing Organization Name and Address Highway Research Center 238 Harbert Engineering Center Auburn University, AL 36830		**10. Work Unit No. (TRAIS)**	
		11. Contract or Grant No.	
12. Sponsoring Agency Name and Address Alabama Department of Transportation 1409 Coliseum Boulevard Montgomery, Alabama 36130-3050		**13. Type of Report and Period Covered** Technical Report	
		14. Sponsoring Agency Code	

15. Supplementary Notes
Project performed in cooperation with the Alabama Department of Transportation.

16. Abstract

The focus of this report is a three-span, continuous, skewed bridge that was constructed in the summer of 2003 as the northbound roadway bridge on US 331 in Montgomery County, Alabama. This bridge deck exhibited extensive transverse and horizontal cracking and was replaced in 2005 before being opened to traffic. The primary objective of this study was to evaluate the mechanisms that may have contributed to horizontal cracking in this bridge deck.

The concrete satisfied all standard slump, total air content, and compressive strength requirements. Core results revealed adequate in-place compressive and splitting tensile strengths. Finite-element analyses were used to rule out excessive skew and differential support settlement as causes of the cracking. Horizontal cracking in this deck was most likely caused by excessive early-age temperature gradients combined with drying shrinkage gradients that produced large shear and normal stresses at the top reinforcement mat location in a concrete with a high coefficient of thermal expansion and high modulus of elasticity. The effect of supplementary cementing materials, water-cement ratio, and placement temperature conditions on the early-age cracking tendency of bridge deck concrete was evaluated by rigid cracking frame testing techniques. Use of either fly ash or ground-granulated blast-furnace slag was found to significantly reduce thermal stresses at early ages. Coefficient of thermal expansion values were determined for concretes made with aggregates found in Alabama.

17. Key Words Concrete bridge deck, cracking, thermal effects, cracking tendency, coefficient of thermal expansion.		**18. Distribution Statement** No restrictions.	
19. Security Classification (of this report) Unclassified	**20. Security Classification (of this page)** Unclassified	**21. No. of pages** 150	**22. Price**

Form DOT F 1700.7 (8-72)

Research Report

ALDOT Research Project 930-645

EVALUATION OF CRACKING OF THE US 331 BRIDGE DECK

Prepared by:
Anton K. Schindler
Mary L. Hughes
Robert W. Barnes
Benjamin E. Byard

Highway Research Center
and
Department of Civil Engineering
at
Auburn University

August 2010

DISCLAIMERS

The contents of this report reflect the views of the authors, who are responsible for the facts and the accuracy of the data presented herein. The contents do not necessarily reflect the official views or policies of Auburn University or the Alabama Department of Transportation. This report does not constitute a standard, specification, or regulation.

NOT INTENDED FOR CONSTRUCTION, BIDDING, OR PERMIT PURPOSES

Anton K. Schindler, Ph.D., P.E.
Mary L. Hughes, Ph.D.
Robert W. Barnes, Ph.D., P.E.
Research Supervisors

ACKNOWLEDGEMENTS

Material contained herein was obtained in connection with a research project “Evaluation of delamination cracking in bridge decks,” ALDOT Project 930-645, conducted by the Auburn University Highway Research Center. Funding for the project was provided by the Alabama Department of Transportation. The funding, cooperation, and assistance of many individuals from each of these organizations are gratefully acknowledged. The contribution of Akash Rao, Kwame Sakyi-Bekoe, and Xin Li during their thesis work is appreciated. The authors would like to acknowledge the contributions of the following individuals:

Larry Lockett	ALDOT, Chief of Materials and Test Bureau, Montgomery
Lyndi Blackburn	ALDOT, Assistant Materials and Test Engineer, Montgomery
Sergio Rodriguez	ALDOT, Special Projects Engineer, Montgomery
Robert King	FHWA, Alabama Division, Bridge Engineer

ABSTRACT

The focus of this report is a three-span, continuous, skewed bridge that was constructed in the summer of 2003 as the northbound roadway bridge on US 331 in Montgomery County, Alabama. This bridge deck exhibited extensive transverse and horizontal cracking and was replaced in 2005 before being opened to traffic. The primary objective of this study was to evaluate the mechanisms that may have contributed to horizontal cracking in this bridge deck.

The concrete satisfied all standard slump, total air content, and compressive strength requirements. Core results revealed adequate in-place compressive and splitting tensile strengths. Finite-element analyses were used to rule out excessive skew and differential support settlement as causes of the cracking. Horizontal cracking in this deck was most likely caused by excessive early-age temperature gradients combined with drying shrinkage gradients that produced large shear and normal stresses at the top reinforcement mat location in a concrete with a high coefficient of thermal expansion and high modulus of elasticity.

The effect of supplementary cementing materials, water-cement ratio, and placement temperature conditions on the early-age cracking tendency of bridge deck concrete was evaluated by rigid cracking frame testing techniques. Use of either fly ash or ground-granulated blast-furnace slag was found to significantly reduce thermal stresses at early ages. Coefficient of thermal expansion values were determined for concretes made with aggregates found in Alabama.

TABLE OF CONTENTS

LIST OF TABLES

LIST OF FIGURES

Chapter 1

Introduction

1.1 BACKGROUND

The focus of this investigation was a three-span, continuous, skewed bridge that was constructed in the summer of 2003 as the northbound roadway bridge over the CSXT railroad on US 331 between Legrand and Montgomery at Station 946 + 40.7085 in Montgomery County, Alabama. This bridge deck exhibited extensive transverse and horizontal cracking and was replaced in May 2005 before being opened to traffic. Examples of the cored locations at some crack locations are shown in Figure 1-1 and the severe extent of cracking on the surface of the deck is shown in Figure 1-2. A picture of the bridge deck is shown in Figure 1-3. Mechanisms that contribute to both transverse and longitudinal cracking in bridge decks have been widely documented (Krauss and Rogalla 1996; Issa 1999). Excessive amounts of wide surface cracks were initially observed; however, horizontal cracks were discovered when cores were extracted from the deck. The horizontal cracks were generally present at the level of the top reinforcement mat; however, in some cases these cracks developed between the top reinforcement mat and the top concrete surface. Typical cores that contained both vertical and horizontal cracks are shown in Figure 1-4. The extent of the horizontal cracking remains unknown; however, of the 26 cores extracted from the deck, 11 contained horizontal cracks.

Figure 1-1: Core holes through cracks in the US 331 bridge deck

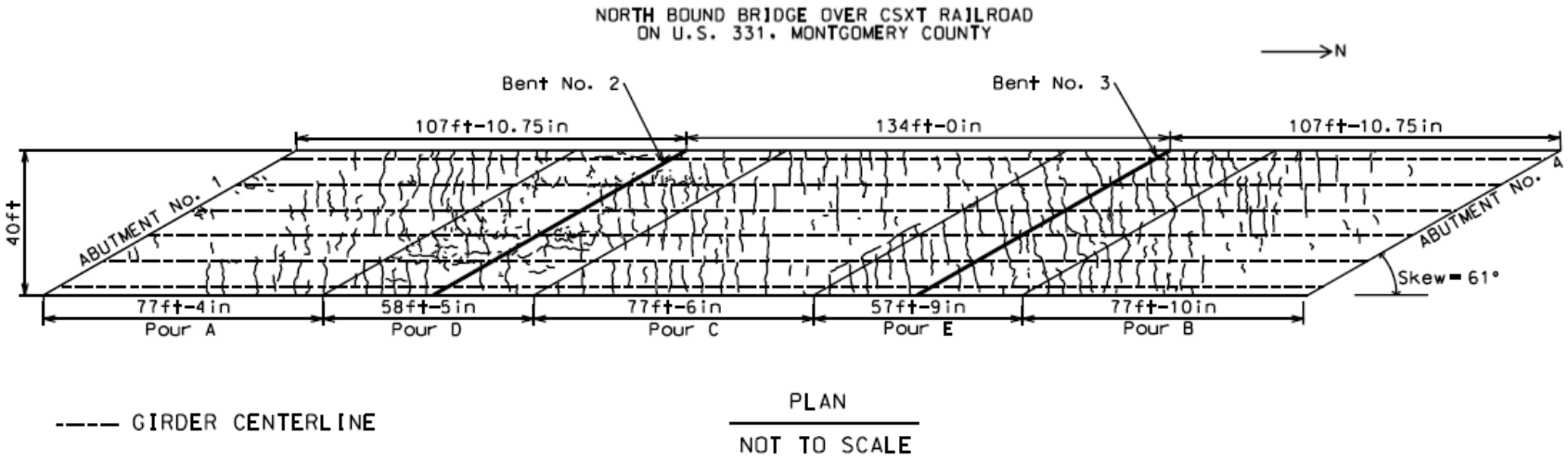

Figure 1-2: Surveyed crack pattern on northbound lanes of the US 331 bridge deck

Figure 1-3: View of the northbound lanes of the US 331 bridge deck

Figure 1-4: Cores from the US 331 deck with vertical and horizontal cracks

The crack surfaces for one of the horizontal cracks in the bridge on US 331 are shown in Figure 1-5. The majority of the cracks occurred around (rather than through) the aggregates, which may be an indication that the horizontal cracks could be due to early-age mechanisms. Even if the horizontal cracks were not caused at an early age the residual stresses induced by large thermal and drying shrinkage gradients may contribute to cracking at a later age.

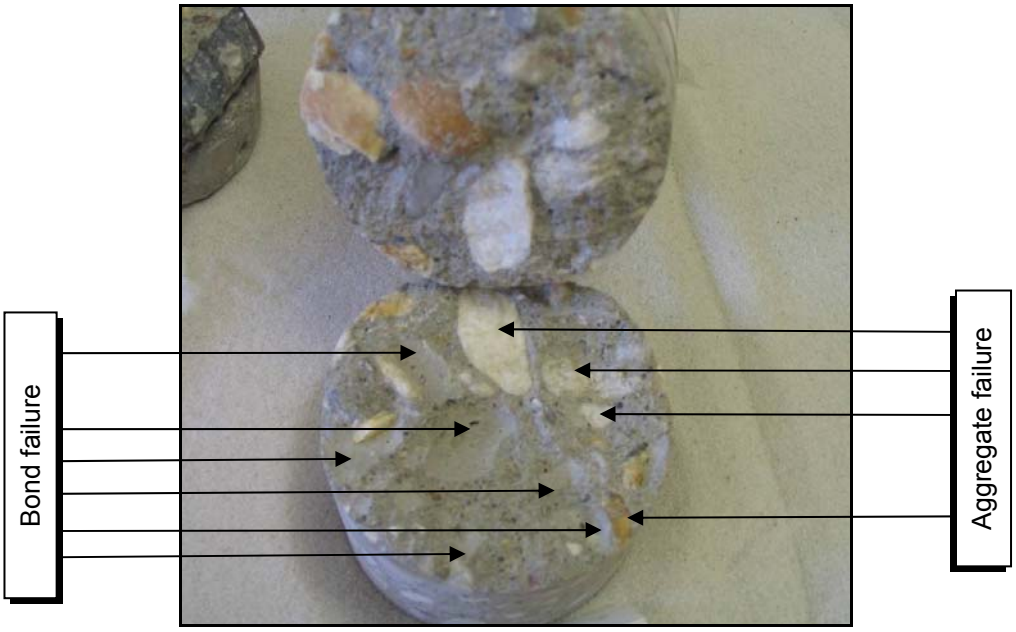

Figure 1-5: Core from deck on US 331 opened along a horizontal crack

Only one published document by Kim and Won (2004) was found that directly discusses mechanisms that may cause horizontal cracking in concrete slabs. Many sources (e.g. ACI 201.1R 1997) document the occurrence of horizontal cracking at the reinforcement mat when corrosion of reinforcement occurs; however, no corrosion was present on the reinforcement of the US 331 bridge. ALDOT personnel were also unfamiliar with these horizontal cracks and were interested in determining the possible cause(s) for the observed distresses.

Kim and Won (2004) explain a possible mechanism for the development of horizontal cracking in continuously reinforced concrete (CRC) pavements. The nature of the horizontal cracking experienced in a CRC pavement in Texas is shown in Figure 1-6. Some similarities between the cores obtained from the bridge on US 331 and the CRC pavement from Texas are evident. The pavements in Texas also revealed that the horizontal cracks occurred around the coarse aggregate, which is an indication of early-age cracking.

Figure 1-6: Core from CRC pavement in Texas with vertical and horizontal cracks (*Courtesy of Dr. Moon Won*)

Kim and Won (2004) provide a mechanism where horizontal cracking is caused by excessive early-age temperature variations that lead to large shear and normal stresses at the reinforcement location in highly crack-prone concretes that tend to have a high coefficient of thermal expansion and high modulus of elasticity. Kim and Won (2004) conclude that the occurrence of horizontal cracking can be minimized by the following means:

- Not placing concrete when the daily temperature differential is significantly large,
- Effectively curing the concrete to avoid high early-age drying shrinkage, and
- Selecting a coarse aggregate type to avoid a high concrete thermal expansion coefficient and a high elastic modulus of concrete.

The bridge deck on US 331 was constructed during June and July of 2003 (months when large temperature gradients would be expected) and contained river gravel coarse aggregate. Cores were tested from the US 331 bridge and the average compressive strength was 6,095 psi and the average modulus of elasticity was 4,500 ksi. The specified design strength for the bridge deck was 4,000 psi. Based on the commonly used ACI 318 relationship, the design modulus of elasticity for the concrete could be expected to be approximately $57\sqrt{4{,}000}$ = 3600 ksi. It is thus clear that the characteristics of the concrete mixture used for the bridge deck did not conform to most of the criteria highlighted by Kim and Won (2004) to minimize the likely formation of horizontal cracks. Based on the forensic evidence collected on the US 331 bridge, the primary failure mechanisms appear to be related to a mixture that is sensitive to cracking, the presence of large thermal gradients, and a high degree of restraint in the continuous bridge deck; however, additional mechanisms will be further evaluated in the report.

1.2 PROJECT OBJECTIVES

The main objectives of this project are as follows:

- Evaluate the mechanism that has caused horizontal cracking in the US 331 bridge deck,
- Determine the extent of horizontal cracking in other bridge decks in Alabama,
- Evaluate the early-age cracking sensitivity of bridge deck mixtures,
- Evaluate the coefficient of thermal expansion of various bridge deck concrete mixtures,
- Analytically evaluate the stress development in bridge decks with geometry similar to the US 331 bridge, and
- Develop recommendations for ALDOT to mitigate the occurrence of horizontal cracking in bridge decks.

1.3 REPORT OUTLINE

Early-age concrete behavior and the mechanisms that contribute to early-age cracking causes are reviewed in Chapter 2. The discussion includes a description of the hydration of cementitious materials, the development of mechanical properties, factors that produce early-age volume change, the coefficient of thermal expansion, early-age creep behavior, and methods to determine early-age stresses.

A review of the US 331 bridge deck, its cracking, all data collected for the bridge, and the mechanisms that more likely contributed to the observed distress are presented in Chapter 3. Additional bridge decks in Alabama were visited to investigate the extent of horizontal cracking in other bridge decks in the state and the findings from these visits are presented at the end of Chapter 3.

The cracking tendency of Alabama concretes made with various supplementary cementing materials and water-cement ratios (w/c) placed under different conditions is assessed in Chapter 4. This was accomplished by testing five concrete mixtures under various, controlled temperature conditions, while measuring the stress development from concrete placement until onset of cracking in rigid cracking frames.

The coefficient of thermal expansion values of Alabama concretes made with various coarse aggregate types and volumes, water-cement ratios, and sand-aggregate ratios are assessed in Chapter 5. All testing was done in accordance with AASHTO TP60 (2004), which was the only available AASHTO or ASTM test available to determine the CTE at the time that this study was completed.

The work document Chapter 6 focuses on using finite-element analysis techniques to gain an understanding of the mechanisms by which excessive cracks might have formed on the US 331 bridge deck. A finite-element model of the US 331 bridge was created and used to numerically predict the stress distribution and cracking behavior of the deck. A parametric study is presented to evaluate the effect of bridge skew angle and differential support settlement on the predicted crack patterns.

Conclusions and recommendations resulting from the work documented in this report are presented in Chapter 7.

Chapter 2

Literature Review

Early-age cracking in bridge deck concrete is a severe problem that can reduce its functional life. Cracking originates from stresses induced by volume change because of thermal, drying, autogenous, and chemical shrinkage, coupled with restraint conditions that prevent movement of the concrete. These stresses develop due to strains induced by early-age volume change as the concrete stiffness increases. Over time, these stresses may exceed the tensile strength of the concrete, which will result in cracking. Early-age concrete behavior and the mechanisms that contribute to early-age cracking causes are reviewed in this chapter. The discussion includes a description of the hydration of cementitious materials, the development of mechanical properties, factors that produce early-age volume change, the coefficient of thermal expansion, early-age creep behavior, and methods to determine early-age stresses.

2.1 HYDRATION OF CEMENTITIOUS MATERIALS

The hydration of portland cement is a chemical reaction during which heat is liberated. Many variables affect the heat generated during this hydration process. Factors such as cement composition, cement fineness, mixture proportions, replacement of cement by supplementary cementing materials (SCMs), and curing temperature can increase or decrease the rate of heat generated during hydration (Mehta and Monteiro 2006). Excessive heat generated, coupled with non-uniform cooling, results in thermal gradients in the concrete elements. This uneven distribution of heat can lead to thermal deformations which, when restrained, can introduce cracking long before the structure is exposed to externally applied loads.

2.1.1 Cement Type

The composition of cement is a major contributor to heat of hydration. Variables such as chemical composition and fineness affect the temperature rise of concrete. Some of these factors can be varied as a technique for controlling temperature, while others must be accepted as given conditions.

2.1.1.1 Cement Composition

The chemical composition of the clinker compounds consists primarily of tricalcium silicate (C_3S), dicalcium silicate (C_2S), tricalcium aluminate (C_3A), and tetracalcium aluminoferrite (C_4AF), which are commonly referred to as Bogue compounds. The relative proportions of these chemical compounds and their fineness determine the different types of cement, as well as the amount of heat they generate during hydration (Bjøntegaard 1999; Mehta and Monteiro 2006).

The hydration of cement is a mixture of simultaneous and consecutive reactions (Bjøntegaard 1999). When the cement is dispersed in water, C_3A, the high-temperature compound of calcium, begins to go into solution and the liquid phase is rapidly saturated with various ionic species. Needle-shaped crystals of Ettringite (calcium trisulfoaluminate hydrate), is the first hydration product to be formed by the reaction of C_3A with water. The reaction of C_3A is followed by the hydration of C_3S. Finally, C_3A and C_4AF react simultaneously after C_3S (Mindess, Young, and Darwin 2002).

The heat evolution of cement as it hydrates is shown in Figure 2-1. The initial reaction (Phase I) is caused by the reaction of C_3A forming ettringite. This process is very fast and a dormant period follows. After the dormant period, the second heat peak (II) is exhibited by the hydration of C_3S. The last heat peak (III) is produced by the transformation of ettringite to monosulfate (Bjøntegaard 1999).

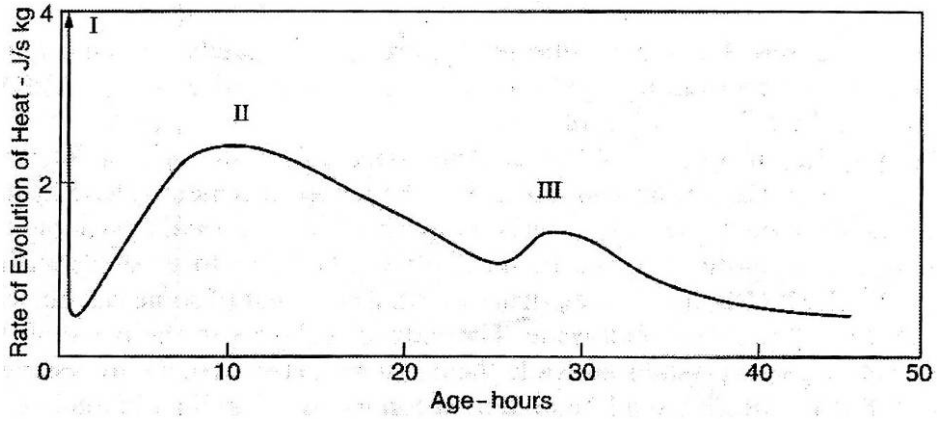

Figure 2-1: Heat evolution of hydrating cement (Bjøntegaard 1999)

Typical heat evolution values and rate of reactions for four primary chemical compounds in a Type I cement are shown in Table 2-1. Type I cement is the standard cement and is most commonly used in general construction applications in the United States (ACI 116R 1997). Type II and IV cements are low-heat generating cements during early ages, due to relatively low C_3A and high C_4AF content (Townsend 1965). Type III cement is high early-age strength cement, due to high C_3A content and fineness, which generates much more heat during hydration than Type I, II, or IV cements.

Table 2-1: Heat evolution of Bogue compounds (Bogue 1929)

Compound	Heat evolution after complete hydration (J/g)	Rate of reaction with water
C_3S	500	"medium"
C_2S	260	"slow"
C_3A	866	"fast"
C_4AF	125	"medium"

2.1.1.2 Fineness

Cement fineness affects the rate of heat generation rather than the magnitude of heat generation (ACI 207.2R 1997). The greater the fineness, the more surface area the cement is exposed to react with the water, and higher is the rate of hydration.

2.1.2 Mixture Proportions

The rate and magnitude of heat generation are affected by the quantity of cement used (ACI 207.2R 1997). This is due to the quantity of reactive products that are available to hydrate and liberate heat. The higher the cementitious materials content, the greater the temperature rise potential.

2.1.3 Replacement of Cement with Supplementary Cementing Materials

To reduce the amount of heat liberated during the hydration of cement, some SCMs can be used as a replacement for portland cement. SCMs such as fly ash and slag cement (a.k.a. ground granulated blast furnace slag) have been found to be effective means of reducing the quantity of cement, therefore reducing the heat due to hydration (ACI 207.2R 1997). Springenschmid and Breitenbücher (1998) stated that it is current practice to reduce the cement content as much as possible in order to reduce heat development.

2.1.3.1 Fly Ash

Fly ash comes from many different sources. The calcium oxide (CaO) content of the fly ash can be used as an indicator of its cementitious nature (Schindler and Folliard 2005). Class C fly ash is classified as fly ash containing more than 20% of CaO. Class F fly ash contains less than 15% CaO (ACI 232.2R 1997). Class F fly ash is generally more pozzolanic in nature as compared to Class C fly ash, which is more cementitious. Therefore, Class F fly ash reduces the total heat of hydration more than Class C (Mehta and Monteiro 2006). The reduction in heat liberation due to

hydration of cementitious systems containing fly ash and cement-only systems are shown in Figures 2-2 and 2-3.

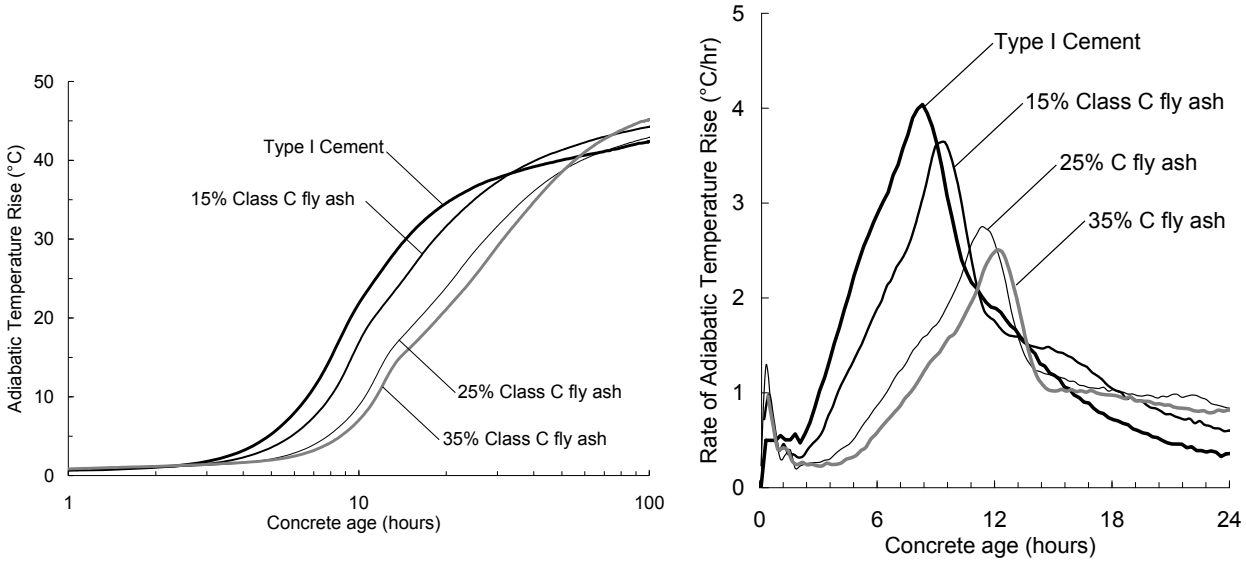

Figure 2-2: Total temperature rise and rate of temperature rise using Class C fly ash as a replacement for portland cement (Schindler and Folliard 2005)

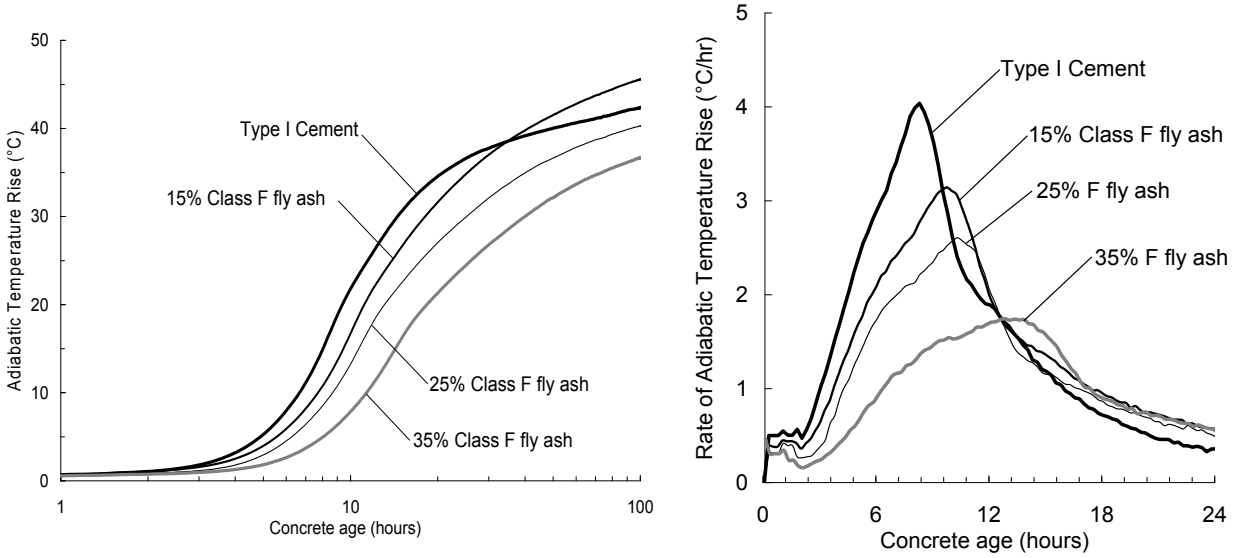

Figure 2-3: Total temperature rise and rate of temperature rise using Class F fly ash as a replacement for portland cement (Schindler and Folliard 2005)

2.1.3.2 Slag Cement

The reduction of early-age heat generation is directly proportional to the slag cement quantity used (ACI 233R 1997). The peak rate of temperature rise is delayed due to the inclusion of slag cement (Sioulas and Sanjayan 2000; Schindler and Folliard 2005), as seen in Figure 2-4.

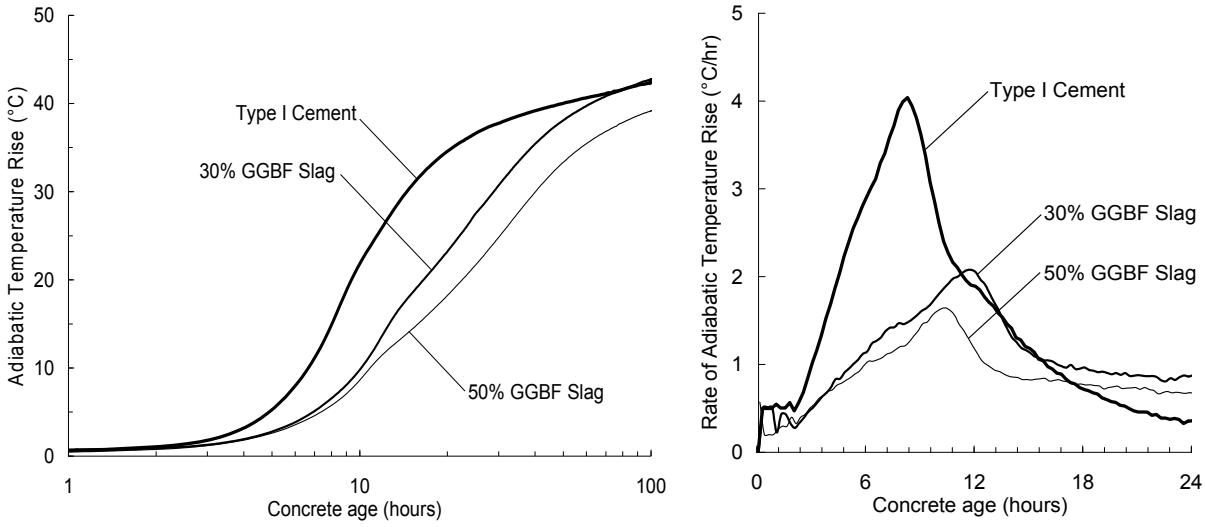

Figure 2-4: Total temperature rise and rate of temperature rise using slag cement as a replacement for portland cement (Schindler and Folliard 2005)

2.1.4 Curing Temperature

The curing temperature has a direct influence on the rate of hydration. If the curing temperature is increased, then the rate of hydration is increased. As the placement temperatures increases, the rate of temperature development rises faster due to the acceleration of hydration.

2.2 SETTING OF CONCRETE

Setting is the change in the concrete from a fluid to a rigid state. It is caused by the sufficient formation of hydration products, which is accompanied by a sudden change in temperature rise in the concrete (Mehta and Monteiro 2006). According to ASTM C 403, initial set is achieved when the concrete paste has reached a penetration resistance of 500 psi. Final set is achieved when the concrete paste has reached a penetration resistance of 4,000 psi. Plots of penetration resistance over time, like the one shown in Figure 2-5, is used to determine initial and final set.

2.3 DEVELOPMENT OF MECHANICAL PROPERTIES

Cracking in early-age concrete is not just a function of stress development. Cracking is also a function of mechanical properties such as tensile strength and elastic modulus. These properties are time- and temperature-dependent. The modulus of elasticity relates strains to stresses, and will be discussed in Section 2.3.3. The tensile strength of the concrete resists the stresses from restrained contraction of the concrete and will be discussed in Section 2.3.2.

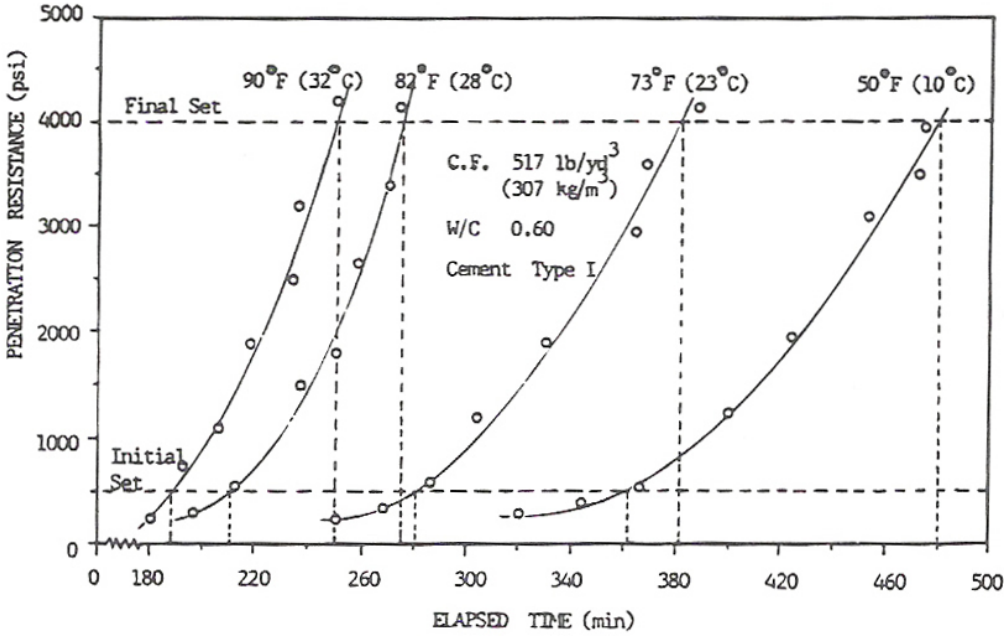

Figure 2-5: Typical plot of penetration resistance versus time for concrete at various temperatures (Dobson 1994)

2.3.1 Compressive Strength

The development of compressive strength in concrete has been widely studied for many years. Factors such as amount and type of cement and admixtures, temperature, curing conditions, and water-to-cementitious materials ratio affect the development of concrete strength (Mehta and Monteiro 2006).

As discussed in Section 2.1, cement type and amount may affect the amount of heat developed in the concrete member. Temperature affects the rate at which the cement hydrates. Therefore, early-age and long-term strength can be affected due to changes in these mixture proportions. Variables such as water-to-cementitious ratio (w/cm), air entrainment, and cement type can be varied to increase or decrease strength. As the w/cm is increased, the compressive strength is decreased (Kosmatka et al. 2002). The decrease in the compressive strength will occur as the total air content of the mixture increases (Kosmatka et al. 2002). The effect of cement type on concrete strength is shown in Figure 2-6. As discussed in Section 2.1.1.1, Types II and IV have low early-age strength due to lower C_3A content. However, Type III cement has high early-age strength due to higher C_3A content.

The curing temperature also affects the rate at which the cement hydrates as discussed in Section 2.1.4. As the curing temperature is increased, the cement hydrates more rapidly. As a result, the concrete develops mechanical properties at a faster pace; however, the long-term strengths are reduced as shown in Figure 2-7.

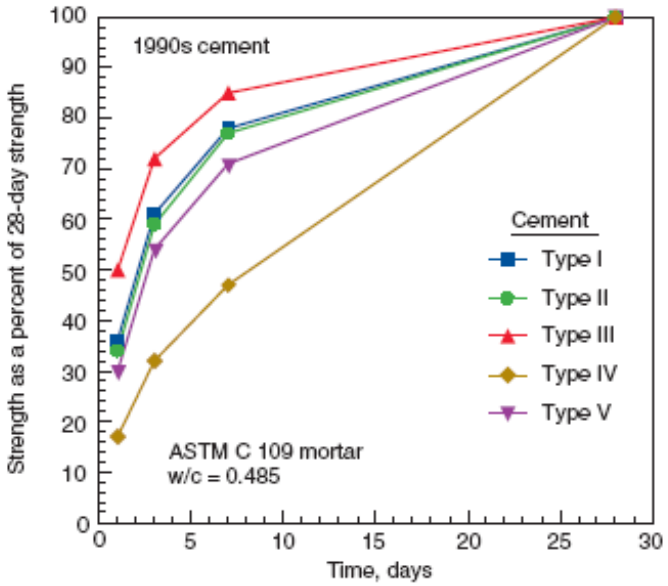

Figure 2-6: Effect of cement type on concrete strength (Kosmatka et al. 2002)

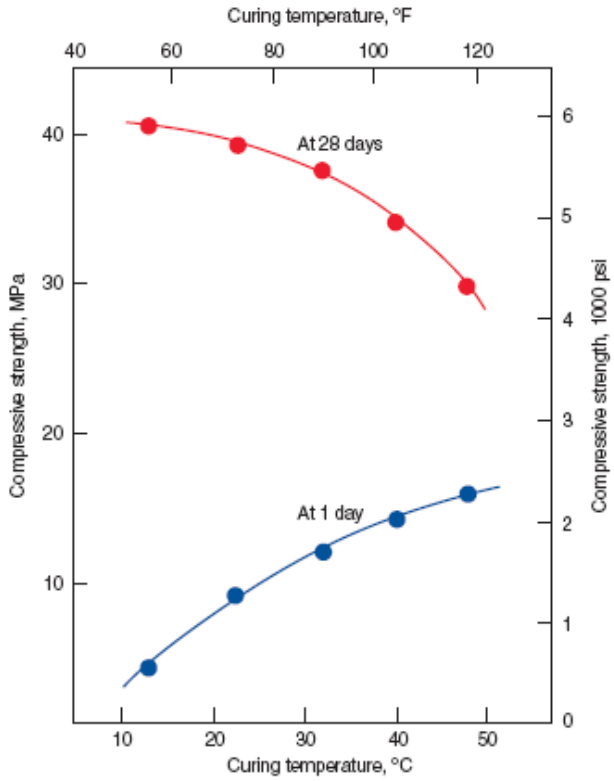

Figure 2-7: Effect of curing temperature on concrete strength (Kosmatka et al. 2002)

2.3.2 Tensile Strength

Tensile strength of concrete develops due to the same factors as compressive strength; however, concrete's tensile strength is much lower than its compressive strength, due to ease of crack propagation under tensile loads (Mindess, Young, and Darwin 2002). The rate of development and magnitude of the tensile strength play an important role in early-age cracking.

Microcracking originates in the interfacial transition zone (ITZ), and cracking develops as load is applied. The ITZ develops from a water film that forms around large aggregate particles as bleeding occurs. As hydration progresses, calcium silicate hydrate (C-S-H) forms to fill the empty voids left behind from the water film. This helps to improve the strength and density of the ITZ (Mehta and Monteiro 2006).

The ITZ is the strength-limiting phase in concrete (Mehta and Monteiro 2006). This is primarily due to the microcracking that can be present in the ITZ before the structure is loaded. It is also the reason why concrete displays inelastic behavior, while its constituents exhibit elastic behavior until fracture.

Aggregate characteristics influence the tensile strength of concrete (Mehta and Monteiro 2006). Aggregate texture has a substantial impact on the tensile strength of concrete. Rough textured or crushed aggregates have shown higher tensile strengths, especially at early ages, than smoother aggregates (Mehta and Monteiro 2006).

2.3.3 Modulus of Elasticity

The development of the elastic modulus of concrete varies in proportion to the square root of the compressive strength gain in concrete (ACI 318 2005). The same factors that alter the development of strength affect the development of the elastic modulus, with some exceptions. The modulus of elasticity is affected primarily by the aggregate type and quantity used in the concrete mixture (Mindess, Young, and Darwin 2002). As the stiffness and amount of the aggregate fraction in concrete increases, the stiffness of the concrete increases, as shown in Figure 2-8.

The modulus of elasticity is also a function of the porosity of the paste fraction of the concrete. As the water-to-cementitious materials ratio is increased, the porosity of the paste fraction is increased. If the porosity is increased, the elastic modulus will decrease (Mindess, Young, and Darwin 2002).

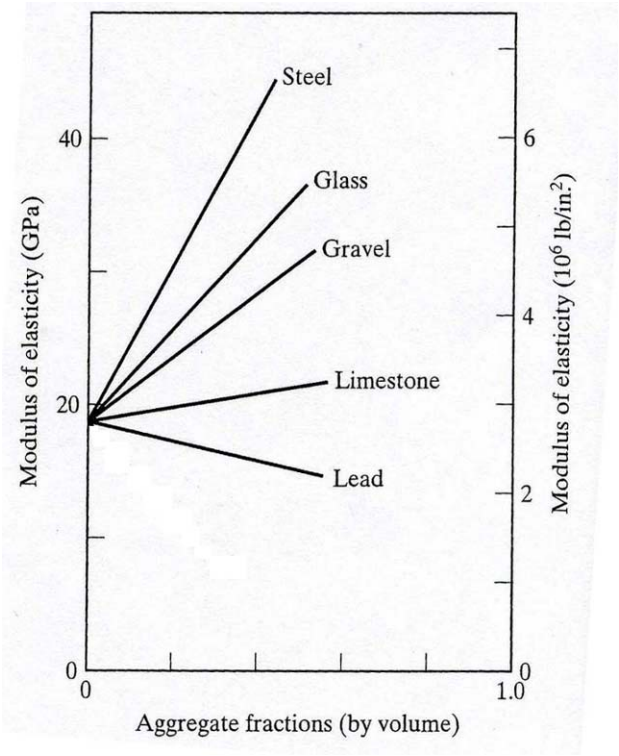

Figure 2-8: Effect of aggregates on modulus of elasticity (Mindess, Young, and Darwin 2002)

2.4 FACTORS THAT PRODUCE EARLY-AGE VOLUME CHANGE

Early-age volume change in concrete is a well-known phenomenon that has been studied for many years. Factors such as thermal changes, drying shrinkage, and autogenous shrinkage are known to produce early-age volume change. If the concrete is restrained from movement, the volume changes will induce compressive or tensile stresses. If these stresses are greater than the corresponding strength of the concrete, then cracking may occur as was the case in the US 331 bridge deck. In this section, the various factors that contribute to early-age volume changes are discussed.

2.4.1 Thermal Effects

Thermal stresses have been a major cause of early-age cracking of bridge deck concrete (Lange and Altoubat 2002). Many factors such as heat of hydration (as discussed previously), environmental conditions (weather and time of placement) and thermal conductivity affect the rate of temperature rise. Concrete, like many other materials, expands when it is heated and contracts when it is cooled. If the concrete is restrained from movement, the change in temperature will induce stresses.

The development of thermal stresses (σ_T) can be calculated by the expression presented in Equation 2-1. For an accurate estimate of the thermal stress, creep effects during early ages and over the structure's life should be accounted for in Equation 2-1 (Schindler and McCullough 2002).

$$Thermal\ Stress = \sigma_T = \Delta T\ CTE \cdot E_c \cdot K_r \qquad \text{Equation 2-1}$$

Where, ΔT = Temperature Change = $T_{zero\text{-}stress} - T_{min}$ (°F),
CTE = Coefficient of Thermal Expansion (strain/°F),
E_c = Creep adjusted Modulus of Elasticity (psi),
K_r = Degree of restraint factor,
$T_{zero\text{-}stress}$ = Concrete zero-stress temperature (°F), and
T_{min} = Minimum concrete temperature (°F).

An illustration of the development of concrete temperatures and thermal stresses over time under summer placement conditions for freshly placed concrete is presented in Figure 2-9. In terms of stress development, the final-set temperature is the temperature at which the concrete begins to resist stresses induced by restraint of external volume changes. In Figure 2-9, it can be seen that due to hydration the concrete temperature increases beyond the setting temperature, line (A). As the expansion of the concrete caused by the temperature rise is restrained, the concrete will be in compression when the temperature peaks, line (B), is reached. The phenomenon of gradual decrease in stress over time is called stress relaxation (Mehta and Monteiro 2006). When the peak temperature is reached the hydrating paste is still developing structure, its strength is low, and high amounts of early-age relaxation may occur when the concrete is subjected to high compression loads (6). When the concrete temperature decreases, the compressive stress is gradually relieved until the stress condition changes from compression to tension, line (C). The temperature at which this transient stress-free condition occurs is denoted the "zero-stress temperature". Note that due to the effects of relaxation, the zero-stress temperature may be significantly higher than the final-set temperature (6). If tensile stresses caused by a further temperature decrease exceed the tensile strength of the concrete, cracking will occur, line (D). Because the thermal stress is proportional to the difference between the zero-stress temperature and the cracking temperature, thermal cracking can be minimized by decreasing the zero-stress temperature. This in turn can be accomplished by (1) minimizing the final-set temperature, (2) minimizing the peak temperature achieved during the high-relaxation phase, or (3) delaying the attainment of the peak temperature. The test setup employed in Chapter 4 of this study restrains concrete specimens to assess the development of thermal stresses (and autogenous effects) in typical bridge deck curing conditions.

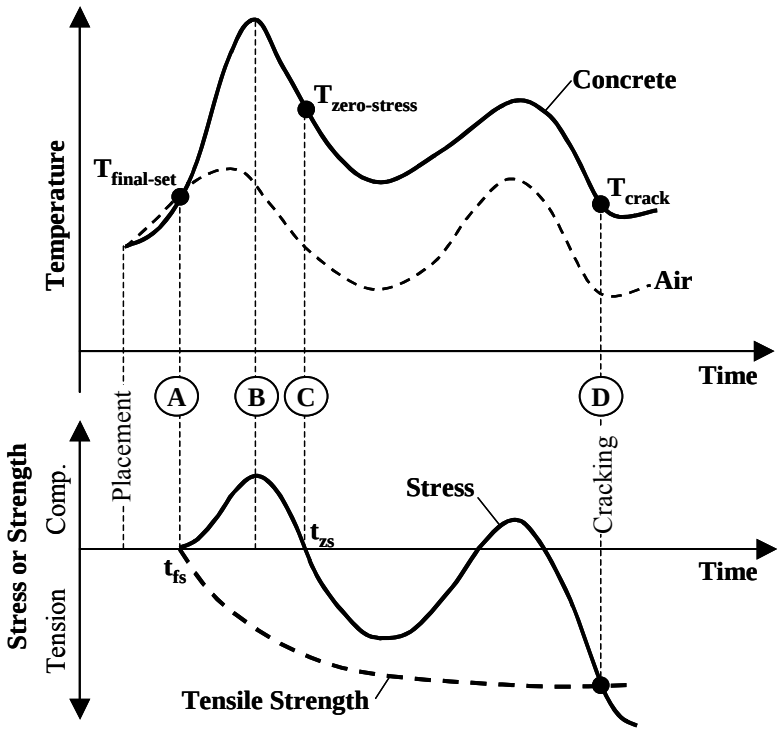

Figure 2-9: Development of early-age thermal stresses (Schindler and McCullough 2002)

However, it is to be noted that there is a significant difference between calculated stress due to the given temperature change, and the actual measured stress. This is due to the viscoelastic nature of the concrete at early ages, which allows much of the compressive stresses to be relaxed. However, due to the relaxation, concrete experiences tensile stresses much earlier than the calculated, and hence a higher risk of cracking at an earlier age than predicted.

2.4.1.1 Coefficient of Thermal Expansion

The coefficient of thermal expansion (CTE) is a key parameter that relates temperature change in the concrete to strain. As indicated in Equation 2-2, the magnitude of strain developed in an unrestrained specimen, is directly proportional to the temperature change and the CTE.

$$\Delta\varepsilon_{Thermal} = \Delta T \cdot CTE \qquad \text{Equation 2-2}$$

where,

$\Delta\varepsilon_{Thermal}$ = change in concrete strain due to temperature change (in./in.), and

ΔT = change in temperature (°F).

The CTE varies as a function of the individual constituents of the concrete (Emanuel and Hulsey 1977). Variables such as aggregate type, water-to-cementitious materials ratio, and age affect concrete's CTE. Changes in concrete's CTE due to the use of different aggregates can be seen in Figure 2-10. Concrete's CTE is directly related to the CTE of the aggregate used in the mixture

proportions (Mehta and Monteiro 2006). As the CTE of the aggregate is increased, the CTE of the concrete is increased.

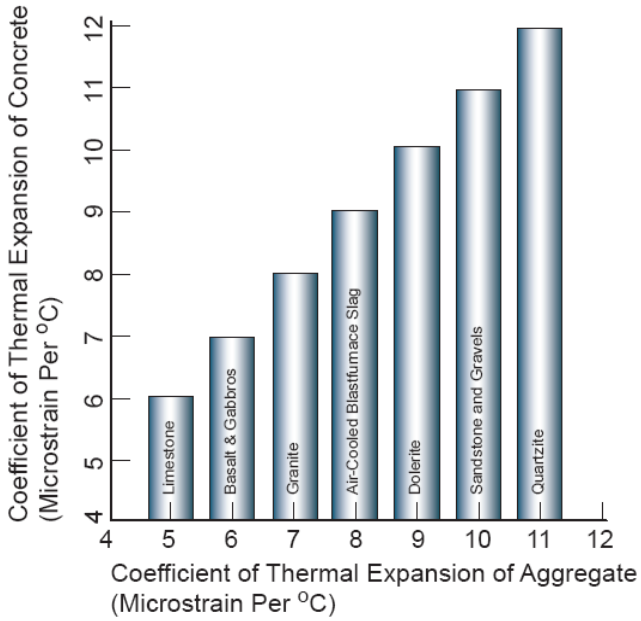

Figure 2-10: Influence of aggregate on the coefficient of thermal expansion of the hardened concrete (Mehta and Monteiro 2006)

2.4.1.1.1 Standard Method of Test for Coefficient of Thermal Expansion of Hydraulic Cement Concrete - AASHTO TP 60 (2004)

AASHTO TP 60 (2004) is a provisional test, and it covers the determination of the CTE of hydraulic cement concrete specimens. Since it is known that the degree of saturation of concrete influences its coefficient of thermal expansion, the moisture condition of the concrete specimens is controlled. Hence for this test, the specimens, 4 in. x 7 in. in size are tested in the saturated condition. A measurement frame with the linear variable differential transformer (LVDT) attached is placed in the water bath and the bath is filled with water. A schematic of the apparatus is shown in Figure 2-11. The movement of the specimen is measured with an LVDT as the temperature of a water bath is repeatedly changed from 50 ^{o}F to 122 ^{o}F ± 2 ^{o}F. The test result is the average of the two CTE values obtained from the two test segments that provide two values within 0.5 x 10^{-6} / ^{o}F of each other. More specifics about this test are provided in Chapter 5 of this report.

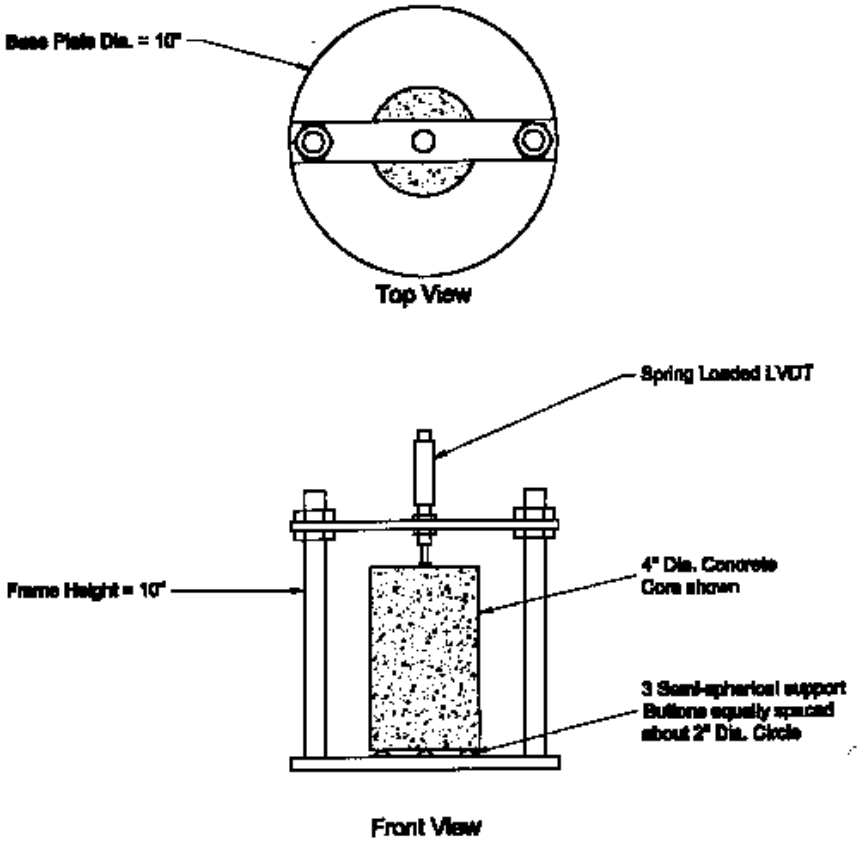

Figure 2-11: Schematic of CTE measuring frame (AASHTO TP 60 2004)

2.4.1.2 Environmental Conditions

Bridges are continuously subjected to changing temperatures, therefore, a significant factor in the behavior and performance is thermal loading due to environmental factors. Thermal stresses induced from seasonal temperatures changes, are linearly proportional (not accounting for relaxation effects) to the differences between material thermal expansion coefficients and differences between concrete stiffness of various elements in the bridge. Through the study conducted by NCHRP Report 380 (Krauss and Rogalla 1996), it is now known that the diurnal temperature changes affect the bridge deck more than the supporting girders and the resulting thermal stresses are proportional to the coefficient of thermal expansion. However, usually, temperature changes are not taken into consideration during design because temperature steel is considered sufficient to control widths after cracking.

When a deck is cast monolithically with the girders, thermal stresses caused by hydration are generally reduced because both the deck and girders generate heat and then cool at the same time. However, thermal stresses are worse in steel-girder bridges (Krauss and Rogalla 1996). Bridge decks in moderate or extreme climates often experience high stresses due to temperature changes. The upper surface of the deck typically heats and cools more quickly,

because it is exposed to direct solar radiation, wind, and humidity. Hence, these factors have to be taken into account when determining the thermal effects on early-age cracking.

2.4.2 Early-Age Shrinkage

Concrete shrinkage is a result of the migration or loss of water from the hydrated cement paste phase. Holt (2001) states that "as water is lost to evaporation (drying shrinkage) or internal reactions (autogenous shrinkage), tensile stresses are generated." As a result of a slow elastic modulus development, large strains may only create small stresses at early ages. However, these stresses at early-ages are more critical because the concrete has not developed much strength. Even if the resulting stresses are small, microscopic cracks may still form. If early cracks are internal and microscopic, long-term shrinkage may cause the cracks to widen and spread. A discussion of drying shrinkage, autogenous shrinkage, and chemical shrinkage can be found in Sections 2.4.2.1, 2.4.2.2, and 2.4.2.3, respectively.

2.4.2.1 Drying Shrinkage

Drying shrinkage occurs when water held by hydrostatic tension in small capillary pores (< 50 nm) of the hydrated cement paste is lost to the atmosphere due to differences in relativity humidity (Mehta and Monteiro 2006). When the voids empty, capillary stresses are generated that result in volumetric shrinkage of the concrete. It is common practice to delay the onset of drying shrinkage by curing bridge decks with cotton mats for 7 days or more after placement. The experimental work in this study was focused on the early-age cracking mechanisms that occur within the first 7 days after placement. Therefore, the effects of drying shrinkage lie outside the scope of this report. Nonetheless, drying shrinkage effects will eventually add to thermal and autogenous shrinkage effects once the deck is exposed to drying.

2.4.2.2 Autogenous Shrinkage

The reaction products formed from cement hydration are smaller that the initial components. The reduction of the absolute volume of the reactants due to hydration is chemical shrinkage. Before setting this phenomenon results in a volumetric change but generates no stress due to the viscoelastic nature of fresh concrete. After setting, chemical shrinkage leads to the creation of internal water filled voids. As water is consumed by the ongoing hydration process the voids empty, and capillary stresses are generated resulting in a volumetric shrinkage. Autogenous shrinkage is the concrete volume change occurring with out moisture transfer to the environment (JCI 1998). Before setting chemical shrinkage and autogenous shrinkage are equal (Holt 2001). When the *w/c* is above 0.42, enough water is provided in the void spaces for hydration, and stresses associated with autogenous shrinkage do not develop (Mindess, Young, and Darwin 2002). Decreasing the *w/c* below 0.42 will thus cause to stresses due to autogenous shrinkage.

A graphic depiction of a sealed concrete's composition change due to the cement hydration reactions is given in Figure 2-12 where C is the cement volume, W is the volume of water, H_y is the volume of the hydration products and V is the volume of voids. This bar graph relates how the autogenous shrinkage is a portion of the chemical shrinkage. While the chemical shrinkage is an internal volume reduction, the autogenous shrinkage is an external volume change.

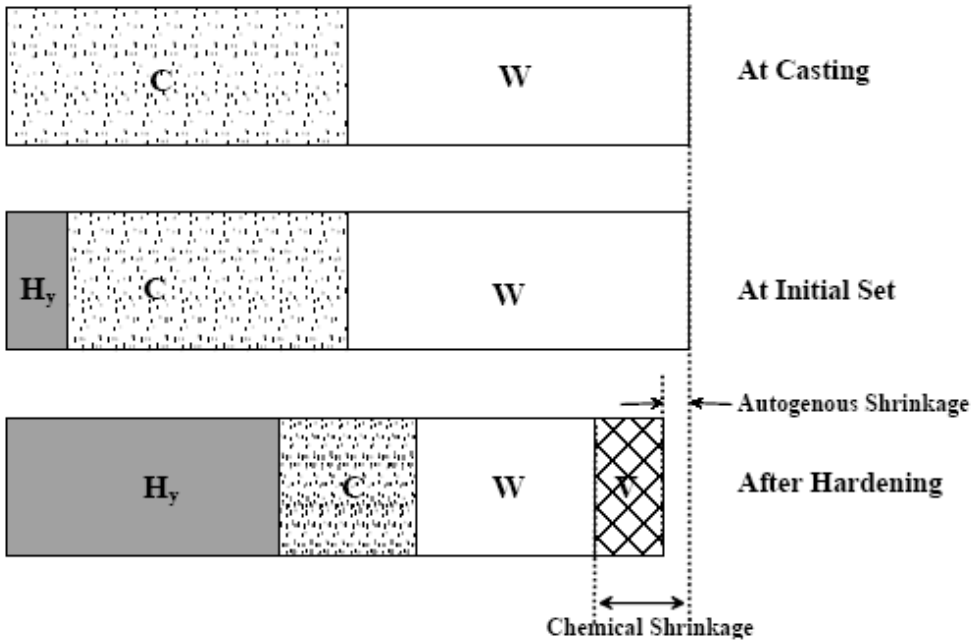

Figure 2-12: Volume reduction due to autogenous shrinkage (Holt 2001)

2.5 DEVELOPMENT OF EARLY-AGE STRESSES

Early-age stresses originate from volume change as a result of thermal, drying, and autogenous shrinkage, coupled with restraint conditions that prevent or alter the movement of concrete. The stresses are time-dependent and are proportional to the restraint against movement. Over time, stresses may exceed the tensile strength of the concrete, which will result in cracking.

2.5.1 Restraint Conditions

Restraint conditions of the concrete element are of utmost importance when determining stresses induced by early-age volume change. Restraint stresses can be divided into two major categories, internal and external. Internal restraint is caused by temperature or gradients that form because of uneven cooling and/or moisture loss within the concrete member. During cooling, the surface of the concrete cools more rapidly than the interior of the element, which creates thermal gradients.

External restraint is caused by the conditions surrounding or supporting the concrete element that prevents free movement. External restraints associated with bridge decks could include, but are not limited to deck form type, deck-girder systems, girder type, girder end constraints, relative stiffness of the girder and the deck. The reduction of the overall restraint of the concrete member can significantly decrease the cracking tendency. Figure 2-13 demonstrates the temperature, stress, and strength development of a concrete element that is fully restrained (100%) from movement. As shown, reducing the restraint factor diminishes the risk of cracking due to the reduction in stresses.

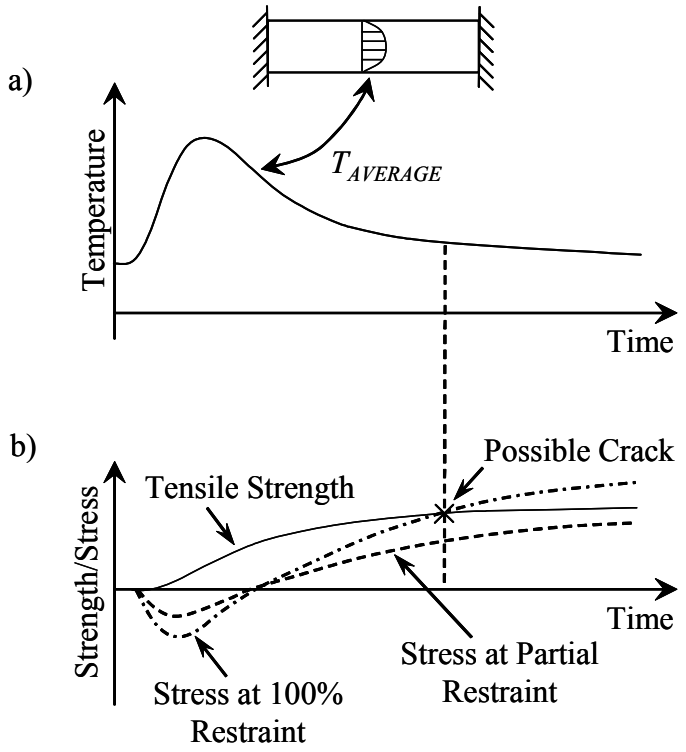

Figure 2-13: Evolution of temperature and thermal stresses for different restraint conditions (Nilsson 2003)

2.5.2 Early-Age Creep Behavior

Early-age concrete undergoes deformations due to volume change as discussed previously. Restraint of these deformations creates stresses in the concrete. Creep and associated relaxation occur due to the viscoelastic response of early-age concrete; therefore, these properties must be considered when assessing the cracking risk of concrete during the first few days after placement.

Creep is the increase in strain with respect to time under a constant load. If a linear-elastic material is subjected to a constant load, then it will respond instantaneously with a deformation that remains constant. However, if the load is removed, then the material will return

to its original shape. Concrete, on the other hand, is not a linear-elastic material especially at early-ages; therefore, understanding early-age nonlinear creep behavior is very important when calculating restraint stresses in early-age concrete (Westman 1999).

Concrete creep can be divided into two major categories: recoverable and irrecoverable deformation (Mehta and Monteiro 2006). Recoverable deformation is recovered fully after unloading due to the elastic nature of the concrete. Irrecoverable deformation causes the concrete paste to behave plastically; therefore, not recovering all deformation after the load is removed. Figure 2-14 illustrates the general behavior of hardening concrete with loading and unloading taking place. Elastic deformation can be recovered instantaneously after the load is removed. The delayed elastic recovery, commonly referred to as creep recovery, is the portion of creep-induced deformation that will be recovered over time. The net effect after loading and unloading has taken place, is the irrecoverable deformation (Emborg 1989).

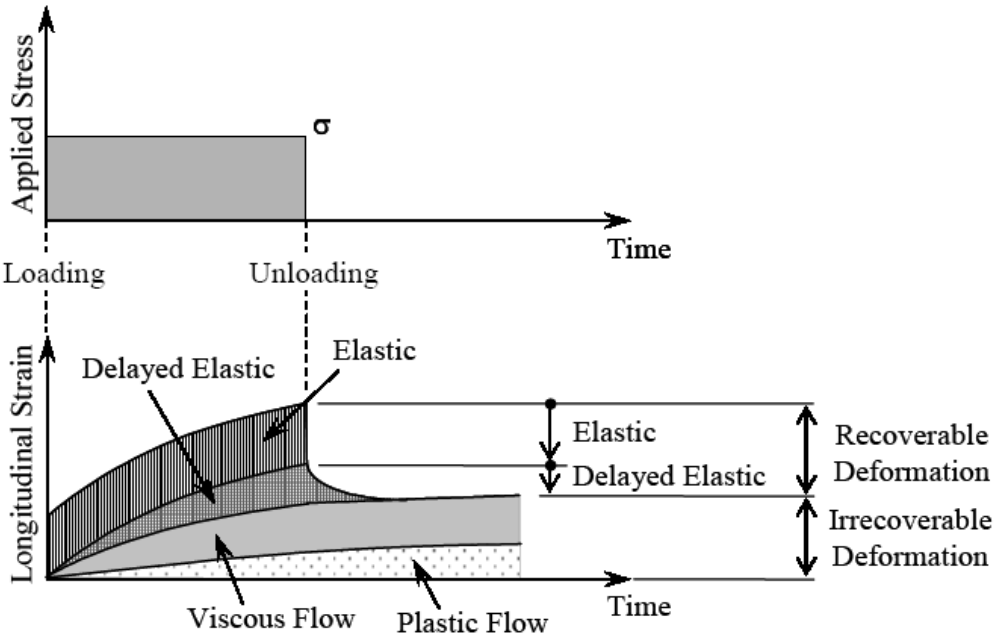

Figure 2-14: Generalized creep behavior of hardening concrete (Emborg 1989)

2.6 METHODS FOR DETERMINING EARLY-AGE STRESSES

The mechanisms that cause internal volume changes in early-age concrete are very complex. The stresses that are generated cannot be determined by measuring deformations alone (Breitenbücher 1990). As a result, accurate measurement of restraint-induced stresses is very difficult. Many laboratory tests have been developed to measure the restraint stresses and quantify the cracking tendency of concrete. Tests such as the concrete ring test, restrained prism test, and temperature-stress testing machine (TST) are methods of determining the cracking tendency of various concrete mixtures (Whigam 2005; Mangold 1998); however, this report only

involves the use of the rigid cracking frame as a testing method, as used by Meadows (2007).

Since many of the mechanisms that affect cracking at early ages are quite complicated at early ages, it is proposed to evaluate the effect of these mechanisms by using cracking frame testing techniques.

2.7 CONCLUDING REMARKS

Cracking in concrete due to early-age volume change is a complex phenomenon and is caused by many variables. Effects such as thermal, drying, and autogenous shrinkage, coupled with restraint conditions, create stresses that can exceed the tensile strength of the concrete. In order to understand the mechanisms driving early-age cracking, the effect of various variables should be should be studied. Quantification of these variables can be an extremely hard task, particularly at early ages, therefore making prediction of cracking tendencies very difficult. A practical way to assess the effect of these variables is to perform restrained cracking tests such as those performed with the rigid cracking frame used in Chapter 4 of this report.

Chapter 3

Review of the US 331 Bridge Deck and Other Bridge Decks in Alabama

A review of the US 331 bridge deck, its cracking, all data collected for the bridge, and the mechanisms that more likely contributed to the observed distress are presented in this chapter. With the assistance of ALDOT personnel, five bridge decks in Alabama were visited to investigate the extent of horizontal cracking in other bridge decks in the state; the findings from these visits are presented at the end of Chapter 3.

3.1 THE US 331 BRIDGE

3.1.1 Description of the US 331 Bridge

The US 331 bridge is a three-span, continuous, skewed bridge constructed in the summer of 2003 as the northbound roadway over the CSXT railroad on US 331 between Legrand and Montgomery at Station 946+40.7085 in Montgomery County, Alabama. A picture of the bridge is shown in Figure 3-1. The plan view and cross section of the bridge are shown in Figure 3-2, along with the framing plan. The reinforced concrete deck has a length of 350 ft, a roadway width of 40 ft and a design thickness of 7 inches. The three span lengths, from the south end to the north end, are 108 ft, 134 ft, and 108 ft, respectively, and the skew angle for the bridge is 61°.

Figure 3-1: View of the northbound roadway bridge over the CSXT railroad on US 331

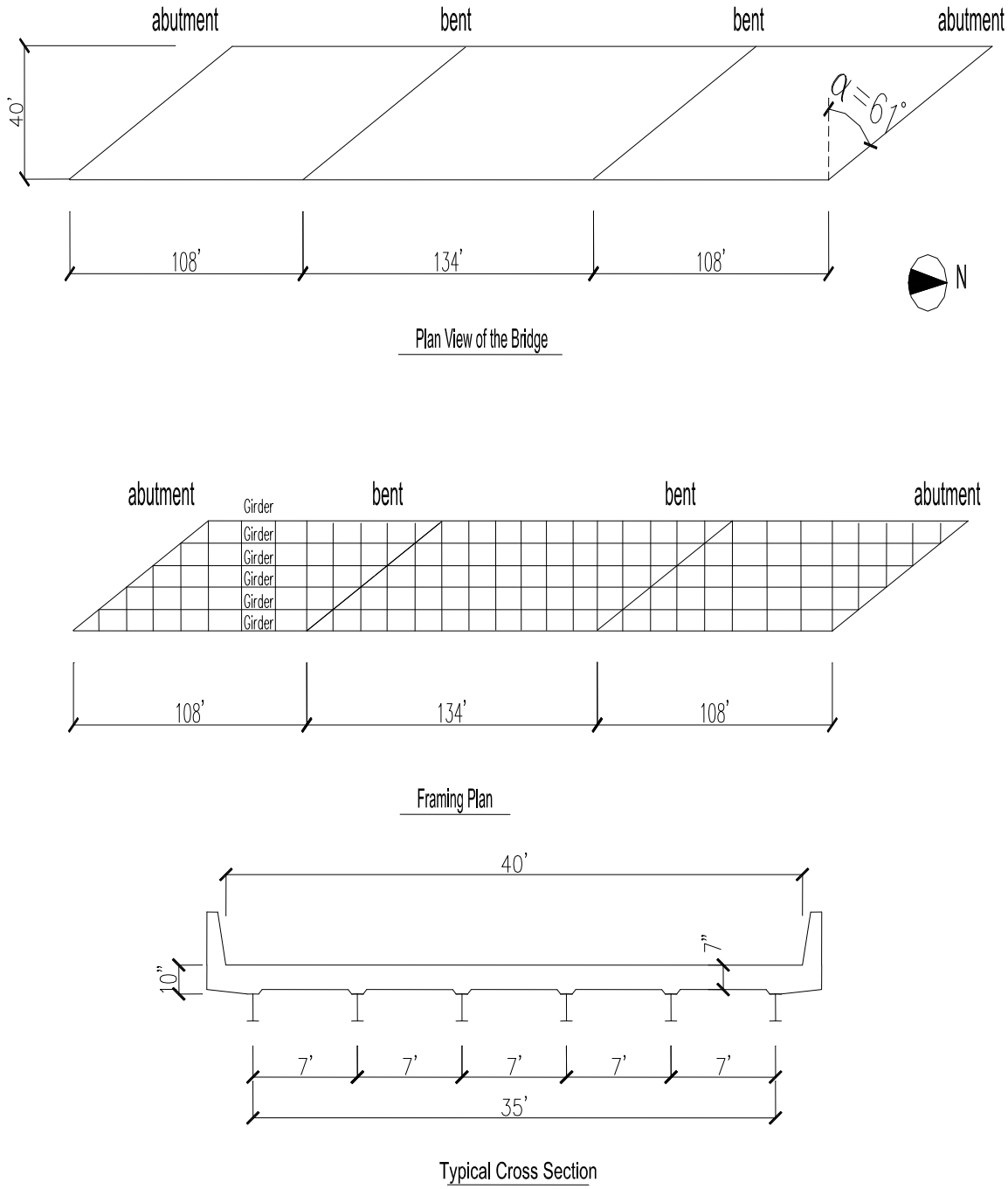

Figure 3-2: Plan view and section of the US 331 bridge

The reinforced concrete deck is supported by six continuous AASHTO M270 Grade 36 steel welded plate girders with a transverse spacing of 7 ft. The web plate dimensions for each girder are ½ in. x 48 in. The flange for each girder measures 1¼ in. x 16 in. in the positive moment regions, and 1¾ in. x 16 in. in the negative moment regions (near the interior bents). The top of the steel flanges are connected to the bottom of the reinforced concrete deck using 96 rows of ¾-in.-diameter x 5 in. equally spaced shear studs over the end span positive moment

regions, and 94 rows of ¾-in.-diameter x 5 in. equally spaced shear studs over the middle span positive moment region. Each of the rows contains three shear studs; one stud was placed directly above the web centerline, and each of the other studs was placed 6 in. on either side of the web centerline.

Intermediate crossframe diaphragms constructed of L4 x 4 x 5/16 in. angles, as shown in Figure 3-3, connect the girders in each span; these diaphragms are represented by the straight vertical lines in the framing plan shown in Figure 3-2. As can be seen in the framing plan, the crossframe diaphragms are perpendicular to the longitudinal direction of the bridge (i.e., they do not follow the 61° skew angle). Additionally, as indicated in Figure 3-2 by the slanted lines, W27 x 84 bearing diaphragms are located between the girders at the abutments and at the interior bents, placed parallel to the skew angle.

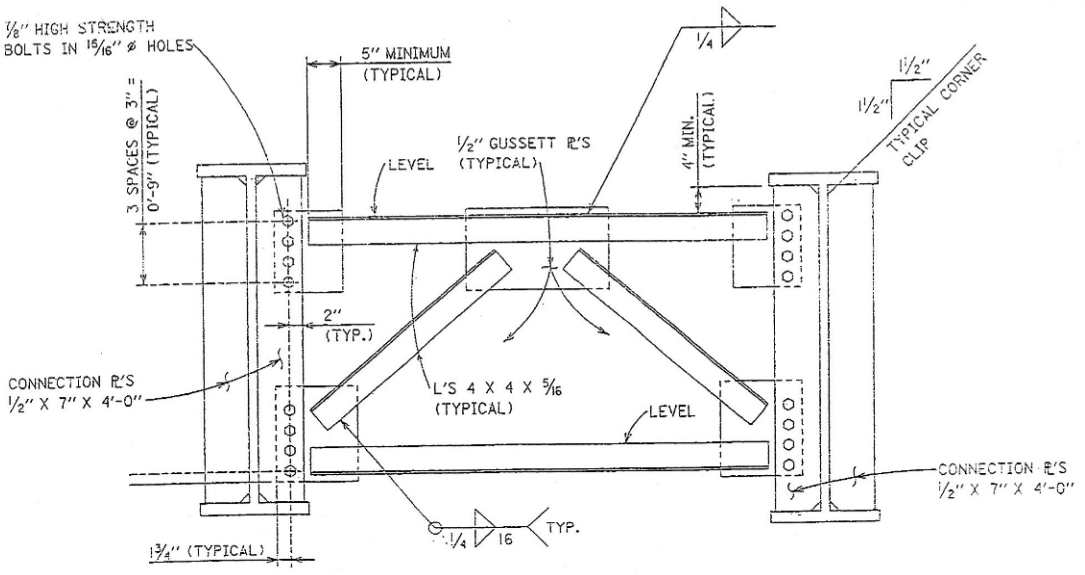

Figure 3-3: Typical intermediate crossframe diaphragm detail (ALDOT detail)

The RC deck slab, as mentioned, had a design depth of 7 in., deepening to 10 in. in a haunch shape above each of the girders. Details of the deck are shown in Figure 3-4. At the top of the slab, No. 4 longitudinal reinforcement was placed directly above the girder centerlines and evenly spaced between the girders at 16.8 in. on center. No. 4 longitudinal reinforcement was also placed in the top of the deck on 12-in. centers between the location above the outermost edge of the top girder flange and the inner edge of the traffic barrier on either side of the bridge. Extra No. 4 longitudinal reinforcement was placed between the main No. 4 bars (previously described) at the top of the slab above each of the interior bents. At the bottom of the slab, eight No. 5 longitudinal reinforcing bars were placed between each pair of girders: located 9 in., 23.5 in., 30.9 in., and 38.3 in. from each girder centerline. In addition, No. 5 transverse reinforcement was placed at the top and bottom of the slab, (above and below the upper and lower longitudinal

reinforcement, respectively), spaced at 5½ in. on center. The design cover was 2.0 in. and 1.0 in. at the top and bottom of the deck, respectively.

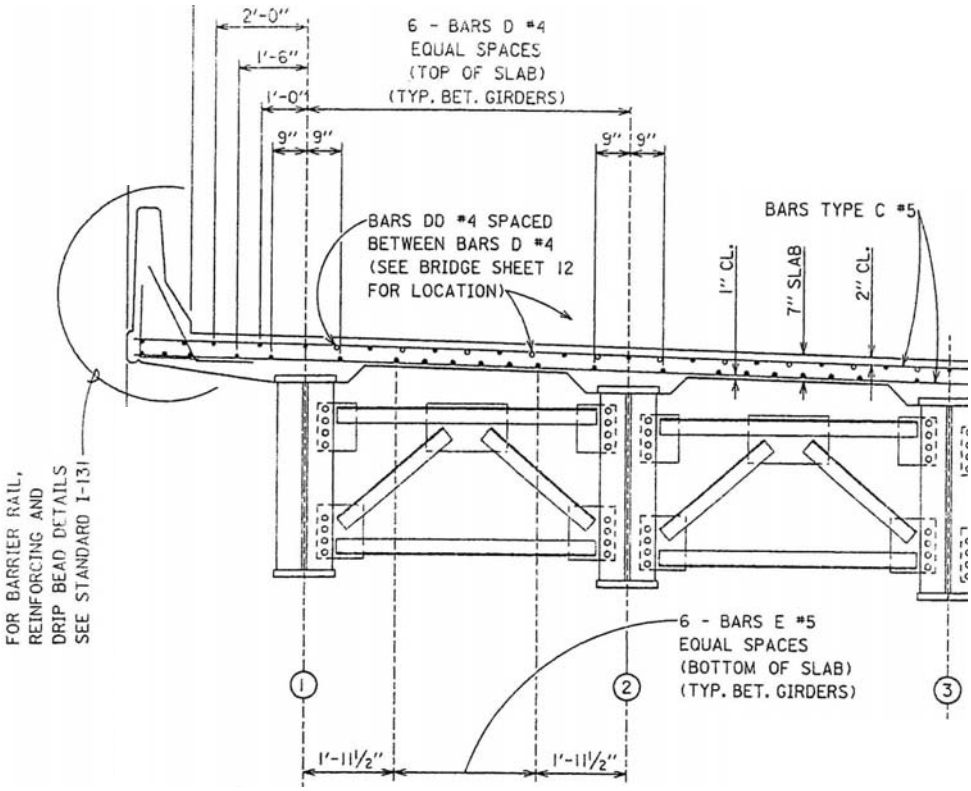

Figure 3-4: Partial section of the bridge at intermediate crossframe location (ALDOT section)

An ALDOT Type AF-1c concrete mixture was used for this bridge deck. The mixture proportions and some key properties of this mixture are presented in Table 3-1. It is important to note that river gravel was used as coarse aggregate.

Table 3-1: Concrete mixture proportions and properties of the US 331 deck

Component	Source	Value
Type I cement content	Siam Cement, Saraburi, Thailand	434 lb/yd^3
Class C fly ash content	Holcim (US) Group, Quinton, AL	186 lb/yd^3
Water content	Local source	275 lb/yd^3
Coarse aggregate content	No. 67 river gravel, Montgomery (Pit #1580)	1,863 lb/yd^3
Fine aggregate content	No. 100 sand, Montgomery (Pit #1580)	1,137 lb/yd^3
Water-reducing admixture	Eucon W-75, Euclid, Cleveland, OH	12 oz/yd^3
Air-entraining admixture	AEA 92, Euclid, Cleveland, OH	2 oz/yd^3
Target slump	-	4 inch
Total air content	-	4 to 6 %
w/cm	-	0.44

The bridge deck was cast in five placements in 2003 as shown in Figure 3-5. First, 80 ft of the end spans were cast on the south side and the north side of the bridge (Pours A and B). Next, an 80-ft portion was cast in the middle of the bridge (Pour C). Finally, the two remaining 54-ft sections above the interior bents were placed (Pours D and E). The girders were unshored during construction.

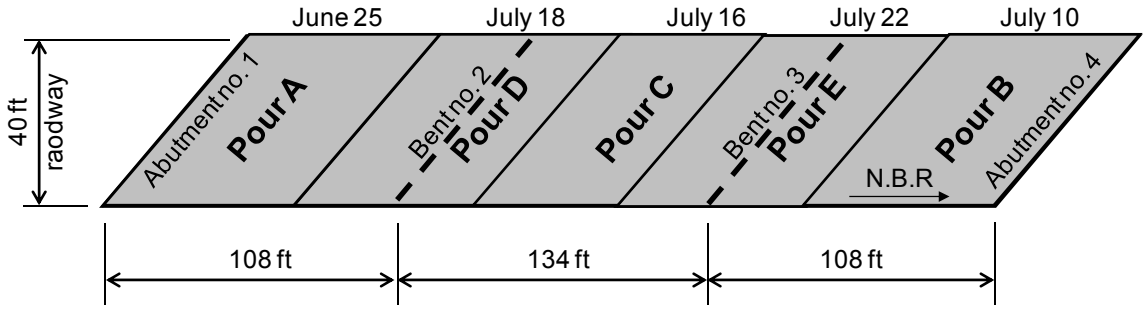

Figure 3-5: Bridge deck placement schedule during the summer of 2003

3.1.2 Cracking of the US 331 Bridge Deck

This bridge deck was placed from June to July 2003; however, since it was part of a roadway still under construction, it was not open to traffic. In the fall of 2004, it was noticed that the surface of this deck exhibited extensive cracking. Some of the cracks in Pour A were repaired with epoxy injection; however, because of the extent of the cracking further investigations were begun.

ALDOT's Materials and Test Bureau investigated the cracking and discovered the presence of various horizontal cracks when coring the bridge deck. The horizontal cracks were generally present at the level of the top reinforcement mat; however, in some cores these cracks also occurred between the top reinforcement mat and the deck surface. Typical cores that contained both vertical and horizontal cracks are shown in Figures 3-6 to 3-8. Some of the apparent severe distress at horizontal crack locations was caused by the coring operation, as the cores had a tendency to spin at the location of a horizontal crack, e.g. bottom of both cores in Figure 3-8. The services of a consultant to perform ground penetrating radar surveys were considered, but were not used due to resource limitations. The extent of the horizontal cracking remains unknown; however, of the 26 cores extracted from the deck, 11 contained horizontal cracks. The number of cores found in each concrete placement section with horizontal cracks was as follows:

- Pour A: two cores,
- Pour D: two cores,
- Pour C: one core,
- Pour E: two cores, and
- Pour B: four cores.

Figure 3-6: Cores from the US 331 deck with vertical and horizontal cracks

Figure 3-7: Cores from the US 331 deck with vertical and horizontal cracks

The nature of the concrete surface at a horizontal crack is shown in Figure 3-9. In this figure, it is clear that bond and aggregate failures occurred at this crack surface.

Figure 3-8: Cores from the US 331 deck with vertical and horizontal cracks

Auburn University and ALDOT staff collectively surveyed the crack locations on the deck by systematically surveying the deck in a 5 x 5 ft grid. The overall result of this surface cracking survey can be seen in Figure 1-2. The location of surface cracks is shown for each of the five concrete placements in Figures 3-10a to 3-10f. A negligible amount of cracks developed parallel to the actual skew of the bridge in Pour D. From this crack survey, it can be concluded that the majority of the surface cracking is perpendicular to the orientation of the steel girders. Note that longitudinal cracks are also present in Pour D; however, these cracks were not as wide as the transverse cracks. Furthermore, there is limited cracking towards the end of the bridge, in the zones where the least longitudinal restraint is provided by the steel girders. It is significant that the cracks are mostly perpendicular to the orientation of the steel girders, as the girders provide

restraint to concrete volume changes; this indicates that this cracking may have been caused by the restraint of concrete volume change effects.

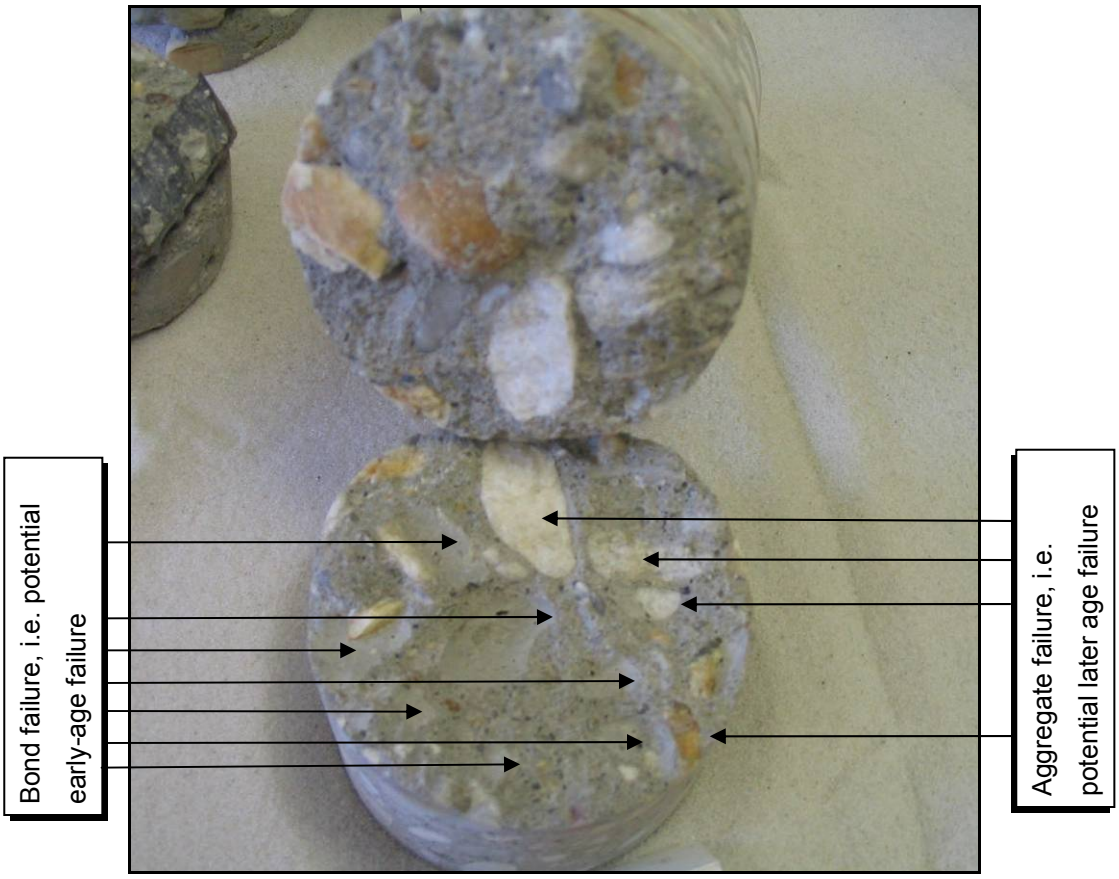

Figure 3-9: Core from deck on US 331 opened along a horizontal crack

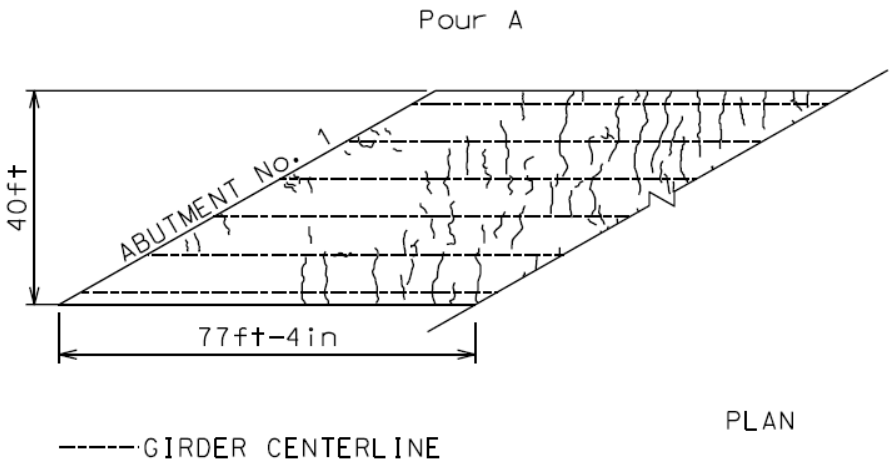

Figure 3-10a: Surveyed crack pattern in Pour A of the US 331 bridge deck

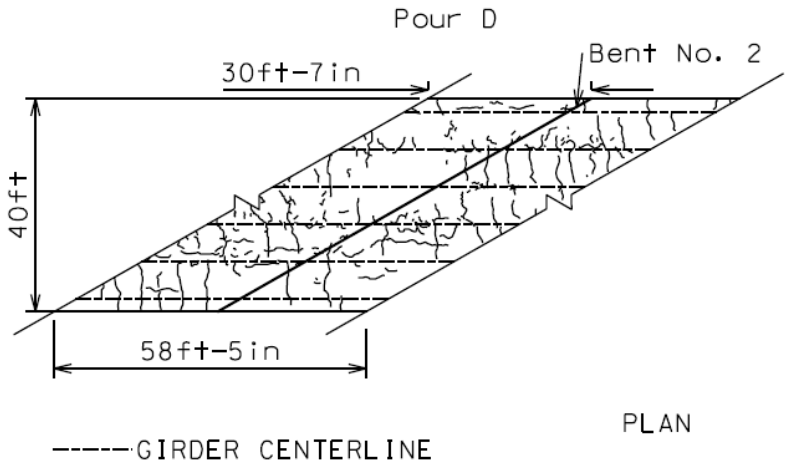

Figure 3-10b: Surveyed crack pattern in Pour D of the US 331 bridge deck

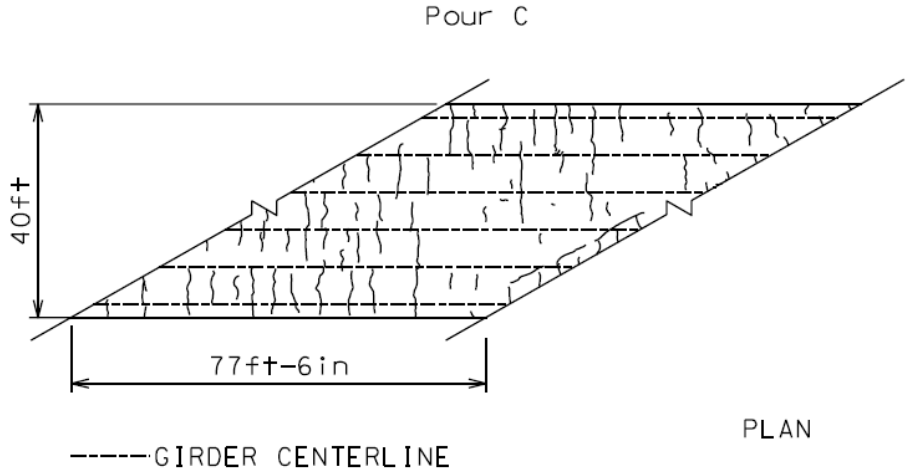

Figure 3-10c: Surveyed crack pattern in Pour C of the US 331 bridge deck

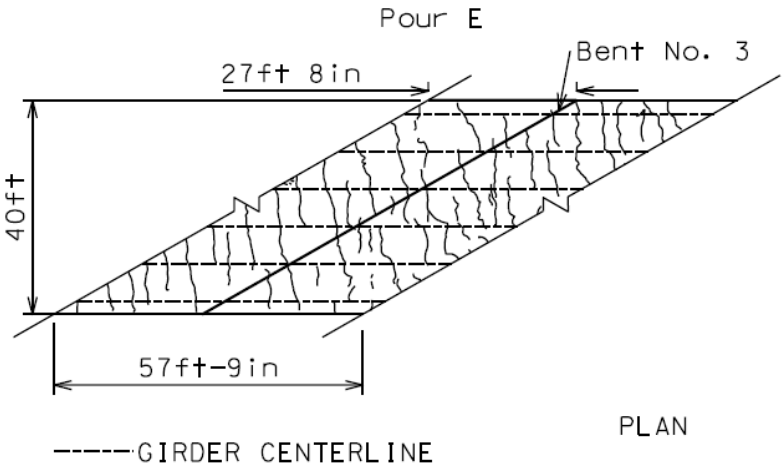

Figure 3-10d: Surveyed crack pattern in Pour E of the US 331 bridge deck

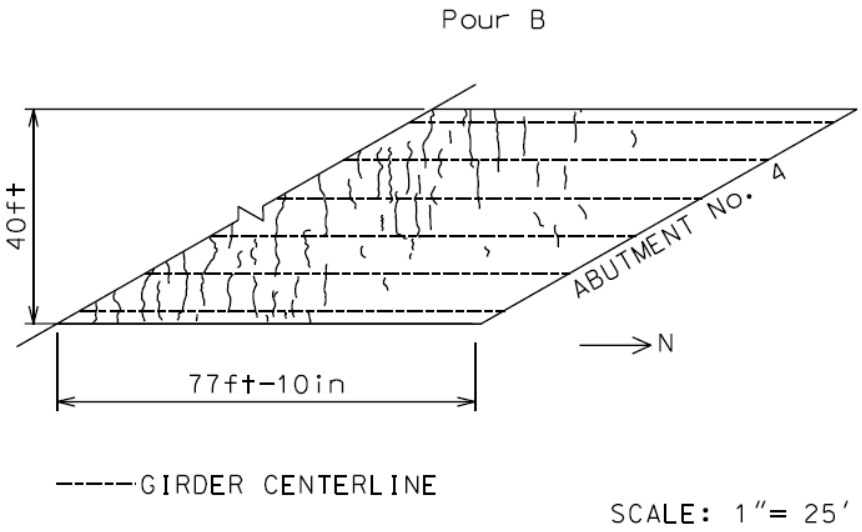

Figure 3-10f: Surveyed crack pattern in Pour B of the US 331 bridge deck

3.1.3 Data Collected for the US 331 Bridge

3.1.3.1 Fresh Concrete Properties

All ready-mixed concrete loads were placed with fresh concrete properties that satisfied ALDOT's specifications for slump and total air content. A summary of the fresh concrete properties and the placement information for each of the five pours is presented in Table 3-2.

Table 3-2: Concrete fresh properties and placement information for each of the five pours

Item	Pour				
	A	**D**	**C**	**E**	**B**
Placement Date	6/25/2003	7/18/2003	7/16/2003	7/22/2003	7/10/2003
Air Temperature Range (°F)	74 to 84	72 to 75	73 to 82	73 to 75	75 to 82
Fresh Conc. Temp. Range (°F)	80 to 83	80	80	80	80
Concrete Volume (yd^3)	90	70	90	70	96
Number of Truck Loads	9	7	9	7	10
Slump range (inch)	3.0 to 4.0	3.5	4.0	3.5 to 4.0	3.5 to 4.0
Total Air Content Range (%)	4.0 to 4.5	4.0 to 4.5	3.5 to 4.0	4.0 to 4.5	3.5 to 4.0

3.1.3.2 Hardened Concrete Properties

3.1.3.2.1 Molded Cylinder Compressive Strengths

The specified design strength for the bridge deck was 4,000 psi at 28 days. ALDOT technicians sampled concrete of some of the ready-mix trucks to make compressive strength cylinders. All sampled concrete satisfied ALDOT's strength requirements, as the average 28-day compressive strength for all loads was 5,150 psi. A summary of the compressive strength results obtained from the molded cylinders for each of the five pours is shown in Table 3-3.

Table 3-3: Concrete compressive strength from molded cylinders for each of the five pours

Item	Pour				
	A	D	C	E	B
Placement Date	6/25/2003	7/18/2003	7/16/2003	7/22/2003	7/10/2003
Average Comp. Strength (psi)	4,930	5,340	5,470	5,170	4,830

3.1.3.2.2 Compressive Strengths of Cores

In November 2004, three 3-in. diameter cores were recovered from each pour by ALDOT's Materials and Test personnel. The strength of all individual cores, except one, exceeded the specified design strength of 4,000 psi. The one core (P3-1) that fell below 4,000 psi came from the center of Pour C; however, two other cores within 26 ft from this core in Pour C produced strengths of 5,070 psi and 5,400 psi. The in-place strength of Pour C's concrete was thus deemed acceptable. The average compressive strength (f_c) of the 3-in. diameter cores sampled in November 2004 was 5,050 psi. A summary of the compressive strength results obtained from the 3-in. diameter cores for each of the five pours is shown in Table 3-4.

Table 3-4: Concrete core compressive strength for each of the five pours

Item	Pour				
	A	D	C	E	B
Placement Date	6/25/2003	7/18/2003	7/16/2003	7/22/2003	7/10/2003
Minimum Core f_c (psi)	4,370	4,770	3,340	5,200	4,060
Average Core f_c (psi)	4,610	5,850	4,600	5,730	4,480

In December 2004, additional 4-in. diameter cores were recovered from each pour by ALDOT's Materials and Test personnel. The strength of all individual cores exceeded the specified design strength of 4,000 psi. The average compressive strength (f_c) of the 4-in. diameter cores sampled in December 2004 was 6,095 psi.

3.1.3.2.3 Modulus of Elasticity of Cores

The 4-in. diameter cores that were recovered in December 2004 were also tested in accordance with ASTM C 469 to determine the concrete's modulus of elasticity. The average compressive strength (f_c) of the 4-in. diameter cores sampled in December 2004 was 4,500 ksi. The specified design strength for the bridge deck was 4,000 psi. Based on the commonly used ACI 318 relationship, the design modulus of elasticity for the concrete was expected to be approximately $57\sqrt{4{,}000}/1000$ = 3,600 ksi. If the ACI 318 relationship is used with the in-place strength of 6,095 psi, the estimated in-place modulus of elasticity is approximately $57\sqrt{6{,}095}/1000$ = 4,450 ksi, which is close to the measured value of 4,500 ksi. The in-place modulus of elasticity is relatively high as it is 24% greater than the design value obtained for a 4,000-psi concrete.

3.1.3.2.4 Splitting Tensile Strength of Cores

The ALDOT inspector's diary did not clearly document the curing method used by the contractor. Bażant and Najjar (1972) presented a fourth-order relationship to define the effect of relative humidity on the strength development. The relationship proposed by Bażant and Najjar (1972) indicates that at a relative humidity of 90% and 80% the concrete strength would be 76% and 16%, respectively when compared to concrete cured at a 100% relative humidity condition. If inadequate curing was applied to the US 331 deck, it was hypothesized that a reduced splitting tensile strength would have been present at the top of the deck as compared to the bottom of the deck. This hypothesis is schematically illustrated in Figure 3-11.

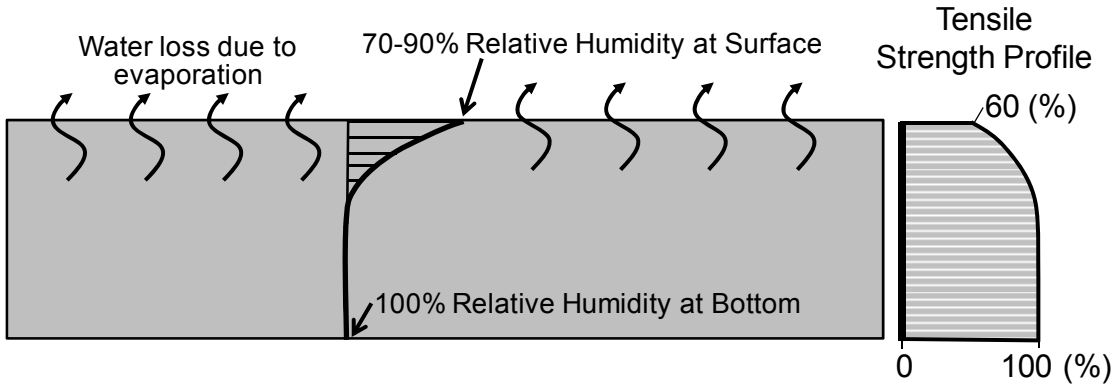

Figure 3-11: Hypothesized impact of inadequate curing on the tensile strength profile

Additional 4-in. diameter cores were recovered in December 2004 to evaluate the hypothesis shown in Figure 3-10. Ground penetrating radar equipment was used to avoid coring through reinforcement. Two groups of nine cores were recovered from both Pours C and D. An example of a group of nine core holes is shown in Figure 3-12. From a group of nine cores, at least 3-in.-thick disks were recovered at the top, middle, and bottom of at least three cores as

shown in Figure 3-12. These 3-in. thick disks were tested in accordance with ASTM C 496 to determine their splitting tensile strength. Because of the deck thickness, some top portions of a core also allowed a bottom portion to be tested; however, only one center portion could be tested from a core. Fifty-eight tests were performed and an average splitting tensile strength of 600 psi was obtained. Based on ACI 207.1R (1996) the relationship between the compressive strength and the tensile strength is as shown in Equation 3-1. The average compressive strength of the 4-in. diameter cores were previously reported to be 6,095 psi. The estimated splitting tensile strength with this compressive strength is 570 psi, which is reasonably similar to the average measured splitting tensile strength. The measured level of splitting tensile strength also indicates that the bond between the aggregates and the paste was as anticipated for most concretes made with this compressive strength.

$$f_{st} = 1.7 \cdot (f_c)^{0.67} \qquad \text{Equation 3-1}$$

where, f_{st} = splitting tensile strength (psi).

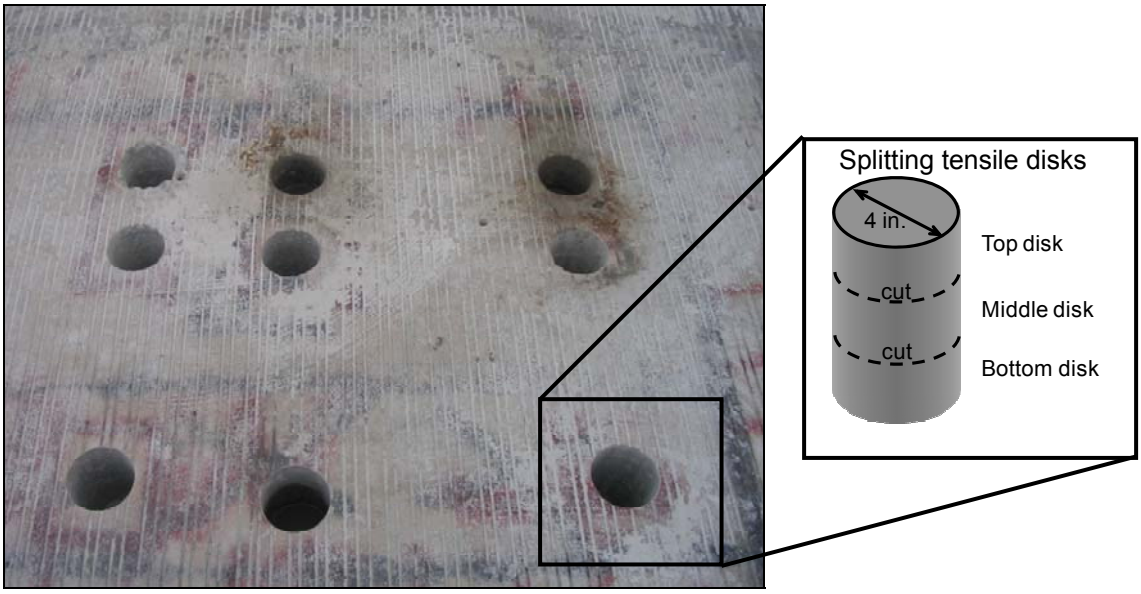

Figure 3-12: Group of nine cores removed for splitting tensile testing

The cumulative distribution of splitting tensile strength at the top, middle, and bottom of the deck is shown in Figure 3-13. The distribution of tensile strengths at the top, middle, and bottom of the deck are very similar. The average strength at the top of the deck is slightly greater than at any of the other locations. The data reveals no apparent loss of splitting tensile strength at the top of the deck, and the average measured splitting tensile strength exceeds the value estimated from the average in-place compressive strength obtained. These results indicate that the cracking on the US 331 bridge deck is probably not attributable to inadequate curing.

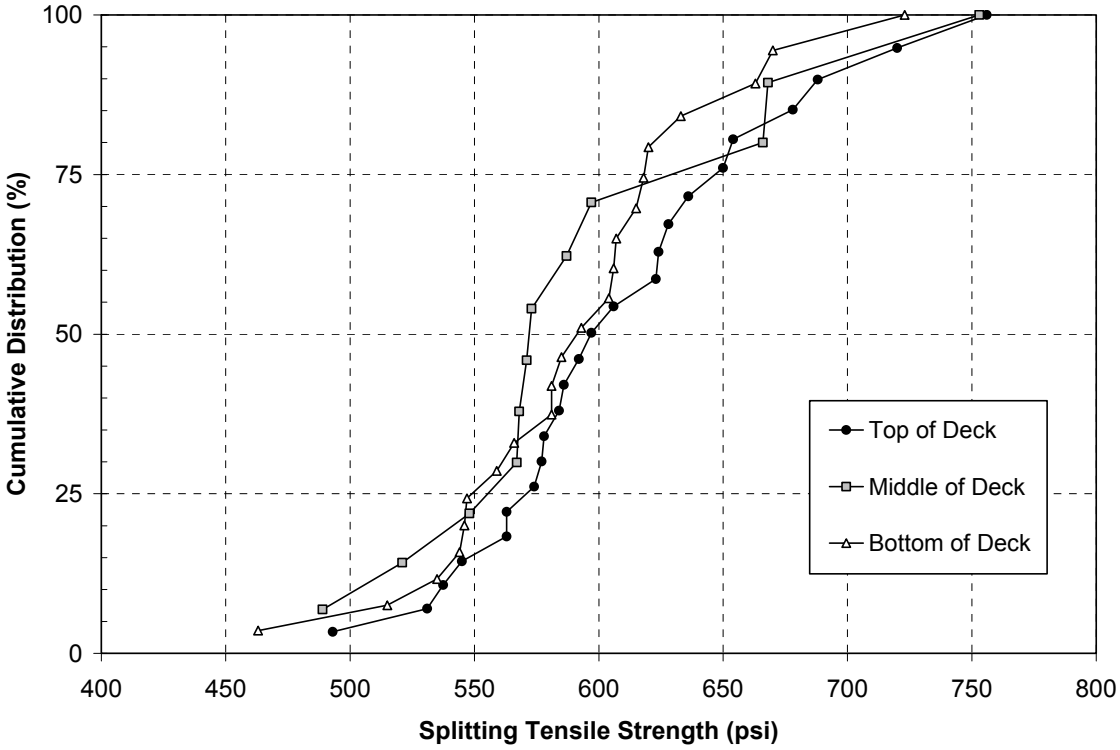

Figure 3-13: Splitting tensile strength distribution of Pour C and D of the US 331 deck

3.1.3.2.5 Concrete Coefficient of Thermal Expansion

Three additional 4-in. diameter cores were recovered from the deck and sent to FHWA's Turner-Fairbank Highway Research Center in McLean, Virginia. The coefficient of thermal expansion (CTE) of the cores was determined in accordance with AASHTO TP 60 (2004) to be 6.83 x 10^{-6} /°F. For reference, Neville and Brooks (1987) report CTE concrete values of 6.8 to 7.3 x 10^{-6} /°F for concrete made with gravel, 5.6 to 6.5 x 10^{-6} /°F for concrete made with sandstone, and 3.4 to 4.1 x 10^{-6} /°F for concrete made with limestone. The CTE obtained from the US 331 bridge is thus typical for concrete made with river gravel; however, it should be noted that this CTE is high as compared to concretes made with limestone.

3.1.3.3 Petrographic Results

A petrographic evaluation was performed on three 3-in. diameter core samples by MACTEC Engineering and Consulting from Atlanta, Georgia. The concrete appeared normal and the most significant statements from this report include the following (Jenkins and Lane 2004):

> "The paste to aggregate bond was poor with mostly pull out around the aggregate when fractured."
>
> "The aggregates were evenly distributed in the concrete. There were no indications of adverse cement aggregate reactions in the concrete. The concrete was well

consolidated and contained approximately 2 percent air. The porosity of the concrete was higher near the top surface than deeper in the concrete. This may be due to drying of the concrete surface and incomplete hydration of the cement near the top of the slab."

3.1.3.4 Deck Thickness and Cover to Reinforcing Bars

The reinforced concrete deck was designed to have a thickness of 7 inches and a cover of 2.0 in. and 1.0 in. at the top and bottom of the deck, respectively, as shown in Figure 3-4. Ground penetrating radar (GPR) was used to determine the as-built average deck thickness and the location of the steel reinforcement. The GPR results were calibrated to the measured deck thickness and reinforcement mat locations visible at open core holes. The GPR results indicated that the average deck thickness between the steel girders was 8.25 in., the average top cover was 3.25 in., and the average bottom cover was 1.0 in. The deck thickness and the top cover depth thus exceeded the design values by 1.25 in.

3.2 DISCUSSION OF CRACKING MECHANISMS FOR THE US 331 BRIDGE DECK

Very limited literature acknowledges the presence of horizontal cracks in bridge decks. Previous research findings were consulted to develop a list of all mechanisms that could have contributed to this type of cracking. Based on the data available, the following mechanisms are all believed to be *unlikely* causes for the severe cracking observed on the US 331 bridge:

- Poor concrete quality—Poor quality concrete was not used in the bridge, which is evident from the quality control data presented in Section 3.1.3 and the core strengths. The concrete satisfied all ALDOT's standard slump, total air content, and compressive strength requirements. Core results revealed an average in-place concrete compressive strength of 6,050 psi and splitting tensile strength of 600 psi, which indicates that concrete with sufficient strength was constructed.
- Excessive reinforcement cover—Although the cover to the top reinforcement was 3.25 in. instead of 2.0 in. it is unlikely that this could have contributed to the severe cracking seen in the bridge. Dakhil et al. (1975) concluded that the cracking tendency should decrease with an increase in cover. NCHRP Report 380 (Krauss and Rogalla 1996) recommended a cover from 1.5 in. to 3.0 in., which is very similar to the as-built condition of the deck.
- Inappropriate deck construction sequence—The deck construction sequence is in accordance with the optimal sequence recommended by Issa (1991) for bridges with a continuous reinforced concrete deck. Based on Issa's recommendation and the fact ALDOT routinely uses this construction sequence without problems, the

deck construction sequence used for this deck should not have caused this type of cracking.

- Inadequate curing—The type of cracking could have been cause by inadequate curing as this will increase drying shrinkage, reduce the strength, and increase the permeability of the surface concrete. Core test results did not reveal a reduction in splitting tensile strength at the top of the deck relative to the middle or bottom regions. This level of splitting tensile strength also indicates that the bond between the aggregates and the paste was as anticipated for most concretes made with this compressive strength. These results indicate that the cracking is probably not attributable to inadequate curing.
- Plastic shrinkage cracking—The type of cracking encountered on the US 331 bridge deck is also not typical of plastic shrinkage cracking as the cracks were through the deck and not just limited to a depth of a few inches.
- Overloading and excessive vibration—It is unlikely that the observed crack pattern was caused by overloading at early ages or vibrations due to the passing of a train underneath the bridge. Any overloading of the deck itself would mainly produce cracking parallel to the girders, which was not observed. Any localized overloading of the girders would produce transverse cracks that are concentrated in the region where the maximum negative moments occur (i.e. over the girder support), which was not observed.
- Excessive bond stresses—High bond stresses around the reinforcement probably did not lead to the observed cracking as the reinforcing bars were adequately spaced and cracking was not limited to locations of maximum steel stress.
- Lack of concrete durability—The observed cracking was not caused by concrete durability mechanisms such as alkali-silica reaction, sulfate attack, or the corrosion of the steel because cracking was observed within a year of construction and there were no indications of products produced by known concrete deterioration mechanisms. Results from the petrographic evaluation (Jenkins and Lane 2004) concluded that there “were no indications of adverse cement aggregate reactions in the concrete”.

In the remainder of this section the more *likely* causes of cracking will be discussed and reviewed based on the data collected for the US 331 bridge.

3.2.1 Likely Causes of Cracking

3.2.1.1 Cracking Due to Thermal and Moisture Gradients

Kim and Won (2004) explain a possible mechanism for the development of horizontal cracking in continuously reinforced concrete (CRC) pavements. The nature of the horizontal cracking found in a CRC pavement in Texas is shown in Figure 3-14. Some similarities between the cores obtained from the bridge on US 331 and the CRC pavement from Texas are evident. The pavements in Texas also revealed that the horizontal cracks occurred around the coarse aggregate, which is an indication of early-age cracking. The crack surfaces for one of the horizontal cracks in the bridge on US 331 are shown in Figure 3-9. The majority of the cracks occurred around (rather than through) the aggregates, which may be an indication that the horizontal cracks could be due to early-age mechanisms. Even if the horizontal cracks were not caused at an early age the residual stresses induced by large thermal and drying shrinkage gradients may contribute to cracking at a later age.

Figure 3-14: Core from CRC pavement in Texas with vertical and horizontal cracks (*Courtesy of Dr. Moon Won*)

Kim and Won (2004) describe a mechanism where horizontal cracking is caused by excessive early-age temperature variations that lead to large shear and normal stresses at the reinforcement location in highly crack-prone concretes that tend to have a high CTE and high modulus of elasticity. Kim and Won (2004) conclude that the occurrence of horizontal cracking can be minimized by the following means:

- Not placing concrete when the daily temperature differential is significantly large,

- Effectively curing the concrete to avoid high early-age drying shrinkage, and
- Selecting a coarse aggregate type to avoid a high concrete thermal expansion coefficient and a high elastic modulus of concrete.

Based on the data collected for the US 331 it was found that the deck was constructed with a high coefficient of thermal expansion of 6.83 x 10^{-6} /°F and a high modulus of elasticity of 4,500 ksi. The bridge was constructed during the summer months, which would produce the highest early-age temperatures and thus the greatest thermal stresses as outlined in Section 2.4.1. The bridge deck is also supported by steel girders and is continuous over three spans, which is a condition that generates a high degree of restraint to any volume change effects. Krauss and Rogalla (1996) conclude in NCHRP Report 380 that "continuous-span structures are more susceptible to cracking than simple-span structures," and that "girder restraint and studs cause significant stresses." The majority of the surface cracking on the US 331 bridge deck is perpendicular to the orientation of the steel girders, which supports the conclusion that these cracks are related to the restraint provided by the steel girders. It is thus clear that the characteristics of the concrete mixture used for the bridge deck did not conform to most of the criteria highlighted by Kim and Won (2004) to minimize the likely formation of horizontal cracks.

The contribution of nonlinear temperature and drying shrinkage stress distributions to produce horizontal cracking is schematically shown in Figure 3-15. Significant stresses develop when a concrete with a high coefficient of thermal expansion and high modulus of elasticity is subjected to large temperature gradients. Related to these variables, Krauss and Rogalla (1996) conclude in NCHRP Report 380 that "Thermal stresses and transverse cracking can be reduced by using concretes with lower coefficients of thermal expansion." Krauss and Rogalla (1996) further conclude that "the concrete modulus of elasticity, adjusted for creep, affects both thermal and shrinkage stresses more than any other physical concrete property."

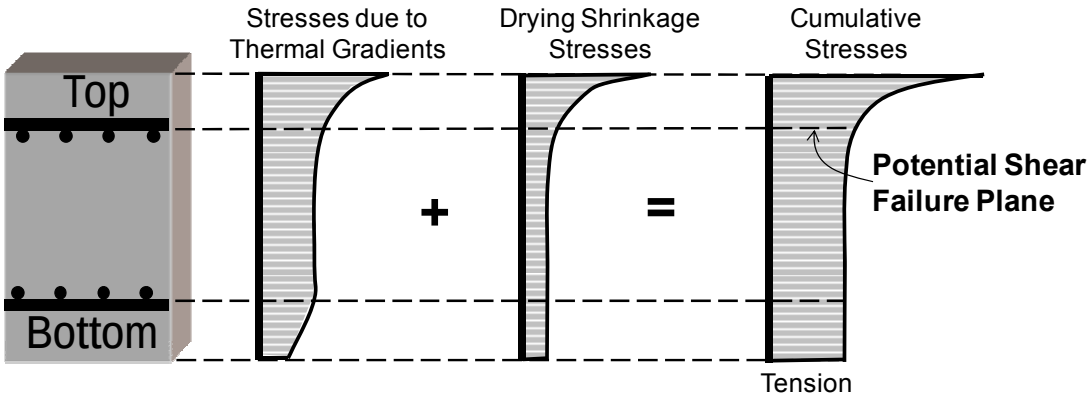

Figure 3-15: Contribution of nonlinear temperature and drying shrinkage stresses to produce horizontal cracking

During the summer months, the combination of heat of hydration and solar radiation effects will cause a peak in temperature rise during the first day, as shown in Figure 3-16. The data in Figure 3-16 were collected during the construction of the South College Street Bridge crossing over I-85 in Auburn, Alabama placed on June 14, 2005. The bridge deck was constructed on stay-in-place metal forms and had a deck thickness of 9.5 in. at the location of the temperature sensors. Additional temperature sensors, as shown in Figure 3-17, were used to determine the temperature gradients at early ages for the South College Street Bridge. The measured results are shown in Figure 3-18. The time of final setting was measured on-site in accordance with ASTM C 403. The temperature profile that corresponds to the equivalent age at which final set occurred in also shown in Figure 3-18. Recall from Section 2.4.1 that the magnitude of the thermal stress is related to the zero-stress temperature, which is elevated during summer construction months due to the combined effects of hydration and ambient conditions. It is clear from the data collected on the South College Street Bridge that temperature differences in excess of 60°F can develop within the first four days after construction. The maximum temperature gradient measured for this bridge was 14 °F. The data from the South College Street Bridge reveal how significant thermal effects can develop in bridge decks.

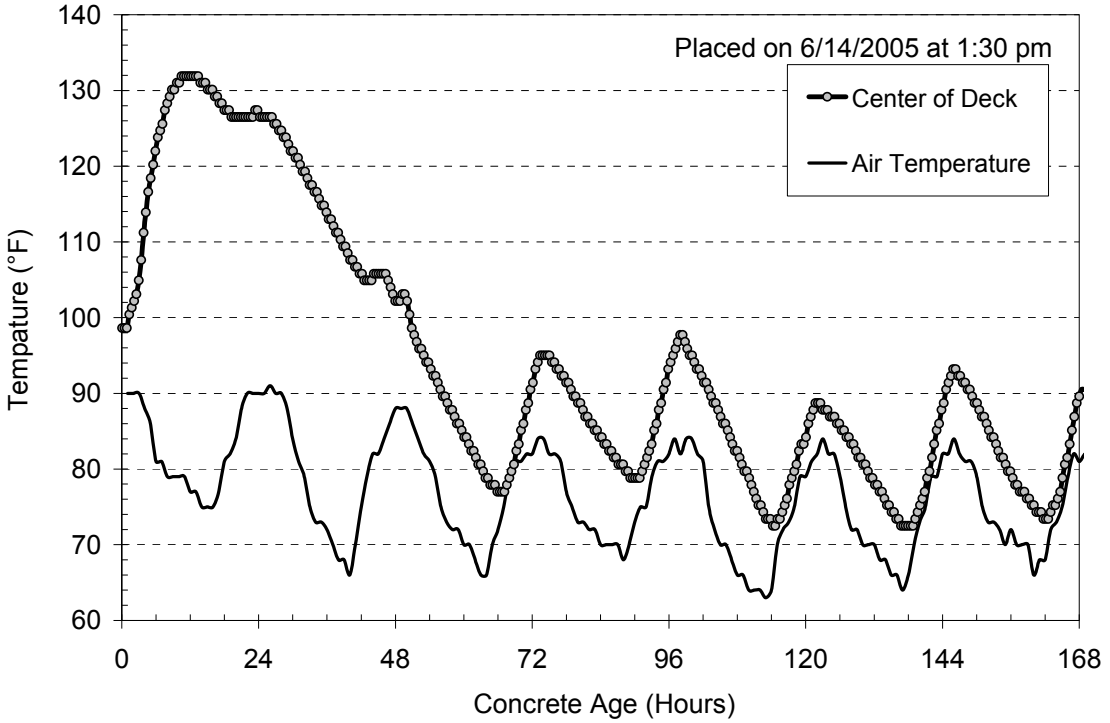

Figure 3-16: Concrete and air temperatures recorded at South College Street Bridge crossing over I-85 built on June 14, 2005

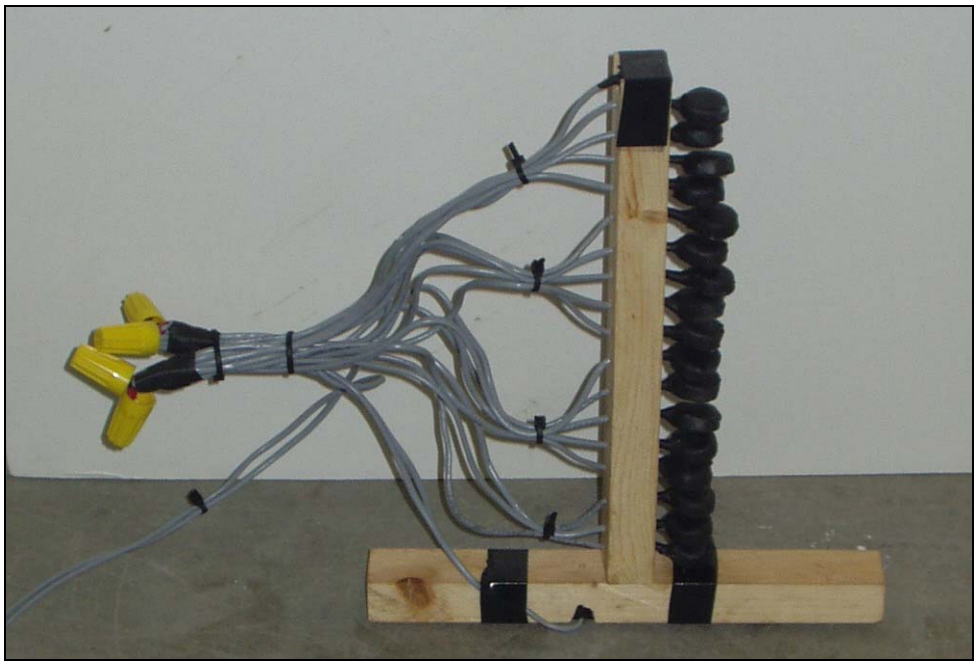

Figure 3-17: Configuration of temperature sensors used to measure the gradients after concrete placement

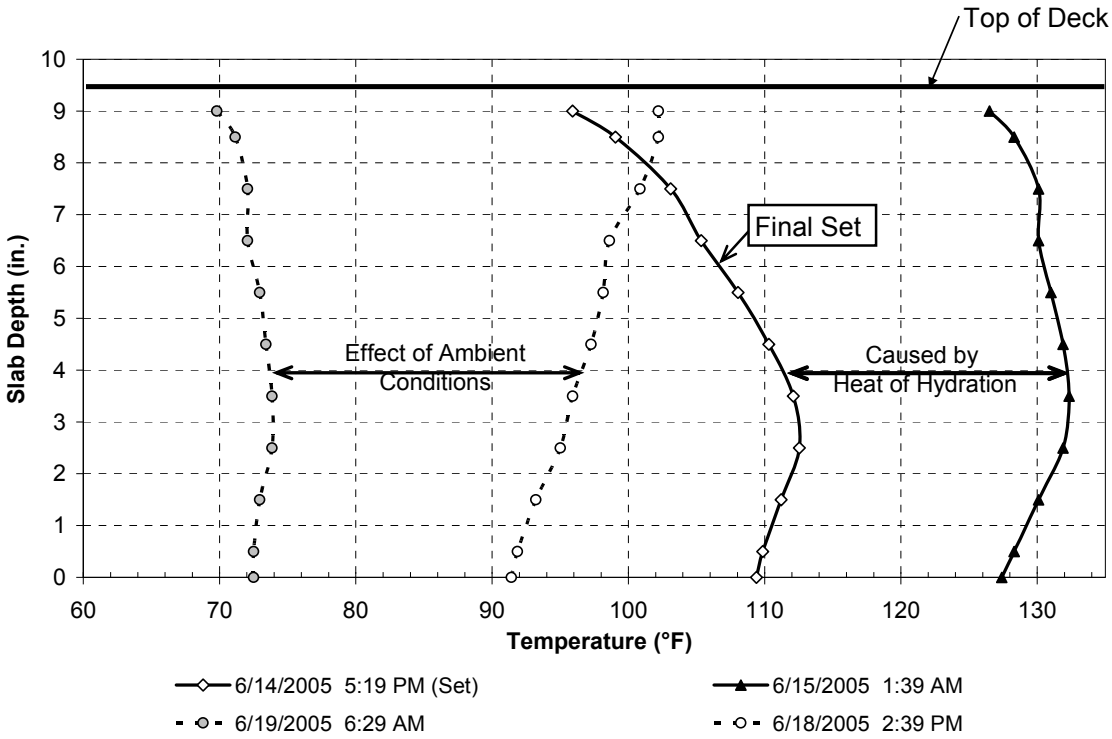

Figure 3-18: Contribution of temperature distributions to produce horizontal cracking

The high coefficient of thermal expansion and high modulus of elasticity of the US 331 bridge may have contributed to it being crack-prone when subjected to significant early-age volume

change effects and a high degree of restraint. Experimental evaluation of the effects of constituent materials on the cracking tendency and early-age behavior of bridge deck concretes made with Alabama materials is described in Chapter 4 of this report. Coefficient of thermal expansion tests will be performed on concretes made with aggregates found in Alabama; this effort is described in Chapter 5. These results will help to provide further evidence to identify the primary cause of the cracking on the US 331 bridge.

3.2.1.2 Effect of Bridge Skew

The US 331 bridge had a skew angle of 61°, which is a significant amount of skew. NCHRP Report 380 (Krauss and Rogalla 1996) concluded that skew "does not significantly affect transverse cracking, but slightly higher stresses occur near the corners." The skew of the bridge may affect the transverse load distribution pattern and it is thus possible that the large skew contributed to the observed distress in this bridge. It is difficult to visualize what effect the skew can have on the distribution of stresses. The effect of various skew angles on the development of stress in the deck was evaluated by finite-element modeling techniques as described in Chapter 6 of this report.

3.2.1.3 Differential Settlement of Bridge Foundation

Differential movement of the bridge foundations could lead to significant deck cracking. The bridge is located south Montgomery in an area were swelling clays are present. No elevations of the bridge were available before the cracking was observed; therefore, no data are available to evaluate this as a potential cause for the observed cracking. Differential settlement of the foundations of this 3-span continuous bridge will tend to cause severe localized cracking at the negative moment regions of the continuous girders. The effect of differential settlement of the bridge foundations was evaluated by finite-element modeling techniques as described in Chapter 6 of this report.

3.3 EXTENT OF HORIZONTAL CRACKING IN OTHER BRIDGE DECKS IN ALABAMA

If the primary failure mechanism involves a cracking-sensitive mixture, large thermal and moisture gradients, and a high degree of restraint in the deck, then this type of cracking may be present in other bridge decks in Alabama. Since the horizontal cracks are not visible on the surface of the deck, it is possible that they are present in other bridges in Alabama, but have gone undetected. The research team worked with ALDOT to identify bridges that may also have horizontal cracking. The criteria used to identify some bridges were as follows:

- continuous bridge deck,
- bridge decks constructed between May and September (warm months), and

- bridge deck mixtures that contain river gravel aggregate (i.e. high modulus of elasticity and coefficient of thermal expansion).

Only a limited number of bridges were identified for the survey. With the assistance of ALDOT personnel, five bridges in Alabama were visited in November and December of 2007. Cores were extracted adjacent to transverse cracks present in the decks in an attempt to find horizontal cracks similar to those found in the US 331 bridge. The five bridge decks discussed below were selected, since they have structural configuration similar to the US 331 bridge. At this stage, it is noteworthy that none of the cores recovered from these decks showed any signs of horizontal cracking.

3.3.1 RS-1402(101): SR 49 over SCL RR in Lineville, Clay County

This bridge deck was visited on November 18, 2007, and a view of this bridge is shown in Figure 3-19. The bridge was built in 1976, has a roadway width of 52 ft, a skew of 39°, and has three spans of 72 ft, 100 ft, and 65 ft. The bridge was built with continuous steel girders. Visual inspection of the concrete revealed that limestone coarse aggregates were used in the bridge deck concrete. The bridge deck was in very good condition with very limited cracking visible on the surface. An example of the type of surface cracking present in the bridge deck is provided in Figure 3-20. Cores were extracted adjacent to transverse cracks; however, no horizontal cracks were present in the cores. The coefficient of thermal expansion of the cores was determined in accordance with AASHTO TP 60 (2004) to be 5.61 x 10^{-6} /°F.

Figure 3-19: View of the bridge deck on SR 49 over SCL RR in Lineville

Figure 3-20: Pictures of the bridge deck on SR 49 over SCL RR in Lineville

3.3.2 APD-237(9): Courtland Bypass over Norfolk Southern Railroad, Lawrence Co.

This bridge deck was visited on November 19, 2007, and a view of this bridge is shown in Figure 3-21. The bridge was built in 1983, has a roadway width of 40 ft, a skew of 49°, and has three spans of 55 ft, 85 ft, and 55 ft. The bridge was built with continuous steel girders. Visual inspection of the concrete revealed that limestone coarse aggregates were used in the bridge deck concrete. Many transverse cracks were visible on the deck, and some of these appeared wide and spalled at the surface. An example of the type of surface cracking present in the bridge deck is provided in Figure 3-22. Cores were extracted adjacent to transverse cracks; however, no horizontal cracks were present in the cores. An inspection of the cores recovered from the cracks also revealed that the transverse cracks were only wide at the surface, as shown in Figure 3-23. The coefficient of thermal expansion of the cores was determined in accordance with AASHTO TP 60 (2004) to be 5.32 x 10^{-6} /°F.

Figure 3-21: View of the bridge deck on the Courtland Bypass over Norfolk Southern RR

Figure 3-22: Picture of the wide surface cracks on the bridge deck on the Courtland Bypass

Figure 3-23: Pictures of the core hole on the bridge deck on the Courtland Bypass

3.3.3 RS-6309(101): SR 216 over L&N RR (Tuscaloosa to Brookwood), Tuscaloosa Co.

This bridge deck was visited on November 20, 2007, and a view of this bridge is shown in Figure 3-24. The bridge was built in 1983, has a roadway width of 44 ft, a skew of 60°, and has three spans of 83.5 ft, 100 ft, and 83.5 ft. The bridge was built with continuous steel girders. Visual inspection of the concrete revealed that river gravel coarse aggregates were used in the bridge deck concrete. The bridge deck was in good condition with some transverse cracks present. An example of the type of surface cracking present in the bridge deck is provided in Figure 3-25. Cores were extracted adjacent to transverse cracks; however, no horizontal cracks were present in the cores. The coefficient of thermal expansion of the cores was determined in accordance with AASHTO TP 60 (2004) to be 7.05 x 10^{-6} /°F.

Figure 3-24: View of the bridge deck on SR 216 over L&N RR

Figure 3-25: Picture of some surface cracks on the bridge deck on SR 216 over L&N RR

3.3.4 BRF-461(7): SR 21 over CSXT Railway at Tunnel Springs, Monroe County

This bridge deck was visited on December 19, 2007, and a view of this bridge is shown in Figure 3-26. The bridge was built in 1988, has a roadway width of 40 ft, a skew of 58°, and has four spans of 66 ft, 88 ft, 83 ft, and 41 ft. The bridge was built with continuous steel girders. Visual inspection of the concrete revealed that river gravel coarse aggregates were used in the bridge deck concrete. Many transverse cracks were visible on the deck that appeared wide at the surface as shown in Figure 3-27. After coring at crack locations, it was determined that these cracks were full-depth, but they do not remain wide for more than ½ in. below the surface as

shown in Figure 3-28. Cores were extracted adjacent to transverse cracks; however, no horizontal cracks were present in the cores. The coefficient of thermal expansion of the cores was determined in accordance with AASHTO TP 60 (2004) to be 6.95 x 10^{-6} /°F.

Figure 3-26: View of the bridge deck on SR 21 over CSXT Railroad at Tunnel Springs

Figure 3-27: Picture of a wide surface crack on the SR 21 bridge deck at Tunnel Springs

Figure 3-28: Picture of the core hole on the bridge deck on SR 21 at Tunnel Springs

3.3.5 RS-4913(102): US 98 over ICG RR West of Wilmer, Mobile County

This bridge deck was visited on December 19, 2007, and a view of this bridge is shown in Figure 3-29. The bridge was built in 1983, has a roadway width of 44 ft, a skew of 39°, and has three spans of 56 ft, 70ft, and 56 ft. The bridge was built with simply-supported prestressed concrete girders. Visual inspection of the concrete revealed that river gravel coarse aggregates were used in the bridge deck concrete. Some wide transverse cracks were present. A picture of the cracking seen on this deck is presented in Figure 3-30. Cores were extracted adjacent to transverse cracks; however, no horizontal cracks were present in the cores. The coefficient of thermal expansion of the cores was determined in accordance with AASHTO TP 60 (2004) to be 7.20 x 10^{-6} /°F.

Figure 3-29: View of the bridge deck on US 98 over ICG RR West of Wilmer

Figure 3-30: Picture of the surface cracking on the US 98 bridge deck

Chapter 4

Cracking Tendency of Bridge Deck Concrete

The high coefficient of thermal expansion and high modulus of elasticity of the US 331 bridge may have contributed to it being crack-prone when subjected to significant early-age volume change effects and a high degree of restraint. Experimental evaluation of the effects of constituent materials on the cracking tendency and early-age behavior of bridge deck concretes made with Alabama materials is evaluated in this chapter. These results will help to provide further evidence to identify the primary cause of the cracking on the US 331 bridge.

4.1 INTRODUCTION

Early-age cracking of concrete bridge decks, typically caused by drying, autogenous, and thermal shrinkage, can have several detrimental effects on long-term behavior and durability. Darwin and Browning (2008) recently reported that "by controlling early age cracking, the amount of cracking at later ages should remain low," and that early-age cracking can significantly increase the rate and amount of chloride penetration (from deicing salts), which may accelerate the rate of the corrosion of embedded reinforcing steel. Transverse cracking occurs in most geographical locations and climates, and in many types of bridge superstructures (Krauss and Ragolla 1996). The work of National Cooperative Highway Research Program (NCHRP) 380 included a survey sent to all U.S. Departments of Transportation (DOTs) and several transportation agencies overseas to evaluate the extent of deck cracking (Krauss and Ragolla 1996). Sixty-two percent of the agencies that responded considered early-age transverse cracking to be problematic. A survey conducted by the Federal Highway Administration (FHWA) found that more than 100,000 bridges suffered from early-age cracking (FHWA 2005).

Concrete cracks when the tensile stress that develops in the structure exceeds its tensile strength. Tensile stresses are induced in bridge decks when concrete volume changes are restrained by the girders. Early-age volume changes occur due to temperature changes, autogenous shrinkage, and drying shrinkage. The amount of stress produced when volume changes are restrained is a function of the modulus of elasticity (or stiffness), stress concentrations, creep, and relaxation of the concrete, which all change based on the maturity of the concrete.

Given the abundance of cracking observed in bridge decks, and the impact of early-age cracking on long-term performance and durability, it is imperative that bridge deck concrete be proportioned and placed to minimize early-age cracking.

4.1.1 Chapter Objectives and Research Methodology

The primary objective of the work documented in this chapter is to evaluate the influence of supplementary cementing materials (SCMs), water-cement ratio (w/c), and placement and curing temperatures on the development of stresses and occurrence of cracking at early ages. Due to the effect of temperature on the development of stresses, cracking in bridge decks is more severe when they are constructed under summer conditions (Krauss and Rogalla 1996). Therefore, the effectiveness of using SCMs under summer placement conditions was determined. This was accomplished by testing five concrete mixtures under various, controlled temperature conditions, while measuring the stress development from concrete placement until onset of cracking.

4.2 EXPERIMENTAL WORK

4.2.1 Experimental Plan and Concrete Mixtures

A control mixture with only portland cement and three mixtures with a SCM used as a partial cement replacement, all having a water-cementitious materials ratio (w/cm) of 0.44, were tested. The mixture proportions are shown in Table 4-1. Since cracking in bridge decks is more severe when placed under summer conditions (Krauss and Rogalla 1996), the influence of using SCMs on early cracking tendency was only evaluated under summer placement conditions. The SCM mixtures had 20, 30, and 50 percent replacement of cement by mass of Class F fly ash, Class C fly ash, and slag cement, respectively. The chemical compositions of the SCMs are presented in Table 4-2. A mixture with only portland cement and a w/c of 0.36 was also tested at two placement temperatures to evaluate the effect of w/c on the cracking tendency. The control mixture was tested at three different temperatures to evaluate the effect of placement and curing temperature on the stress intensity and occurrence of cracking at early ages.

4.2.2 Testing to Quantify the Early-Age Cracking Potential of Concrete

The rigid cracking frame (RCF), shown in Figure 4-1, comprises of two mild steel crossheads and two 4-inch diameter Invar side bars. The test setup was adapted from the configuration developed by Dr. Rupert Springenschmid as documented by RILEM Technical Committee 119 (1998).

Table 4-1: Concrete mixture proportions and properties

Component	Mixture Identification				
	CTRL	**30C**	**20F**	**50S**	**0.36**
Water content, lb/yd	273	273	273	273	250
Type I cement content, lb/yd^3	620	434	496	310	696
Class F fly ash content, lb/yd^3	0	0	124	0	0
Class C fly ash content, lb/yd^3	0	186	0	0	0
Slag cement content, lb/yd^3	0	0	0	310	0
Coarse aggregate content, lb/yd^3	1950	1854	1854	1854	1950
Fine aggregate content, lb/yd^3	1149	1213	1208	1223	1146
Type D admixture dosage,oz/yd^3	37	37	37	37	0
Type F admixture dosage, oz/yd^3	0	0	0	0	35
Target slump, inch	4	4	4	4	4
Total air content, percent	2	2	2	2	2
w/cm	0.44	0.44	0.44	0.44	0.36

Table 4-2: Properties of cementitious materials

Parameter	Portland Cement	Class C Fly Ash	Class F Fly Ash	Slag Cement
Silicon dioxide, SiO_2 (%)	21.1	36.1	51.9	38.6
Aluminum oxide, Al_2O_3 (%)	4.82	18.1	24.6	9.16
Iron oxide, Fe_2O_3 (%)	3.07	6.4	4.04	0.54
Calcium oxide, CaO (%)	63.1	25.2	13.4	35.8
Magnesium oxide, MgO (%)	3.39	5.73	2.1	13.0
Alkalies (Na_2O + 0.658K_2O) (%)	0.56	2.19	0.92	0.57
Sulfur trioxide, SO_3 (%)	2.91	2.3	0.44	0.19
Loss on ignition, LOI (%)	0.85	0.4	0.43	0.48
Tricalcium silicate, C_3S (%)	51.6	--	--	--
Dicalcium silicate, C_2S (%)	21.4	--	--	--
Tricalcium aluminate, C_3A (%)	7.58	--	--	--
Tetracalcium aluminoferrite, C_4AF (%)	9.34	--	--	--
Blaine fineness (m^2/kg)	350	--	--	--
Bulk specific gravity	3.15	2.63	2.34	2.91

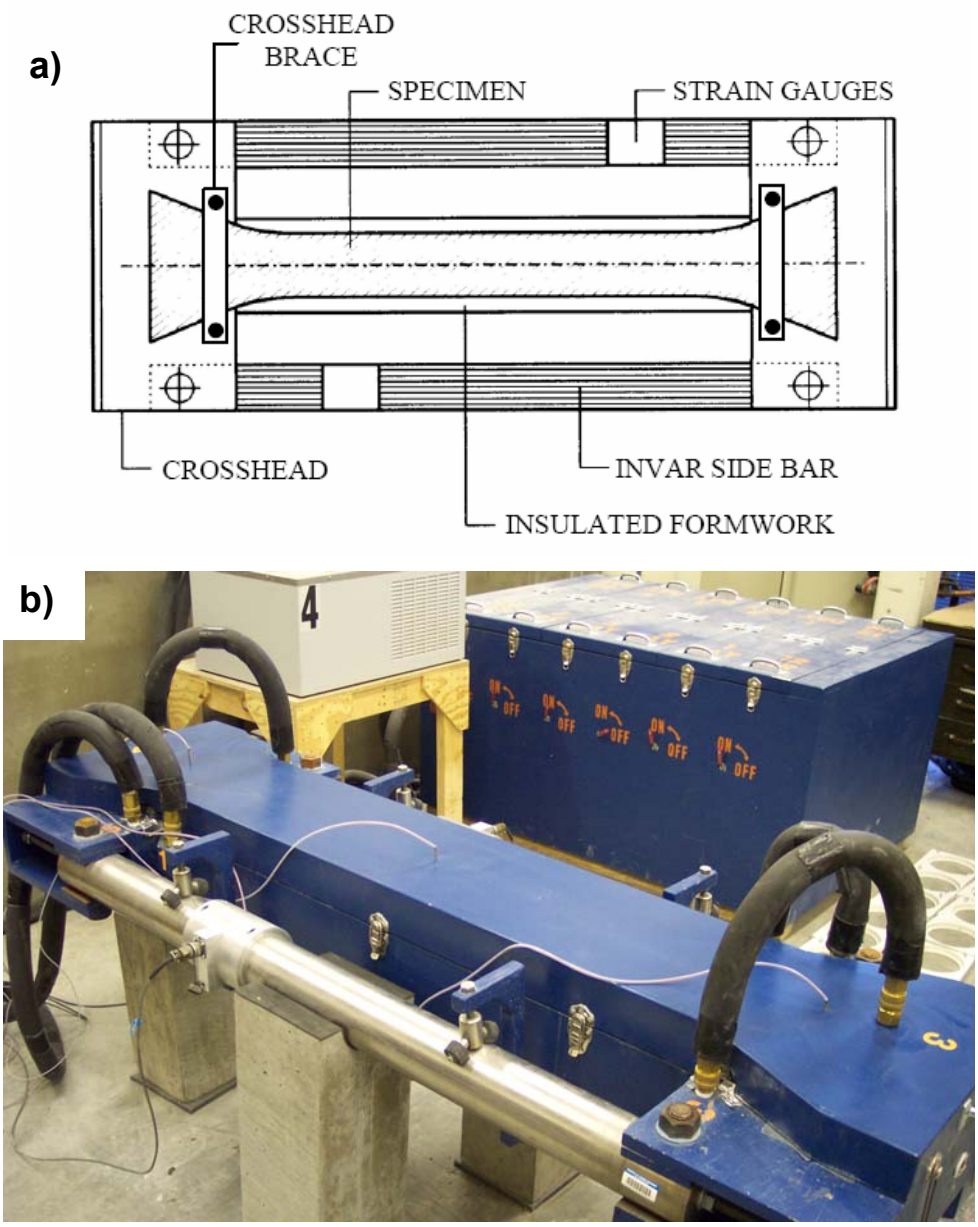

Figure 4-1: Rigid cracking frame test setup: (a) Schematic of test (Mangold 1998) (b) Actual equipment used

Concrete in the fresh state is consolidated in the RCF, and its stress development is measured continuously until cracking occurs. The 6 × 6 × 49 in. concrete specimen is restrained by dovetailed crossheads at each end. The dovetail is gradually tapered to reduce stress concentration and is lined with teeth that grip the concrete. To prevent slippage of the concrete, crosshead braces are used at the end of the crosshead to restrain opening of the crosshead as the concrete goes into tension. The formwork shown includes 0.5-in. diameter copper tubing throughout. A mixture of water and ethylene glycol is circulated from a temperature-controlled water bath through the formwork to control the curing temperature of the concrete sample. The

formwork of the RCF is lined with plastic to reduce friction between the concrete and the form and to seal the concrete specimen on all surfaces. Because of the presence of the sealed plastic layer around the concrete specimen, no moisture is lost and drying shrinkage effects do not develop while the forms are in place on the RCF.

When concrete in the RCF starts to hydrate and volume changes due to temperature and autogenous shrinkage effects develop, the Invar bars provide restraint against movement and stress develops in the concrete. Concrete stress development is monitored using strain gauges mounted on the Invar bars, which are calibrated to the bar forces, which equilibrate the concrete stresses. The concrete stresses generated are a function of the relaxation, coefficient of thermal expansion, modulus of elasticity, temperature history, and maturity of the concrete. The RCF captures the combined effect of all these phenomena under controllable temperature conditions.

Each mixture was placed in the RCF and was cured to a temperature profile developed to reflect the temperature profile of a bridge deck on a given placement date. The ConcreteWorks software program (Poole et al. 2006) was used to predict the concrete temperature history of each specific mixture as it would develop in an 8-in. thick bridge deck. The development of the temperature profile is discussed in a following section.

4.2.3 Testing to Quantify the Early-Age Unrestrained Shrinkage of Concrete

A free shrinkage frame (FSF) similar to the one used by Bjøntegaard (1999) was used to determine the unrestrained uniaxial strain of the concrete specimen and is shown in Figure 4-2. The FSF consists of a thermally insulated box with 0.5-in. diameter copper tubing, and a supporting Invar steel frame. The box serves as the formwork for the freshly placed concrete and the system to match cure the concrete to any temperature profile. A 6 × 6 × 24 in. concrete specimen is cast with two sacrificial steel plates connected with an Invar rod to a linear variable displacement transducer to measure linear expansion and contraction. The fresh concrete is placed on a double layer of plastic with a lubricant in between to minimize the friction, and facilitating free movement of the concrete specimen. When concrete in the FSF is cured to a temperature history that represents that expected in an 8-in. thick bridge deck, the measured strain is caused by thermal and autogenous effects only. Each mixture was tested in the FSF using the same temperature profile used in the RCF.

4.2.4 Concrete Mechanical Properties

A match-curing box was used to cure 6 × 12 in. cylindrical specimens to allow testing of the mechanical properties of the concrete. The match curing box can be seen in the background of Figure 4-1b. All cylinders were cured to the same temperature history as the concrete specimens in the RCF and the FSF. Twenty-four cylinders were made per mixture, and two were tested for modulus of elasticity as per ASTM C 469 and compressive strength as per ASTM C 39, and two

were tested for splitting tensile strength as per ASTM C 496 at concrete ages of ½, 1, 2, 3, 7, and 28 days.

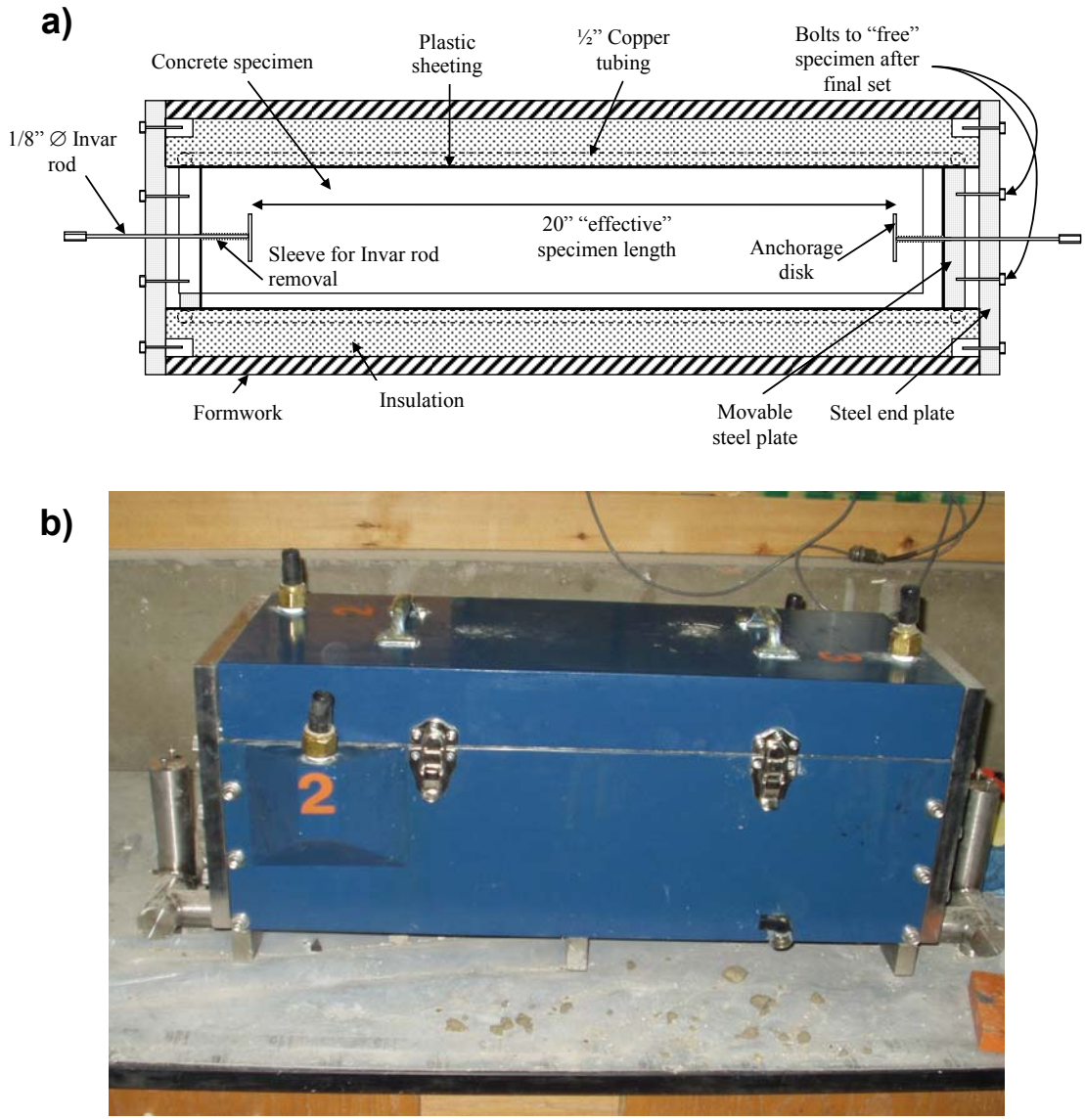

Figure 4-2: Free shrinkage frame test setup: a) Schematic of test (Meadows 2007) b) Actual equipment used

4.2.5 Modeling of Bridge Deck Temperatures

The temperature profile that an in-place concrete element experiences is a function of the geometry of the element, the concrete mixture proportions, the chemical composition of the cementing materials, the hydration parameters of the cementing materials, the placement

temperature, the thermal conductivity of the aggregate, and environmental effects such as ambient temperature, wind speed, and incoming solar radiation.

To assess the effect of placement and curing temperature, the concrete modeling software ConcreteWorks (Poole et al. 2006) was used to determine the temperature profile that an 8-in. thick bridge deck constructed on stay-in-place metal forms would to experience. In the model it is assumed that external curing is provided by a curing blanket with R-value of 2.9 $hr \cdot ft^2$ °F/BTU. Three placement situations were investigated: summer, fall, and winter conditions. Bridge deck temperatures for summer, fall, and winter placements were determined for Montgomery, Alabama on construction dates of August 15, October 15, and January 15, respectively. The average daily temperatures for this location and these summer, fall, and winter placement dates are about 95°F, 73°F, and 50 °F, respectively. Semi-adiabatic calorimetry was used to determine the hydration parameters of each mixture (Schindler and Folliard 2005). Using the hydration parameters, as well as the placement date, city, bridge geometry, aggregate type and thermal conductivity, mixture proportions, placement temperature, wind speed, ambient relative humidity, and percent cloud cover, a temperature profile was generated.

4.2.6 Temperature Conditions and Material Conditioning

The control mixture was tested at each of the three temperature conditions to evaluate the effect of placement and curing temperature on time to initial cracking. When mixtures were tested at a temperature other than fall conditions (73 °F placement temperature), the raw materials were placed in an environmental chamber and conditioned to obtain fresh concrete temperatures of approximately 95 °F and 50°F for summer and winter placement conditions, respectively. As discussed previously, the mixtures with SCM replacements were tested only under summer placement conditions. The no-SCM 0.36 mixture was tested at summer and fall placement conditions.

4.2.7 Materials

4.2.7.1 Cementitious Materials

Type I portland cement, manufactured by Lafarge North America in Calera, Alabama was used in all the concrete mixtures. The result of the chemical analysis and fineness for the cement is shown in Table 4-2. The following SCMs were used:

- Class C fly ash—distributed by Holcim Ltd. (Quinton, Alabama),
- Class F fly ash—distributed by Boral Materials (Cartersville, Alabama), and
- Grade 120 slag cement—distributed by Buzzi Unicem (New Orleans, Louisiana).

The properties of the SCMs as tested by an external lab are shown in Table 4-2. Note that this Class C fly ash is from the same source used during the construction of the US 331 bridge deck.

4.2.7.2 Aggregate

The coarse aggregate for the project was an ASTM C 33 No. 67 gradation, siliceous river gravel. The fine aggregate used throughout the project was siliceous river sand. Both aggregate types were obtained from Martin Marietta Materials' quarry located in Shorter, Alabama.

4.3 RESULTS AND DISCUSSION

The zero-stress time and temperature and the cracking time and temperature for all tests are summarized in Table 4-3. For placement under the same temperature conditions, the later the time to cracking and the lower the cracking temperature, the better the resistance to early-age cracking of a mixture.

Table 4-3: Summary of important values obtained from RCF tests

Mixture	Placement Temperature (Condition)	RCF Test Results			
		Zero Stress		Cracking	
		Time, hrs	Temp., °F	Time, hrs	Temp., °F
CTRL	50 °F (Winter)	20.5	58.2	76.3	51.5
	73 °F (Fall)	12.3	103.2	47.1	71.3
	95 °F (Summer)	11.2	134.3	42.7	88.7
0.36	73 °F (Fall)	16.8	109.2	41.7	76.3
	95 °F (Summer)	14.5	131.4	39.5	92.1
30C	95 °F (Summer)	17.9	117.6	122.5	83.8
20F		13.7	125.9	73.8	83.8
50S		33.6	108.9	173.4	69.3

4.3.1 Influence of Temperature

The temperature profile data and the RCF and FSF results for the control mixture at all three placement conditions are presented in Figure 4-3. Decreasing the placement and curing temperatures delays and decreased the temperature peak shown in Figure 4-3a, which decreased the zero stress temperature and increased the zero stress time as shown in Table 4-3.

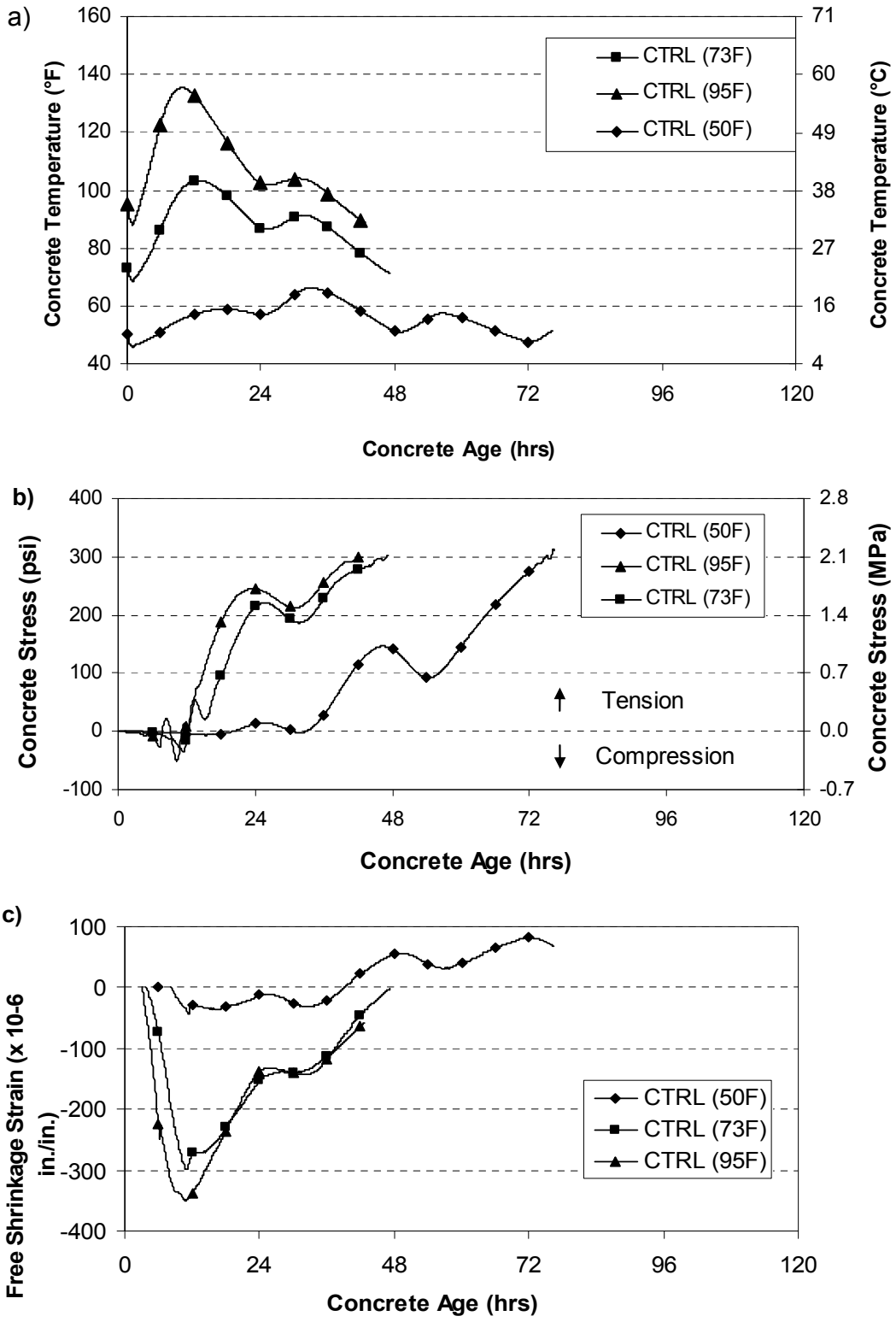

Figure 4-3: Measured results for the control mixture placed under summer, fall and winter placement conditions a) Temperature profiles b) Stresses from RCF, and c) FSF strains

Decreasing the placement and curing temperature reduced stresses and delayed cracking as shown in Figure 4-3b. The free shrinkage data, shown in Figure 4-3c, reveal that a decrease in placement and curing temperature causes a decrease in thermal strain, which in turn leads to reduced stresses. Breitenbücher and Mangold (1994) also found that decreasing the temperature of the fresh concrete significantly increased the time to cracking. These results confirm that the thermal stresses that develop during summer placements are much higher than those that develop during winter placements.

4.3.2 Influence of Fly Ash and Slag Cement

The temperature profile data and the RCF and FSF results for the control mixture and the SCM mixtures for the summer placement condition are presented in Figure 4-4. The splitting tensile strength and modulus of elasticity development for the control and SCM mixtures are shown in Figure 4-5.

Increasing the replacement of cement with an SCM decreased the rate of hydration and maximum temperature reached, as shown in Figure 4-4a. The reduction in rate of hydration delayed the rate of splitting tensile strength and modulus of elasticity development, as shown in Figure 4-5. The reduced rate of temperature development and stiffness development that accompanied the use of SCMs increased the time to zero stress, decreased the zero-stress temperature, and increased the time to cracking show in Table 4-3.

The 30% Class C ash mixture had not cracked at 120 hours. Inspection of Figure 4-4b indicates that this mixture had undergone more than two complete days of approximately identical temperature cycles at that point and was unlikely to crack under continued application of the intended temperature profile. In an effort to determine the cracking temperature and stress, it was artificially cooled at a rate of 1.8 °F/hr to induce cracking, which occurred 2.5 hours later. Similarly, the 50% slag cement mixture did not crack under the summer temperature profile. However, similar artificial cooling of this specimen was unintentionally delayed until 168 hours. It cracked after about 5 hours of artificial cooling. The control mixture and the 20% Class F fly ash mixture each cracked under the effects of the summer placement temperature profile without artificial cooling. Considering that the true cracking times for the 30% Class C ash mixtures and 50% slag cement mixtures would have been even greater than the values reported in Table 4-3, it is evident that the cracking times for the SCM mixtures were significantly greater than the cracking time for the control mixture when placed under summer conditions.

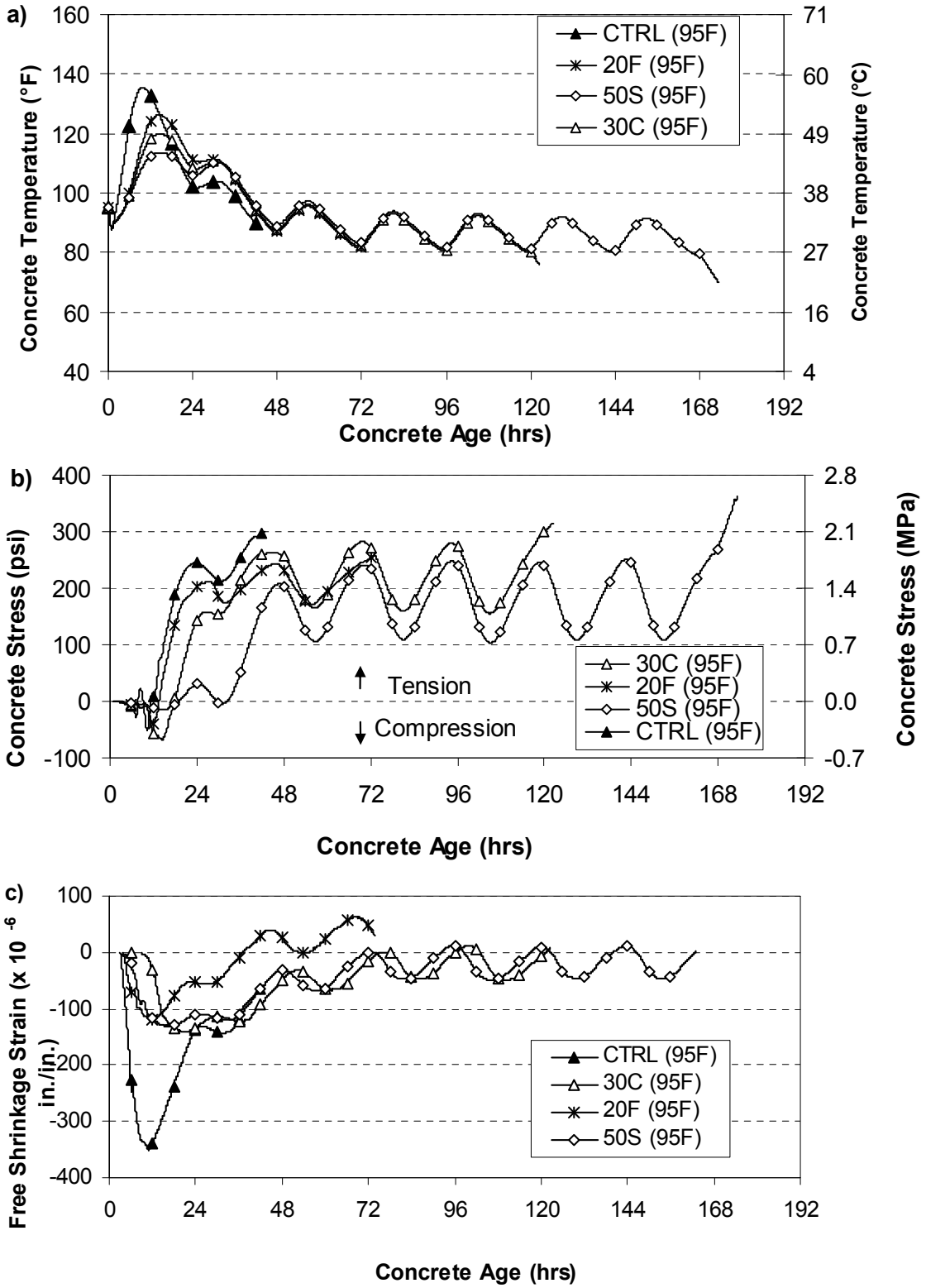

Figure 4-4: Measured results for the control and SCM mixtures placed under summer conditions a) Temperature profiles b) Stresses from RCF, and c) FSF strains

The use of SCMs caused a significant reduction of the free shrinkage in the first 24 hours relative to the control mixture as shown in Figure 4-4c. This reduction in free shrinkage strain and the reduced rate of modulus of elasticity development resulted in a reduced stress development when SCMs were used. The 50% slag cement and 30% Class C fly ash mixtures increased the time of cracking by more than 100 percent over the control mixture placed under summer conditions. Although the 20% Class F fly ash mixture was not as effective in reducing the cracking tendency of the concrete, it too reduced the cracking tendency of the control mixture. These findings are significant the results shown in Figure 4-5a indicate that the use of SCMs reduces early-age splitting tensile strength; however, the combined effect of reduced rate of heat generation and modulus of elasticity development results in an overall improvement in cracking resistance.

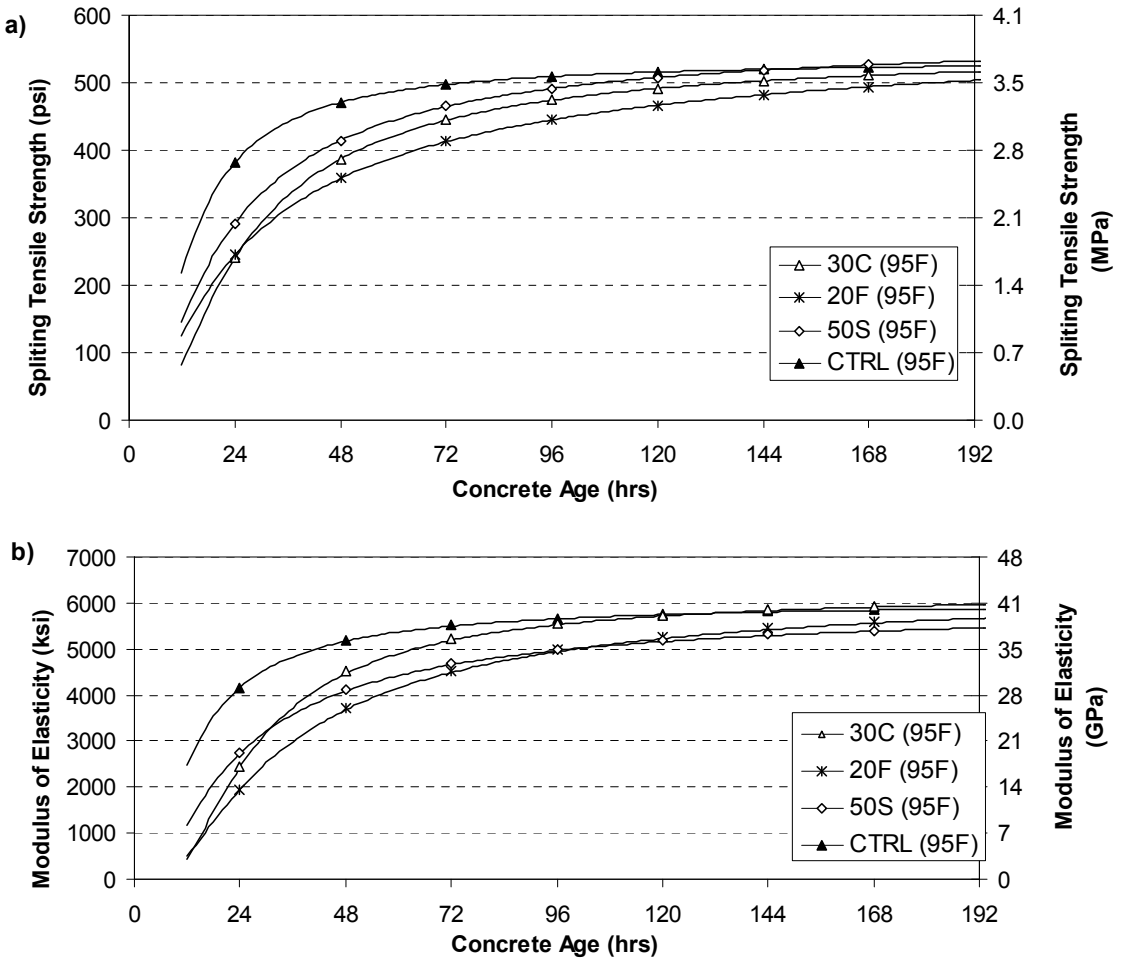

Figure 4-5: Measured results for the control and SCM mixtures a) Splitting tensile strength development, and b) Modulus of elasticity development

Springenschmid and Breitenbücher (1998) found fly ash to reduce the cracking temperature. In the present study, it was found that the use of fly ash or slag cement caused a

reduction in the cracking temperature. In their study, Breitenbücher and Mangold (1998) concluded that slag cement reduces temperature rises and tensile stresses. These findings are also valid for the slag cement mixtures evaluated in this study. From the results of this study, it may be concluded that the use of SCMs under hot weather conditions can substantially reduce the development of tensile stresses due to thermal and autogenous shrinkage effects.

4.3.3 Influence of Water-to-Cement Ratio

The temperature profile data and the RCF and FSF results for the control and *w/c* of 0.36 mixtures placed under summer and fall conditions are presented in Figure 4-6. As shown in Table 4-1, the *w/c* was decreased by increasing the cement content and decreasing the water content to maintain a constant paste volume. The increase in cement caused an increase in peak temperatures as shown in Figure 4-6a. The increased peak temperature decreased the time to cracking.

4.4 CONCLUSIONS

Early-age cracking in bridge decks is a severe problem that may reduce its functional life. Testing of restrained and unrestrained specimens was done under temperature conditions that match those in an 8-in. bridge deck to explore early-age cracking mechanisms of bridge deck concretes. The influence of supplementary cementing materials (SCMs), water-cement ratio (w/c), and placement and curing temperature was evaluated. Five concrete mixtures were made under various controlled temperature conditions, while measuring the stress development from concrete placement until cracking. The results of this study support the following conclusions:

- Higher placement and curing temperatures result in higher thermal stresses. Decreasing the placement and curing temperature can reduce stresses and delay cracking.
- The use of SCMs can be very effective in delaying cracking under summer placement conditions. Increasing the replacement of cement with an SCM decreases the rate of hydration and maximum temperature. The resulting reduction and delay in the development of tensile stresses more than compensates for the slower development of early-age tensile strength associated with cement replacement by SCM. The combined effect of reduced rate of heat generation and modulus of elasticity development results in an overall improvement in cracking resistance.
- The mixtures with 30% Class C Fly ash and the 50% slag cement replacements were most effective in delaying cracking under summer placement conditions, when thermal stresses are most severe.
- Decreasing the w/c while maintaining a constant paste content leads to an increase in cement content, an increase in peak temperature, and a decrease in time to cracking.

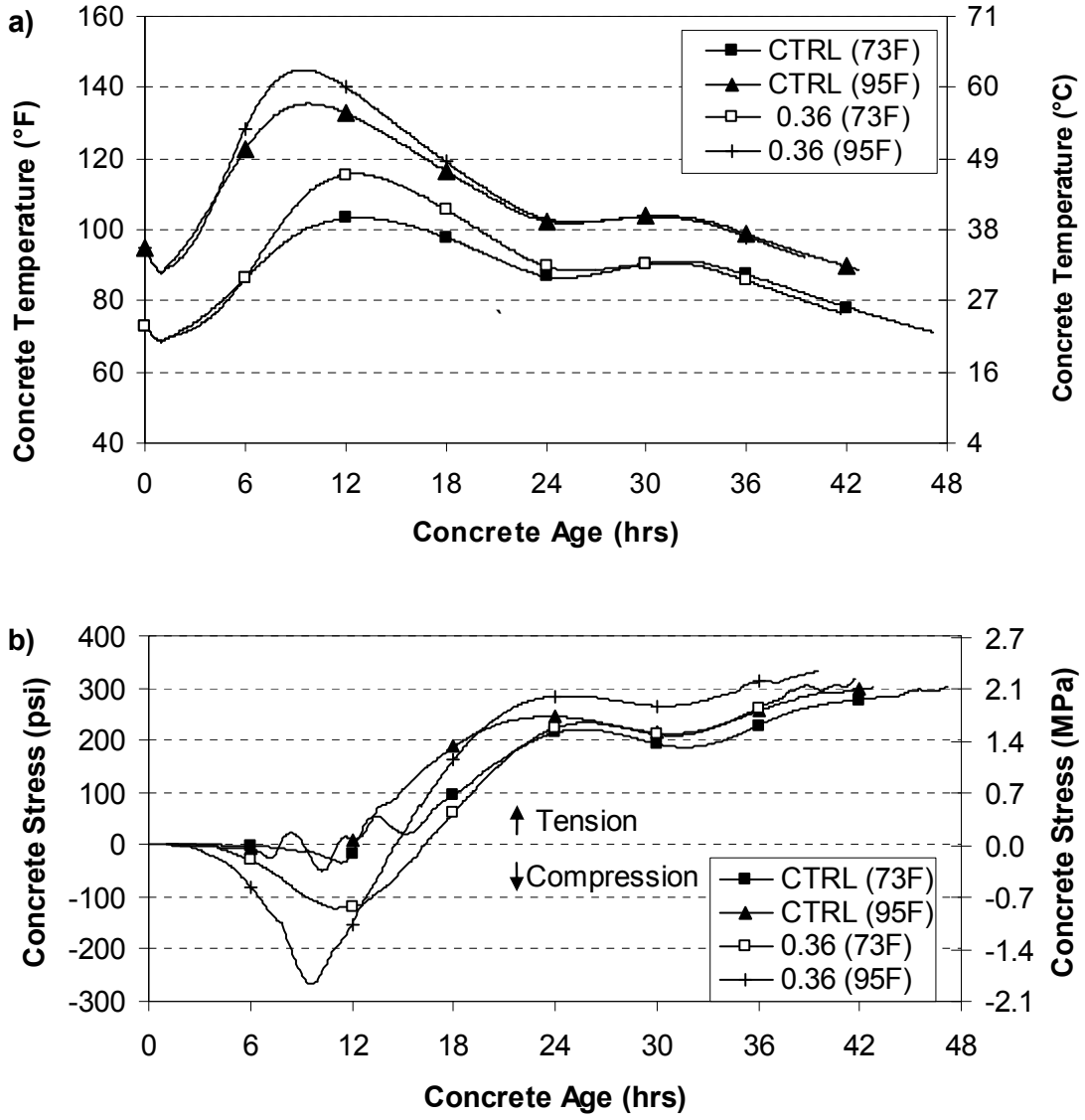

Figure 4-6: Measured results for Control and 0.36 Mixtures placed under summer and fall conditions a) Temperature profiles b) Stresses from RCF

Chapter 5

Coefficient of Thermal Expansion of Bridge Deck Concrete

5.1 INTRODUCTION

In this section, the work performed to determine the coefficient of thermal expansion (CTE) of various concretes made with Alabama materials is discussed. The set configuration used complied with AASHTO TP60 (2004), which was the only available AASHTO or ASTM test available to determine the CTE at the time that this study was completed. The setup used for the AASHTO TP 60 test is shown in Figure 5-1.

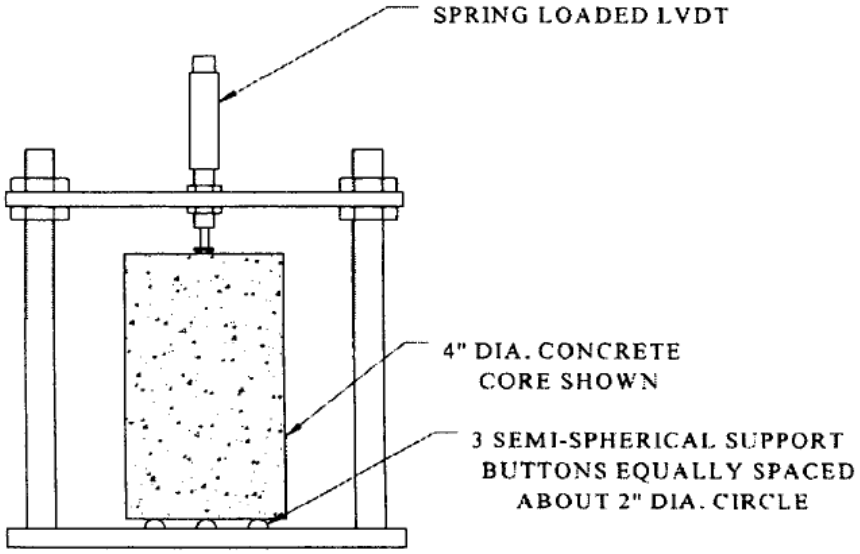

Figure 5-1: Coefficient of thermal expansion test setup (AASHTO TP 60 2004)

5.2 EXPERIMENTAL TESTING PROGRAM

The testing program was developed to evaluate the effects of coarse aggregate type and volume, water-cement ratio, and sand-aggregate ratio on the concrete CTE. Fifty-four concrete samples were tested at the concrete age of 28 days for their CTE. The experimental testing program used is defined in Table 5-1.

Siliceous river gravel, dolomitic limestone, and granite are the coarse aggregates and siliceous sand is the only fine aggregate used. The sand-aggregate ratios used in this study were 0.40, 0.45, and 0.50, with the water-cement ratios being 0.32, 0.38, and 0.44. These ranges of sand-aggregate ratio and water-cement ratio capture those typically used in the Alabama

concrete industry. For each coarse aggregate type, nine concrete mixtures were made and tested. Type I portland cement was used and all samples were tested in the saturated state as required by AASHTO TP 60 (2004).

Table 5-1: Experimental testing program

Coarse Aggregate Type	Fine Aggregate Type	Sand - Aggregate Ratio (By Volume)	Water - Cement Ratio	Concrete Sample Identification
Siliceous River Gravel	**Siliceous Sand**	0.40	0.32	RG-40-32
			0.38	RG-40-38
			0.44	RG-40-44
		0.45	0.32	RG-45-32
			0.38	RG-45-38
			0.44	RG-45-44
		0.50	0.32	RG-50-32
			0.38	RG-50-38
			0.44	RG-50-44
Dolomitic Limestone	**Siliceous Sand**	0.40	0.32	DL-40-32
			0.38	DL-40-38
			0.44	DL-40-44
		0.45	0.32	DL-45-32
			0.38	DL-45-38
			0.44	DL-45-44
		0.50	0.32	DL-50-32
			0.38	DL-50-38
			0.44	DL-50-44
Granite		0.40	0.32	GR-40-32
			0.38	GR-40-38
			0.44	GR-40-44
		0.45	0.32	GR-45-32
			0.38	GR-45-38
			0.44	GR-45-44
		0.50	0.32	GR-50-32
			0.38	GR-50-38
			0.44	GR-50-44

5.3 SAMPLE IDENTIFICATION

The methodology adopted to identify the laboratory-prepared concrete samples is shown below in this section. The sample identification method was developed with consideration of the type of

coarse aggregates used, the sand-aggregate ratio, and the water-cement ratio. The concrete sample identification for all the mixtures tested as part of this study is shown in Table 5-1.

Coarse Aggregate Type	**Sand-Aggregate Ratio**	**Water-Cement Ratio**
RG	**40**	**32**
DL	**45**	**38**
GR	**50**	**44**

Identification Code:

Coarse Aggregate Type	**Sand-Aggregate Ratio**	**Water-Cement Ratio**
RG = Siliceous River Gravel	40 = 0.40	32 = 0.32
DL = Dolomitic Limestone	45 = 0.45	38 = 0.38
GR = Granite	50 = 0.50	44 = 0.44

***Example*:**

RG-40-32 = Concrete made with siliceous river gravel, with a sand-aggregate ratio of 0.40, and a water-cement ratio of 0.32.

5.4 COEFFICIENT OF THERMAL EXPANSION EQUIPMENT

The equipment and procedure used for the concrete CTE test in accordance with AASHTO TP 60 (2004) is described in this section. This test method determines the CTE of concrete sample maintained in a saturated condition, by measuring the length change of the sample due to a specified temperature change. The measured length change is corrected for any change in length of the measuring apparatus (previously determined), and the CTE is then calculated by dividing the corrected length change by the temperature change and then the sample length.

5.4.1 Circulator

The Polyscience circulator model 9612 shown in Figure 5-2 was used. It provides precise temperature control of fluids for open- or closed-loop circulation to attached external equipment. This model features a 28-liter reservoir with a maximum fill level of about 1 in. below the top of the reservoir. For optimum cooling efficiency, the fluid level in the reservoir is kept above the coils at all times. All parts exposed to moisture are corrosion-resistant 300-series stainless steel. The operational temperature range is from -13 ºF to 302 ºF with a temperature stability of ± 0.018 ºF. The read out accuracy is ± 0.45 ºF. The circulator has a duplex pump that permits circulation to and from an attached external open bath.

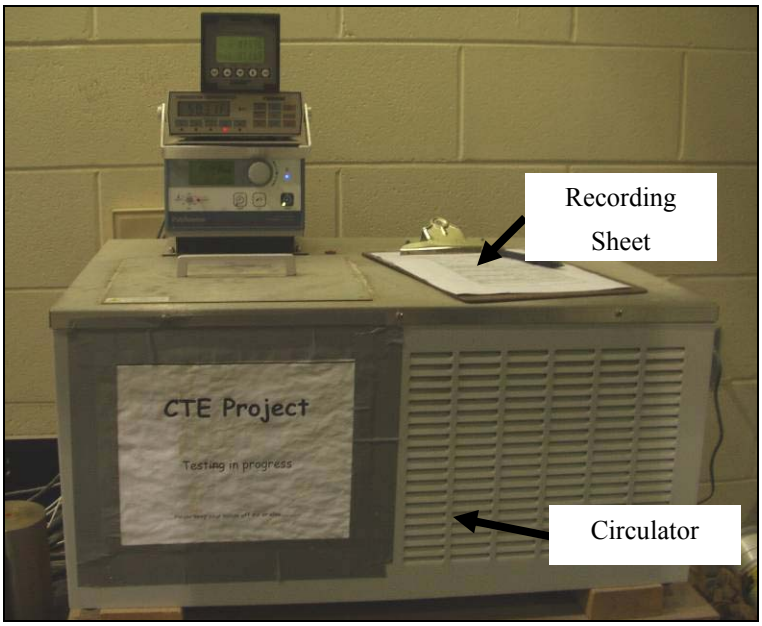

Figure 5-2: Circulator used for temperature control

5.4.2 Linear Variable Differential Transformer Readout

A Schaevitz MP2000 linear variable differential transformer (LVDT) readout was used and it is shown in Figure 5-3. The Schaevitz MP2000, from Measurement Specialties, is an integrated microprocessor-based LVDT readout controller. It is designed to provide excitation and to display the calibrated voltage of alternating current (AC) operated LVDTs. The MP 2000 provides real-time readings of LVDT displacement on a liquefied crystal display (LCD), and it has two output channels, A and B.

5.4.3 Linear Variable Differential Transformer

The LVDT used in this study is shown in Figure 5-4. It uses AC and has a ±0.125 in. (3.18 mm) range. It was manufactured by Measurement Specialties Incorporated and has the model number GCA-121-125. The GCA series gage head is made from stainless steel, which enables it to perform in environments containing moisture, dirt, and other contaminants. Electronic components are hermetically sealed for added protection against hostile conditions. Additionally, these LVDTs were protected from moisture by the use of heat-shrink tubes as shown in Figure 5-4. The other specifications of these LVDTs are shown in Table 5-2. As can be seen, it is rated to perform well in a wide range of temperatures, i.e. -65 °F to 300 °F, and has a linearity of ± 0.25 % of full range output, which makes it suitable for this study. The LVDT requires calibration on its first use. The next section describes the calibration procedure.

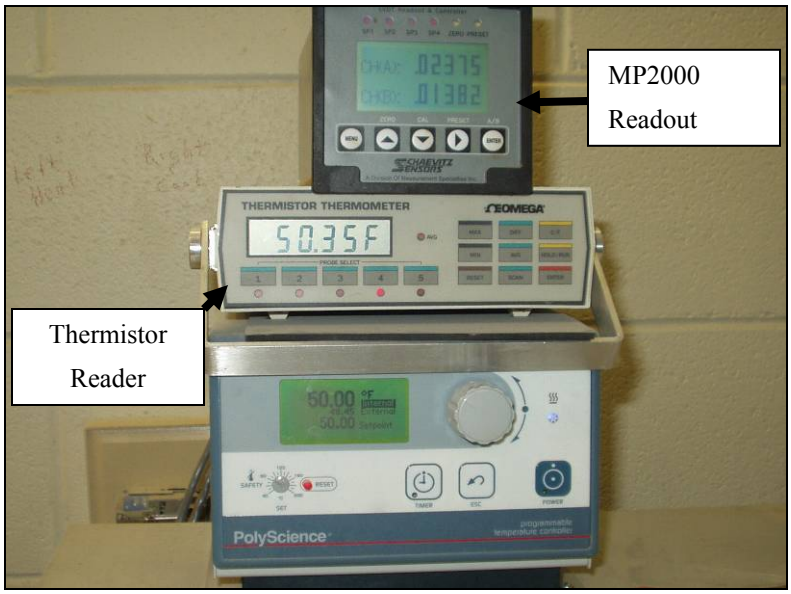

Figure 5-3: Thermistor display and MP2000 Readout

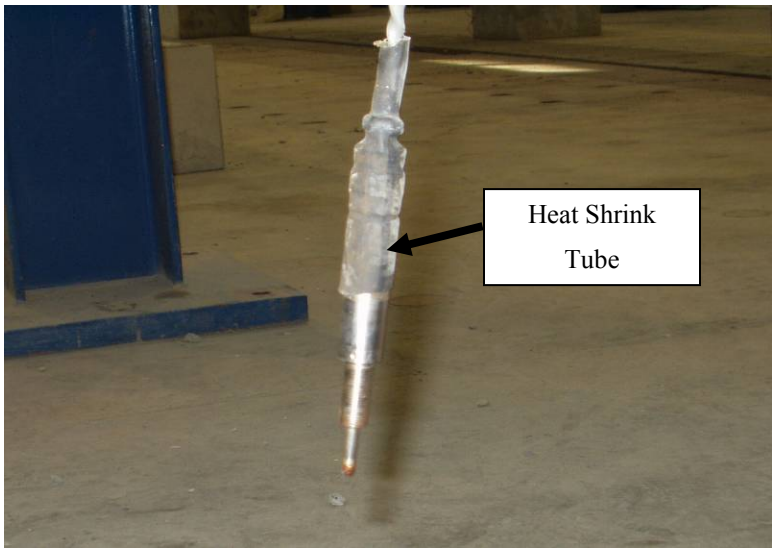

Figure 5-4: Typical linear variable differential transformer

Table 5-2: Specifications of an AC-LVDT operated model (Measurement Specialties, Inc. 2008)

Property	Specification
Frequency Range	400 Hz to 10 kHz
Linearity	±0.25% of full range output
Repeatability	0.000025 in. (0.0006 mm)
Operating temperature range	-65 °F to 300 °F (-55 °C to 150 °C)
Housing Material	AISI 400 series stainless steel
Electrical Termination	6-pin connector

5.4.3.1 LVDT Calibration Procedure

A micrometer screw gage was used to induce a controlled displacement of 0.100 in. in known increment to the LVDT as shown in Figure 5-5. The amount of displacement exceeds the largest displacement anticipated during a CTE test.

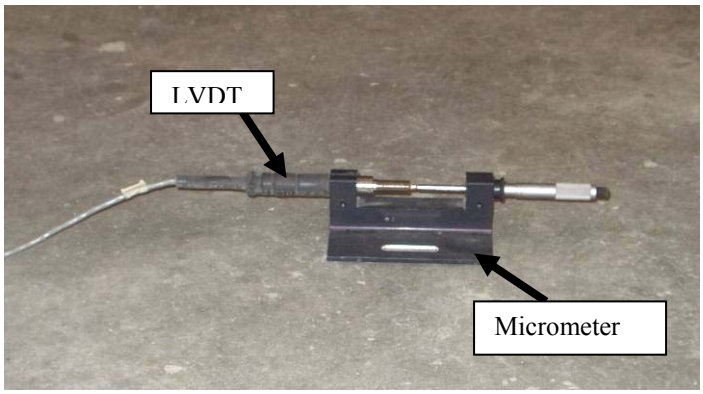

Figure 5-5: LVDT connected to a micrometer screw gage

5.4.4 External Water Tank

A rectangular stainless steel tank was used as shown in Figure 5-6. It has dimensions of 23 in. (length) x 21 in. (width) x 20 in. (height) with an insulated-wall thickness of 1 in. Each wall of the tank is insulated to minimize temperature loss during the test.

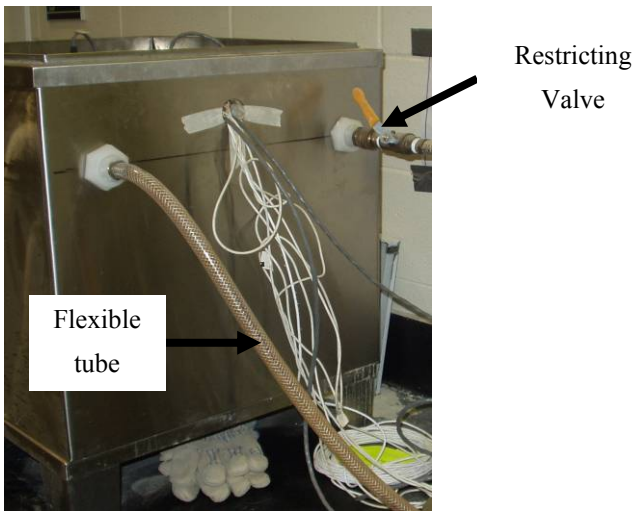

Figure 5-6: External water tank

5.4.5 Thermistor Reader

A thermistor is a temperature-sensing element composed of sintered semiconductor material, which exhibits a change in resistance proportional to a small change in temperature (Omega

Engineering, Inc. 2008). The thermistor reader used is shown in Figure 5-3. It was manufactured by Omega Engineering, Inc. and has the model number 5830. It is a portable instrument, which measures and displays the temperature of up to five different readings from -22 °F to 212 °F. The thermistor reader reads thermistor probes and displays the readings on a five digit LCD on the front panel.

5.4.6 Thermistor Probes

The thermistor probes with model number ON-403-PP, manufactured by Omega Engineering, Inc., were used as shown in Figure 5-7. The probes were made of stainless steel with a diameter of 1/8 in. and a length of 4 ½ in.

Figure 5-7: Thermistor probe

5.4.6.1 Calibration of the Thermistor Reader

The Omega thermistor reader required calibration before use. Five resistors, 106.2K Ohm ± 0.05%, each wired across a separate standard 1/4" phone plug and hence marked "Hi Cal" and Five resistors, 407.1 Ohm ±0.05 %, each wired across a separate standard ¼ in. phone plug and hence marked "Lo Cal" were required for the calibration.

5.4.7 Frames

The frame used in this study is shown in Figure 5-8. The frame is made of Invar and has a total height of 13.75 in. The supporting vertical bars have a diameter of 0.75 in. The base plate has dimensions of 10.25 in. (length) x 10.25 in. (width) x 0.75 in. (thickness). The cross bar with dimensions of 9.75 in. (length) x 2.0 in. (width) x 0.75 in. (thickness) is positioned by nuts at a height of about 8.0 in. above the top of the base plate.

Figure 5-8: Manufactured Invar frame

5.4.8 Assembly of the Components for the AASHTO TP 60 (2004) Test

The complete setup for the AASHTO TP 60 (2004) is shown in Figure 5-9. The circulator was connected to the external water tank by means of suction and pressure flexible tubing. A flow-restriction valve (shown in Figure 5-6) was installed on the pressure (outlet) tubing and adjusted to match the return suction (inlet) flow rate.

Figure 5-9: AASHTO TP 60 (2004) test setup

The circulator's water reservoir was filled to a level of 1 in. below its top, while the water level in the external water tank was filled such that the level matched that of the water level in the circulator's reservoir. The cables of the thermistor probes were plugged into the rear of the thermistor reader with the temperature probes positioned using Plexiglas sheets in the external

water bath (see Figure 5-10) specifically prepared to hold these probes. The LVDTs were then connected by cables to the MP2000 reader. The LVDT was held in position on the Invar cross bar by a nut. The cross bar was then fixed onto the Invar frames by nuts. Two frames were used, and they were made to sit side by side in the external water tank.

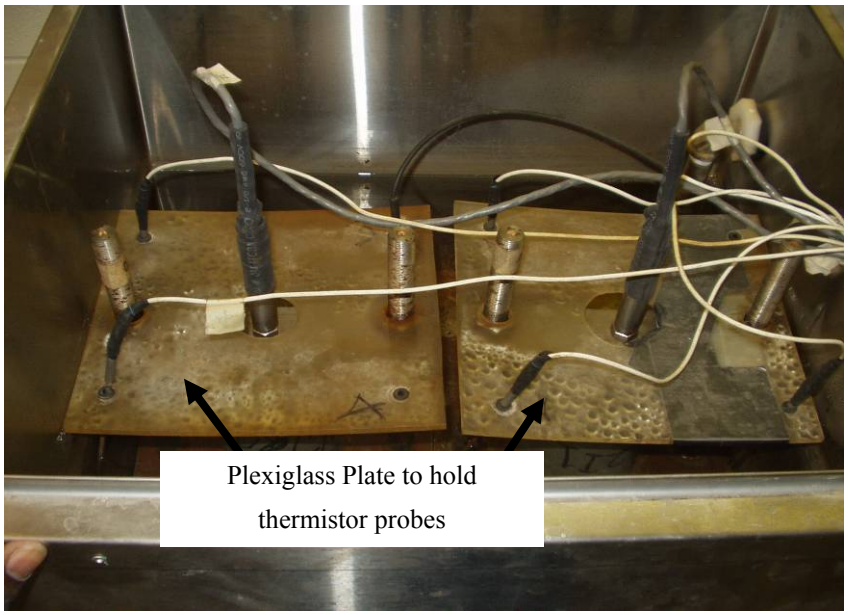

Figure 5-10: External water bath for the two Invar frames containing concrete samples

5.5 LABORATORY PROCEDURES

This section briefly describes the procedures for the laboratory work undertaken. All concrete mixing was conducted in an enclosed, air-conditioned concrete laboratory. Portland cement was received and stored in standard 94-lb sacks. The coarse and fine aggregates were stored in sealed 55-gallon drums. The aggregates were replenished from large stockpiles stored outdoors at Sherman Industries ready-mixed concrete plant in Auburn, Alabama.

5.5.1 Batching and Mixing

Prior to batching, moisture corrections were performed on both the fine and coarse aggregates. Once the moisture corrections were performed, all materials were batched using weight batching into 5-gallon buckets. In an attempt to prevent moisture gain or loss, the buckets were sealed with lids. The total batch size made was three cubic feet, usually with about 50 % being waste. The mixing room where all the concrete was mixed is shown in Figure 5-11. The procedure used to mix concrete was in accordance with AASHTO T 126 (2001).

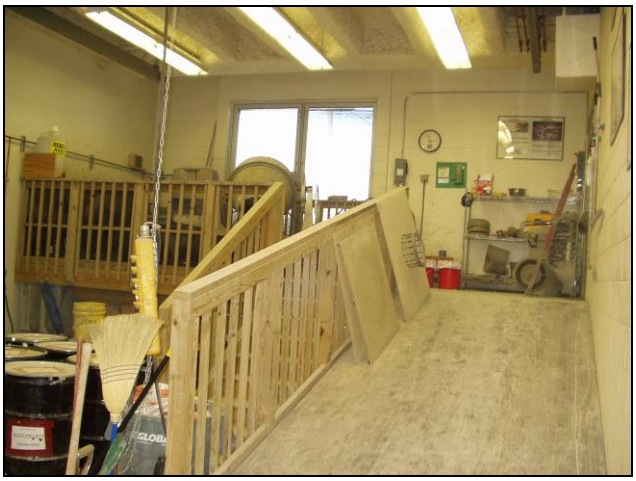

Figure 5-11: Concrete mixing room

5.5.2 Assessment of Fresh Concrete Properties

On completion of mixing, the following tests were performed to assess fresh concrete properties according to the standards indicated:

- slump in accordance with ASTM C 143 (2003),
- unit weight in accordance with ASTM C 138 (2001),
- total air content in accordance with ASTM C 231 (2004), and
- fresh concrete temperature in accordance with ASTM C 1064 (2004).

5.5.3 Sample Preparation

The AASHTO TP 60 (2004) procedure requires that tests should be carried out on 4 in. diameter x 7 in. high concrete samples. Therefore, before mixing, the 4 in. x 8 in. plastic cylinder molds were trimmed to 7 in. in height using an electric-powered saw blade.

All test specimens were made in accordance with ASTM C 192 (2002). Nine cylinders were made for each concrete batch. This comprised of six 4 in. x 7 in. cylinders and three 6 in. x 12 in. cylinders. Each 6 in. x 12 in. cylinder was made in three equal lifts of concrete, and each layer was rodded 25 times with a 5/8-in. tamping rod. For the 4 in. x 7 in. (100 mm x 175 mm) cylinders, each was made in two equal lifts of concrete, and each layer rodded 25 times with a 3/8-in. tamping rod. The sides of the molds were slightly tapped with a rubber mallet each time a layer was rodded. A wooden trowel was then used to strike off the surface of the concrete sample. Next, the cylinders were covered with plastic caps to prevent any loss of moisture. Typical concrete samples in the hardened state with their identification numbers are shown in Figure 5-12.

Using the ASTM C 192 (2002) test method, the concrete samples were stripped after a concrete age of 24 hours and transferred to the moist curing room, where they were kept until a

concrete age of 28 days and then prepared for the hardened concrete testing. The moist curing, apart from helping in hydration, also helps to keep the concrete samples saturated for the CTE test as required by AASHTO TP 60 (2004).

Figure 5-12: Typical tested samples ready to be discarded

5.5.4 Assessment of Hardened Concrete Properties

The following hardened concrete property tests were performed on each concrete sample prepared.

5.5.4.1 Compressive Strength Testing

The compressive strength testing was conducted on the three 6 in. x 12 in. cylinders using a compressive testing machine manufactured by Forney. All three samples were tested in accordance with ASTM C 39 (2003).

5.5.4.2 Coefficient of Thermal Expansion

Fifty-four samples were tested for their coefficient of thermal expansion (CTE). This test was conducted in accordance with the specifications of AASHTO TP 60 (2004). The CTE test was carried out on two 4 in. x 7 in. concrete samples at a time, hence two Invar frames A and B were used at a time. The frames were made to sit side-by-side in the external water bath. With the samples removed from the curing room, their dimensions (length and diameter) were measured using a vernier caliper and recorded. The length and diameter measurements were taken at four different points along the circumference to ensure accuracy. The samples were next setup in the

frames, making sure that the lower end of the sample was firmly seated against the support buttons, and that the LVDT tip was seated against the upper end of the sample.

The temperature of the water bath was set to 50 °F on the circulator. It was allowed to remain at this temperature until thermal equilibrium of the concrete samples was reached as was indicated by consistent readings of the LVDT to the nearest 0.00001 in. taken over a one-half hour period at 10-minute intervals.

The temperature readings were then recorded to the nearest 0.2 °F, and the LVDT readings were recorded to the nearest 0.00001 in. These were the initial readings. Next, the temperature of the water bath was set to 122 °F (50 °C). When the bath reached this temperature, it was allowed to remain at this temperature until thermal equilibrium of the concrete samples was reached, as explained earlier.

The temperature readings from each of the four sensors and LVDT readings were then recorded. These formed the second set of readings. The temperature of the water bath was next set to 50 °F (10 °C) on the circulator. The bath was allowed to remain at this temperature until thermal equilibrium of the sample was reached. The temperature readings of the four sensors and LVDT readings were again recorded as stated previously. These were the final readings for a complete cycle. The whole process was repeated two more times and the average CTE computed from the test data.

5.5.4.2.1 Correction for Frame Movement

Since the Invar frames expand and contract simultaneously with the concrete sample, a correction factor for the Invar frames had to be determined and applied in accordance with AASHTO TP 60 (2004). To determine the correction factor, the AASHTO TP 60 (2004) test was run on stainless steel calibration samples (shown in Figure 5-13). This calibration test was performed for each frame.

Figure 5-13: Stainless steel samples used in determining the correction factor

5.6 RAW MATERIALS USED

This section presents the properties of all the raw materials used in this portion of this study.

5.6.1 Aggregates

Three types of coarse aggregates, namely siliceous river gravel, dolomitic limestone, and granite, were used in this study. They were of gradation No. 67 according to ASTM C 33 (2003). These aggregates were selected for this study since they are the types of aggregates commonly used by the Alabama concrete industry. The type of fine aggregate used was siliceous sand. The different types of aggregates together with their properties are defined in Table 5-3. The gradation plots of these aggregates are also shown in Figures 5-14a – 5-14d.

Table 5-3: Aggregate properties

Aggregate Type	Source	Gradation	Bulk Specific Gravity	Absorption Capacity (%)
Siliceous River Gravel	Martin Marietta, Shorter, Alabama	No. 67	2.568	0.820
Dolomitic Limestone	Vulcan Materials, Calera, Alabama	No. 67	2.753	0.378
Granite	Florida Rock Industries, Forest Park, Georgia	No. 67	2.687	0.640
Siliceous Sand	Martin Marietta, Shorter, Alabama	ASTM C 33 Sand	2.626	0.301

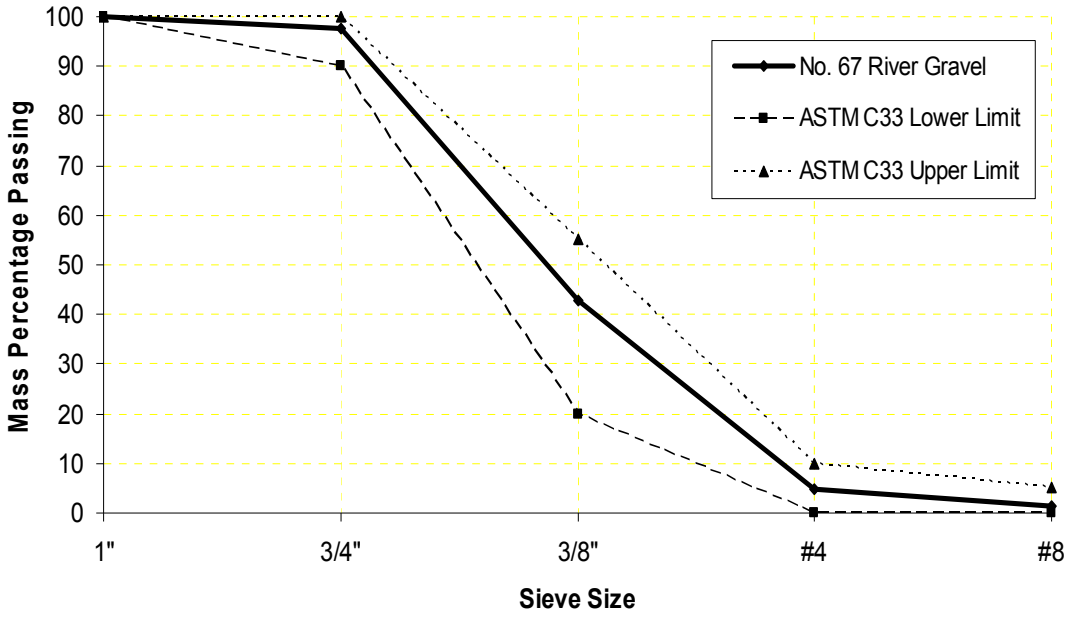

Figure 5-14a: Gradation test results for Martin Marietta No. 67 Siliceous River Gravel

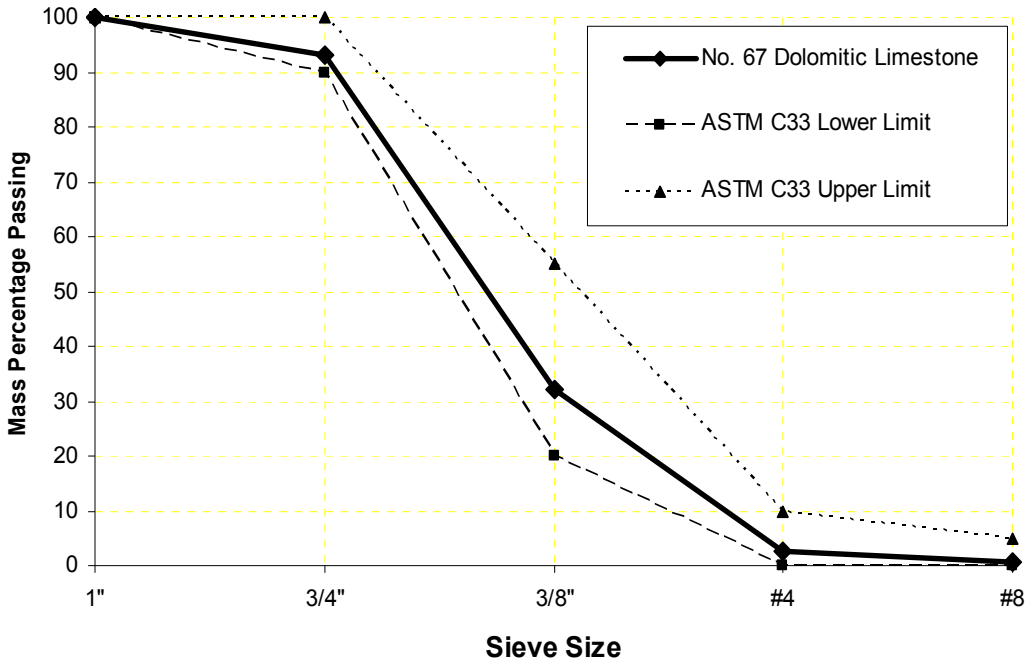

Figure 5-14b: Gradation test results for Vulcan Materials No. 67 Dolomitic Limestone

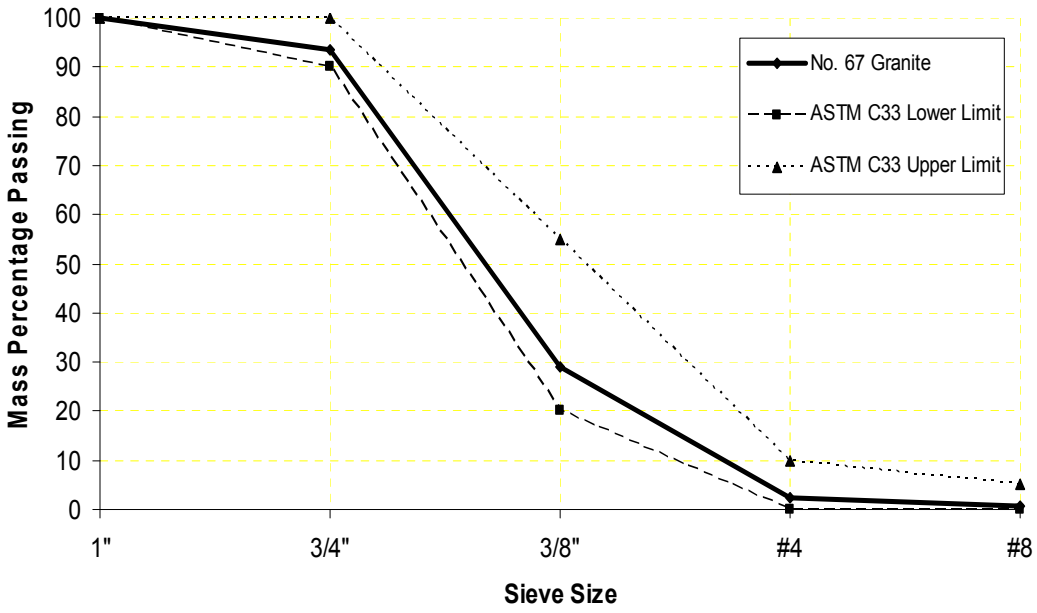

Figure 5-14c: Gradation test results for Florida Rock Industry No. 67 Granite

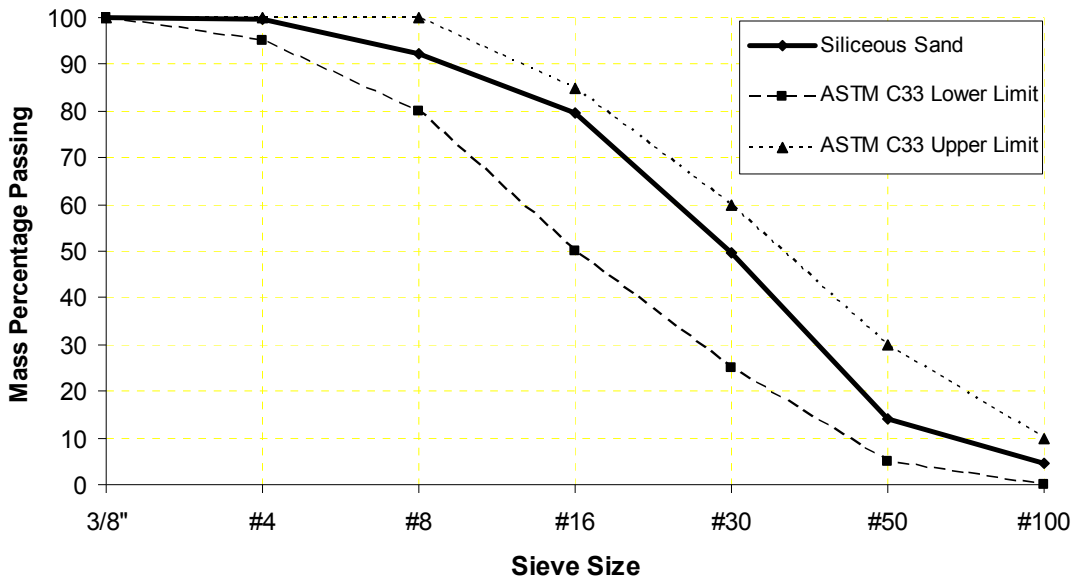

Figure 5-14d: Gradation test results for Martin Marietta, Shorter Siliceous Sand

5.6.1.1 Assessment of Aggregate Chemical Composition

Samples of the aggregate were prepared for their chemical composition testing. The preparation involved crushing the aggregate samples to minus 3/8-in. in size. They were then sent to Wyoming Analytical Laboratories in Golden, Colorado for chemical composition testing. The chemical test involved the determination of the oxide residues in the compound. The proportions of these oxide residues in the various aggregates are shown in Table 5-4.

5.6.2 Chemical Admixtures

Chemical admixtures were used as needed in the concrete mixtures to control the slump and the total air content of the fresh concrete. All chemical admixtures were supplied by BASF Admixtures, Inc. Pozzolith 200N was used as a low-range water-reducing admixture, the dosage of which depended on the water-cement ratio used. Polyheed 1025 was used as a medium-range water-reducing admixture, the dosage of which also depended on the water-cement ratio used. MB AE 90 was used as the air-entraining admixture.

5.6.3 Cementitious Materials

Only Type I portland cement was used for this portion of the study. The Type I portland cement used was manufactured by Lafarge in Calera, Alabama.

Table 5-4: Chemical analysis results from Wyoming Analytical Laboratories

Oxide Residue	Percent by Weight			
	River Gravel	Dolomitic Limestone	Granite	Siliceous Sand
SiO_2	99.20	3.12	65.87	97.42
AL_2O_3	0.21	0.23	13.99	1.12
Fe_2O_3	0.24	0.11	3.26	0.48
CaO	0.03	40.16	5.68	0.08
MgO	0.05	11.82	1.69	0.07
Na_2O	0.05	0.01	3.90	0.03
K_2O	0.02	0.07	2.16	0.37
TiO_2	0.03	0.00	0.42	0.14
MnO	0.01	0.01	0.10	0.01
CO_2	0.07	44.31	2.62	0.17
Others	0.09	0.18	0.31	0.11

5.7 PRESENTATION AND DISCUSSION OF RESULTS

The results obtained from the laboratory testing program are presented and discussed in this section. The effect of the coarse aggregate type and volume, water-cement ratio, and sand-aggregate ratio on concrete CTE are statistically analyzed and discussed. At the end of the chapter, results from this experimental work are compared with those of the FHWA.

5.7.1 Coefficient of Thermal Expansion Results

The two main hardened concrete properties tested were the compressive strength and coefficient of thermal expansion (CTE) of concrete at a concrete age of 28 days. A summary of the test results is shown in Table 5-5.

Table 5-5: CTE and compressive strength test results at a concrete age of 28 days

Concrete Sample Identification	CTE ($x10^{-6}$ in./in./°F)	Compressive Strength (psi)
RG-40-32	7.01	8270
RG-40-38	7.07	7520
RG-40-44	7.23	7580
RG-45-32	6.82	8580
RG-45-38	6.93	7490
RG-45-44	6.86	6420
RG-50-32	6.94	8960
RG-50-38	6.82	7250
RG-50-44	6.87	6330
DL-40-32	5.66	9800
DL-40-38	5.59	8730
DL-40-44	5.52	8340
DL-45-32	5.31	9150
DL-45-38	5.61	8790
DL-45-44	5.45	7200
DL-50-32	5.41	9910
DL-50-38	5.54	7770
DL-50-44	5.62	7250
GR-40-32	5.64	10300
GR-40-38	5.48	8390
GR-40-44	5.37	7430
GR-45-32	5.69	10600
GR-45-38	5.52	8670
GR-45-44	5.57	7990
GR-50-32	5.91	10260
GR-50-38	5.75	8400
GR-50-44	5.47	7820

From Table 5-5 it is evident that the CTE of the concretes made with river gravel are greater than those of granite and dolomitic limestone. The average CTE for concretes made with various aggregates are summarized in Table 5-6.

Table 5-6: Average CTE for concretes made with the different coarse aggregates

Coarse Aggregate Type	Average Concrete CTE ($x\ 10^{-6}$ /°F)
River Gravel	6.95
Granite	5.60
Dolomitic Limestone	5.52

5.7.2 Statistical Analysis and Inferences from CTE Test Results

The CTE test results were analyzed using the analysis of variance (ANOVA), generalized linear models (GLM), and the t-test methods. A P-value indicates the probability of error of the statement that a factor has a significant effect on the measured parameter. A lower P-value for a factor means that such factor has a higher level of significance. A probability of error (α) level of 0.05 was used, which is associated with the 95^{th} percent confidence level. A factor is significant if the P-value of the factor is equal or less than 0.05. The coefficient of determination, r^2, gives the proportion of the variance of one variable that is predictable from the other variable. It is a measure that allows one to determine how certain one can be in making predictions from a certain linear relation. The coefficient of determination is such that $0 < r^2 < 1$. A coefficient of determination of 1 means that 100 % of the total variation in the dependent variable can be explained by the linear relationship between the independent variable and the dependent variable while for a coefficient of determination of 0, it implies that the total variation in the dependent variable cannot be explained by the linear relationship.

Statistical analyses were performed to determine the effect of course aggregate type, water-cement ratio, and sand-aggregate ratio on concrete CTE. The P-values and r^2-values obtained from the statistical analysis are summarized in Table 5.6. From the results shown in Table 5-7 it can be concluded that the coarse aggregate type has the most significant effect on the concrete CTE. This is evident from the very high r^2-value of 0.96085 and a P-value of < 0.0001. The sand-aggregate ratio, with an r^2-value of 0.00302 and a P-value of 0.960 has a greater effect on the concrete CTE than the water-cement ratio. The water-cement ratio with an r^2-value of 0.00076 and a P-value of 0.991 has the least effect on the concrete CTE.

Table 5-7: Summary of p-values and correlation coefficients

Parameter	P-Value	Correlation Coefficient
Coarse aggregate type	< 0.0001	0.961
Sand-aggregate ratio	0.960	0.003
Water-cement ratio	0.991	0.001

5.7.3 Comparison of Results with those Published in Literature

In this section, results from the laboratory-tested samples are compared with results from the FHWA's Turner-Fairbank Highway Research Center (TFHRC) in McLean, Virginia. The research at TFHRC was carried out as part of the Long Term Pavement Performance (LTPP) program of the Strategic Highway Research Program (SHRP) where hundreds of cored samples were tested. The results obtained from this study performed at Auburn University (AU) are compared with those from FHWA in Figure 5-15.

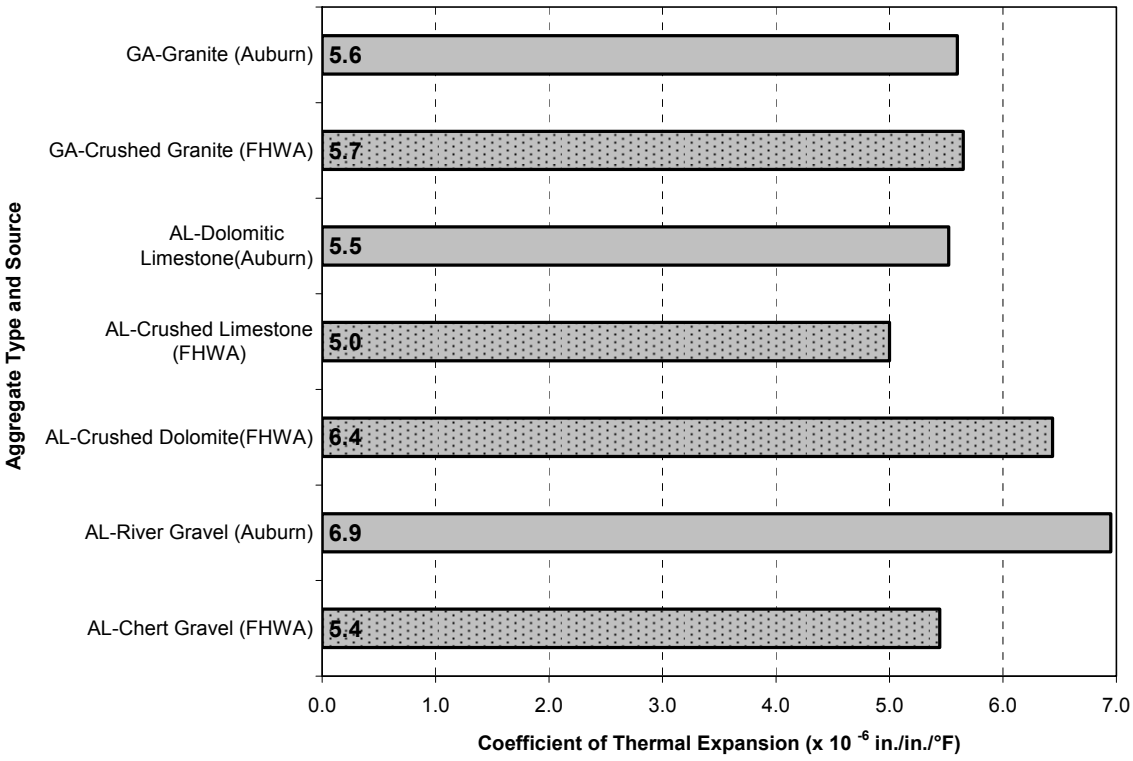

Figure 5-15: Comparison of results from Auburn University with those of FHWA

It may be seen from Figure 5-15 that the CTE-values are very similar for concretes made with granite coarse aggregate. However, for concretes made of gravel the results showed a major difference in the CTE values obtained. Similarly, for concretes made of dolomitic limestone (in the case of AU study) and limestone and dolomite (in the case of FHWA), the result are considerably different. However, the value of the CTE obtained for concrete made with gravel in the Auburn University study compare well with those reported in literature: 6.8 x 10^{-6} /°F (Neville and Brooks 1987) and 6.6 x 6.8 x 10^{-6} /°F (Mehta and Monteiro 2006).

5.8 CHAPTER CONCLUSIONS

The following conclusions are made based on the results of the experimental work presented and discussed in this section:

- The CTE values obtained for concretes made with aggregates found in Alabama are reported in Table 5-8.
- The sand-aggregate ratio and water-cement ratio do not have as much influence on the concrete CTE as does the coarse aggregate type.

Table 5-8: Coefficient of thermal expansion values for concretes made of common aggregate types used in the Alabama Concrete Industry

Coarse Aggregate Type	Average Concrete CTE (x 10^{-6} /^{o}F)	Concrete CTE Range (x 10^{-6} /^{o}F)
River Gravel	6.95	6.82 –7.23
Granite	5.60	5.37 – 5.91
Dolomitic Limestone	5.52	5.31 – 5.66

Chapter 6

Analytical Evaluation of Bridge Deck Cracking

6.1 INTRODUCTION

The work in this chapter focuses gaining an understanding of the mechanisms by which premature cracks might have formed on the US 331 bridge deck, so that the occurrence of such cracking in future newly-constructed bridge decks could be prevented. To investigate the development of stresses inherent in a bridge of this type, a refined finite-element model of this continuous, skewed, composite bridge was created and used to predict the stress distribution and cracking behavior of the deck. This modeling effort was accomplished using the commercial finite-element package ABAQUS, which has the capability to produce stress contours and cracking distribution of a model. After the model was shown to accurately represent the physical characteristics of the given bridge, a parametric study was conducted, in which various factors that were believed to possibly influence the cracking behavior, specifically bridge skew angle and differential support settlement, were systematically varied in the model, and the resulting crack patterns were compared.

6.1.1 Chapter Objectives and Research Methodology

The primary objectives of the work documented in this chapter are to 1) numerically predict the development of stresses and the cracking behavior for a three-dimensional finite-element model of the US 331 bridge, and 2) use that model as a basis to conduct a parametric study to assess the influence of bridge skew angle and varying bridge support settlement conditions on the development of stresses and the subsequent extent and location of cracking in continuous composite bridges of this type. Since the US 331 bridge deck was removed and replaced prior to the beginning of this research effort, it was not possible to conduct field studies on the damaged deck. Therefore, numerical studies were chosen as an alternative method to gain an understanding of the physical mechanisms that could have contributed to the development of global stresses that led to the premature cracking.

6.2 DEVELOPMENT OF FINITE-ELEMENT MODEL

6.2.1 Review of the US 331 Bridge

The plan view and section view of the three-span, continuous, skewed bridge that was recently constructed on US 331 near Montgomery, Alabama are shown in Figure 3-1, along with the framing plan. The reinforced concrete (RC) deck has a length of 350.92 ft, a width of 40 ft and a design thickness of 7 inches. The three span lengths, ranging from the south end to the north end, measure 108.24 ft, 134.43 ft, and 108.24 ft, respectively, and the skew angle for the bridge measures 61° (all the skew angles in this chapter are defined as shown for angle α in Figure 3-1). There are "expansion" support conditions (i.e., roller supports) imposed at the abutments and at the left interior bent, and a pinned boundary condition is imposed at the right interior bent.

The reinforced concrete deck (prior to its demolition) was supported by six continuous AASHTO M270 Grade 36 steel welded plate girders with a transverse spacing of 7 ft. The web plate dimensions for each girder are ½ in. x 48 in. The flange for each girder measures 1¼ in. x 16 in. in the positive moment regions, and 1¾ in. x 16 in. in the negative moment regions (near the interior bents). The top of the steel flanges were connected to the bottom of the reinforced concrete deck using 96 rows of ¾-in.-diameter x 5 in. equally spaced shear studs over the end span positive moment regions, and 94 rows of ¾-in.-diameter x 5 in. equally spaced shear studs over the middle span positive moment region. Each of the rows contained three shear studs: one stud was placed directly above the web centerline, and each of the other studs was placed 6 in. on either side of the web centerline.

Intermediate crossframe diaphragms constructed of L4 x 4 x 5/16 in. angles, as shown in Figure 3-2, connect the girders in each span; these diaphragms are represented by the straight vertical lines in the framing plan shown in Figure 3-1. As can be seen in the framing plan, the crossframe diaphragms are perpendicular to the longitudinal direction of the bridge (i.e., they do not follow the 61° skew angle). Additionally, as indicated in Figure 3-1 by the slanted lines, W27 x 84 bearing diaphragms are located between the girders at the abutments and at the interior bents, placed parallel to the skew angle.

The RC deck slab, as mentioned, had an average depth of 7 in., deepening to 10 in. in a haunch shape above each of the girders. The bridge deck was cast in three stages. First, 80 ft of the end spans were cast on the south side and the north side of the bridge. Next, an 80 ft portion was cast in the middle of the bridge. Finally, the two remaining 54'-10¾" sections above the interior bents were cast. As a result, after the final deck concrete was poured over the intermediate supports (but while the concrete was still fresh), since the construction was unshored, the girders were required to support the weight of the wet concrete, and were assumed to have undergone all deflection before the concrete in these closure pours set. Due to this sequencing, it is assumed that the stresses produced in the deck closure castings were not

affected by dead loads, since the deck's own weight was supported solely by the steel girders, but were affected only by any additional live load to which they were subjected. Test data collected from core samples taken from the deck exhibited an average concrete compressive strength of approximately 5,300 psi.

6.2.2 Model Characteristics

6.2.2.1 Model Assumptions

To study the behavior of the bridge deck, a refined 3D finite-element model of the bridge was developed using the commercial finite-element software package ABAQUS. Several general assumptions were made to simplify the development of the model without loss of accuracy in the representation. First, material properties were held constant for all concrete components and for all steel components of the bridge. Secondly, it was decided that the deck haunches located directly above the girders would not be explicitly modeled, so that the deck was modeled using a constant thickness. Thirdly, the crossframe diaphragms placed between the girders were simplified as equivalent steel beams in the model. Details of the equivalency calculation will be provided in the following section.

6.2.2.2 Deck and Girders

Based on the bridge information and modeling assumptions described above, the main components of the bridge were modeled using the ABAQUS elements shown in Table 6-1 below. The overall model and a close-up view are presented in Figures 6-1 and 6-2.

Table 6-1: Finite elements selected for the main bridge components

Component	Element Type
RC Deck	Shell Elements
Steel Girders	Beam Elements
Diaphragms	Beam Elements
Reinforcement	Rebar Elements
Interaction between deck and girders	TIE Function
Parapet	Ignored

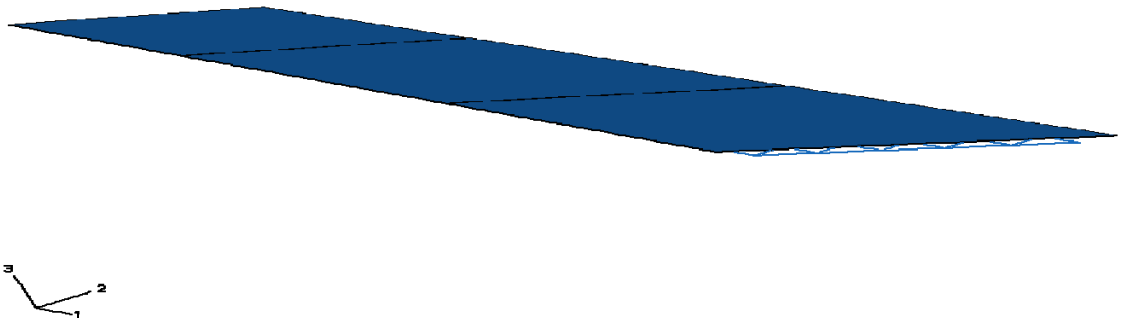

Figure 6-1: Three-dimensional finite-element model of US 331 bridge

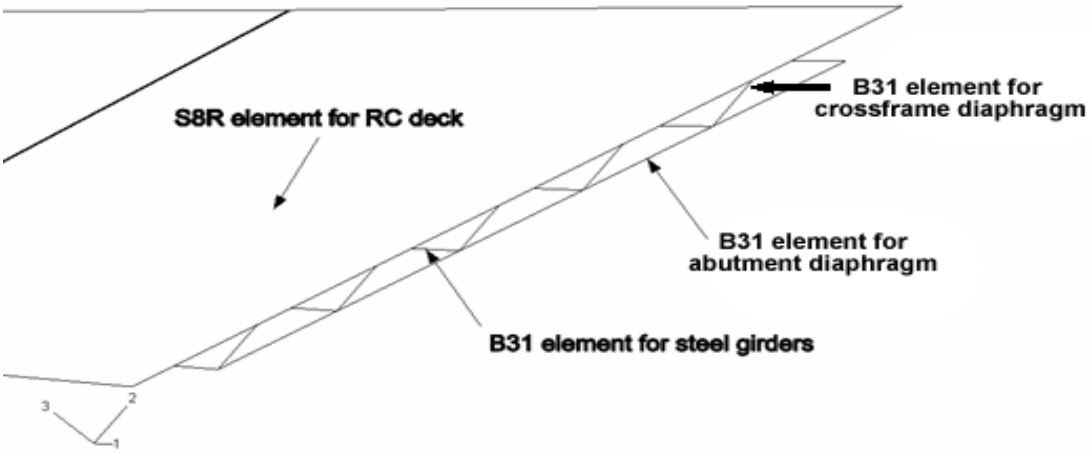

Figure 6-2: Close-up view of bridge model with element types indicated

The concrete deck was modeled using ABAQUS's S8R elements, which are eight- node, second-order, general-purpose thick-shell elements with reduced integration. The S8R elements can reflect the influence of shear flexibility in laminated composite shell models (ABAQUS 2006b). In the skew sensitivity study presented in the ABAQUS Benchmark manual (ABAQUS 2006a), plates with varying skew angles were modeled using different shell elements of ABAQUS. The results proved that, with the finest mesh (14 x 14 for a 1.0 m x 1.0 m plate), S8R elements showed the smallest error (0.5%, 0.2%, and 0.8% for center-slab deflection and maximum and minimum moment, respectively), when the skew was as severe as 60°. This result indicates that S8R elements with a sufficiently refined mesh are the most likely ABAQUS elements to provide results that are quite accurate for simulating deck behavior for decks with large skew angles.

The top and bottom reinforcement in the concrete deck was represented using the "Rebar layer" option of ABAQUS. With this function, layers of reinforcement can be defined as a part of the reinforced concrete section properties. These layers are superimposed on the shell elements of the concrete deck and are treated as a smeared layer with a constant thickness equal to the area of each reinforcing bar divided by the reinforcing bar spacing (ABAQUS 2006b). Bar diameters and spacings corresponding to the No. 4 and No. 5 longitudinal rebar and No. 5 transverse rebar described above were provided as input for ABAQUS to define the rebar layers.

The steel girders and diaphragms were modeled with B31 elements, which are three-dimensional, two-node Timoshenko linear beam elements. B31 elements allow transverse shear strain to be represented, and can be subjected to large axial strains. The ABAQUS Analysis manual stated that these shear-deformable beam elements (B31) should be used in any simulation that includes contact (ABAQUS 2006b). That was one of the primary reasons that this type of element was selected, since deck and girder contact was considered important in this model. These elements are displayed as a line in ABAQUS, though the cross-sectional dimensions for each beam element are directly defined by the user, so that the effects of the cross-sectional properties can be represented. Nominal dimensions for the steel plate girders, and for the W27 x 84 shapes used for the abutment and bent diaphragms, were specified directly to ABAQUS.

As mentioned previously, dimensions for an equivalent wide-flange shape were used to represent the crossframe diaphragms. This technique was used because, to span between the plate girders, in the finite-element model, a specific node had to be identified for attachment of the diaphragms to the beams. Since the girders were being represented by linear beam elements, there was only one node available for attachment to the girders (located at the centroid of the beam's profile). Therefore, attachment nodes could not be identified near the top and bottom of the girder, where the actual location of the attachment of the L4 x 4 x 5/16 crossframe diaphragm members occurs (via a gusset plate connection).

The method of virtual work was used to establish equivalent shear and bending stiffnesses for the bridge's actual crossframe dimensions. From the bending stiffness analysis, it was determined that only the top and bottom chords of the crossframes carry "bending" stresses, so it was deemed that the equivalent beam used to represent the crossframe diaphragm should have top and bottom flanges with cross-sectional areas equal to the cross-sectional area for the L4 x 4 x 5/16 angle (2.40 $in.^2$) used for the top and bottom chords of the actual diaphragm. It was decided that the equivalent beam should have a web height of 36" (the approximate distance between the centroids of the top and bottom L4 x 4 x 5/16 crossframe shapes). An appropriate web thickness was then determined based on the shear stiffness associated with the shearing deformation of a beam of rectangular cross section. The final cross-sectional dimensions chosen for the equivalent beam, then, were 0.24" x 10" for the top and bottom flanges, and 0.0583" x 36" for the web. The equivalent beams were rigidly attached in the model to the girder node on either end.

The selection of the element size and mesh density was very critical for obtaining accurate results, because most finite-element modeling results are sensitive to these parameters. A group of previous researchers found that selection of relatively small elements will eliminate unrealistically low predicted strengths due to the effects of stress concentrations (Barth and Wu 2006). It is also warned in the ABAQUS manual that a coarse mesh will cause S8R elements to have a great loss of accuracy if they are used to model a skewed plate. Therefore, a reasonably fine mesh was selected in this model. The length of the deck was divided into 400 transverse strips, giving a length of approximately 10.5 in. for each element in the longitudinal direction. Each transverse strip of the deck, then, was divided into 64 elements, giving a width of approximately 8.6 inches in the transverse direction for each element. The deck has only one shell element through the thickness, but information regarding stresses, strains, etc. are available from ABAQUS at any point in the thickness of that element using the section point definition feature of ABAQUS. The steel girders had the same number of elements in the longitudinal direction as the deck. This relatively fine mesh spacing was shown to provide accurate results when compared to theoretical values (as will be described later), while allowing the cost (in terms of model run time) of the computer simulation to remain affordable.

6.2.2.3 Material Modeling

Both the concrete and steel were defined as linear elastic materials in this model. (A simulation incorporating nonlinear material properties for the concrete deck will be described in a following section.) Table 6-2 lists the specific material properties that were input to ABAQUS for both materials. The average splitting tensile strength was defined as 600 psi, according to data obtained from early field testing of the deck material.

Table 6-2: Material properties of the US 331 bridge model

Material	Modulus of Elasticity, E	Poisson's Ratio, ν	Density, ρ
Concrete	4.42×10^6 psi	0.15	0.086 lb/in^3
Steel	29×10^6 psi	0.32	0.286 lb/in^3

6.2.2.4 Load and Boundary Conditions

The applied load for this finite-element (FE) model consisted of a light traffic load equal to approximately 87 psf. A "normal", AASHTO-specified service live load was not applied in the model because the deck studied here was newly constructed, and regular vehicular traffic had not yet been allowed on the bridge.

Gravity effects for the bridge were not included, per se, since they were believed not to affect the cracking behavior of the deck, due to the sequential casting sequence described

earlier. In addition, temperature effects were not incorporated. Pin and roller boundary conditions were considered to reflect the abutment and bent restraints; these conditions were used in the model for both the RC deck and girders, as shown in Figure 6-3.

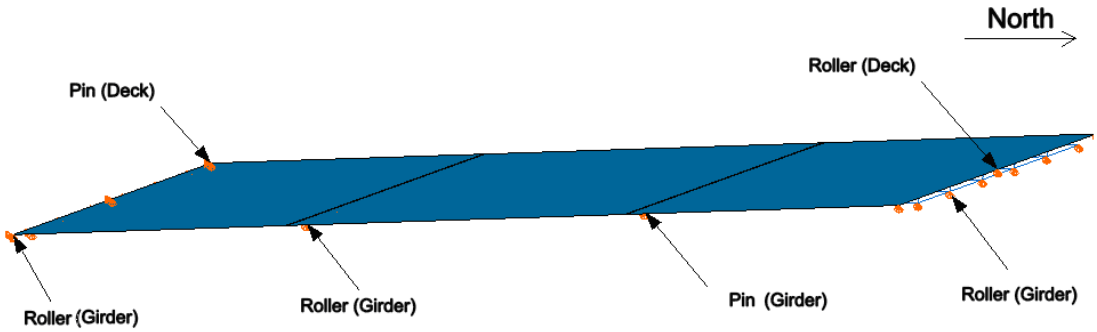

Figure 6-3: Boundary conditions for the US 331 bridge model

6.2.2.5 Interaction between the Deck and Girders

The "Tie" function of ABAQUS was used to simulate the interaction between the concrete deck and the steel girders. Full composite action was assumed between these two very different materials and no slip was allowed at the interface. Tie is a relatively new surface-based connection, which can be used to tie two surfaces together (the connection is a surface-to-surface connection, rather than a node-to-node connection). The essence of the Tie function is similar to that for a node-to-node connection, in which a rigid beam element is used to connect two nodes, but its surface-based property makes it more efficient to implement than traditional node-to-node rigid beam connections.

When connected with a surface-to-surface Tie constraint, the translational degrees of freedom of the slave surface are eliminated (elimination of the rotational degrees of freedom is optional) and each node of the slave surface will have the same motion as the point on the master surface to which it is closest (ABAQUS 2006b). For the present model, a Tie connection was created between two surfaces: the bottom surface of the deck and the top surface of girder top flange. The deck bottom surface was defined as the master surface, and the top flange surface was designated as the slave surface so that a load applied to the deck could be transferred from the deck to the girders. However, in reality, at the location of the piers, the girders are not able to deflect with their corresponding deck master, due to the boundary condition supports that are applied to the piers. Therefore, the master-slave relationship had to be reversed at the pier locations to allow for a realistic deflected shape for the continuous bridge. Figure 6-4 gives the modeling details of the tie connections and boundary conditions surrounding the pier locations.

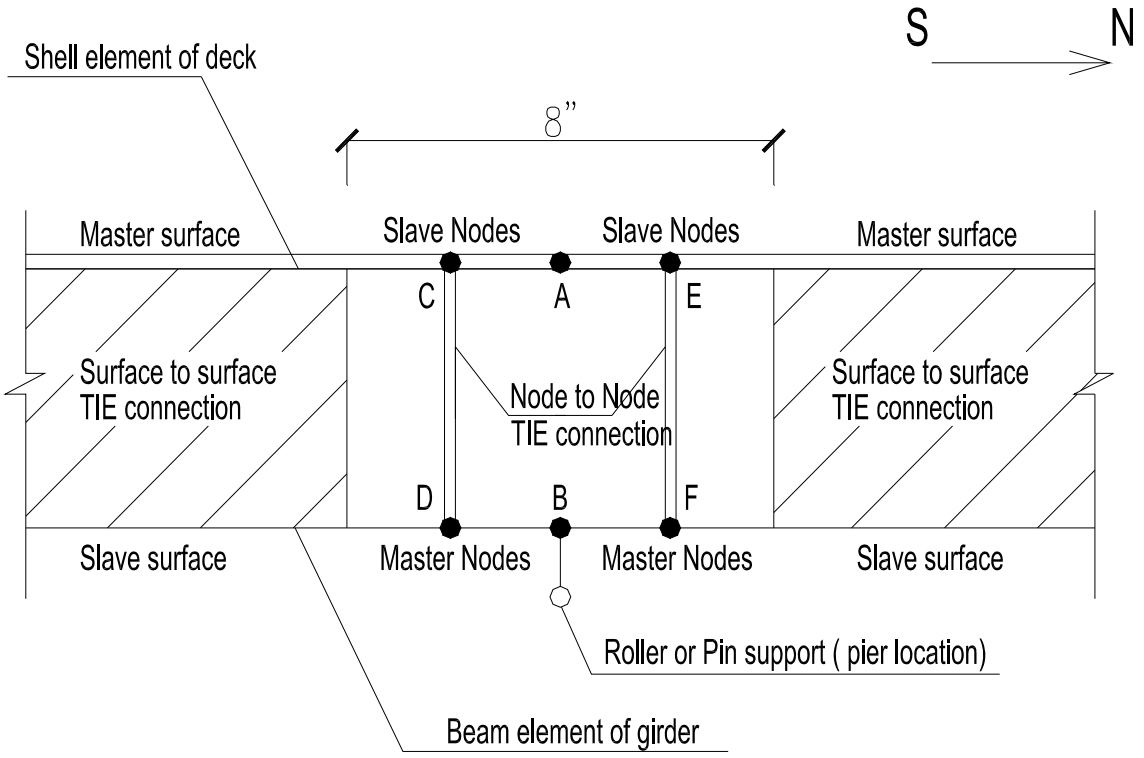

Figure 6-4: Interaction modeling at the piers (elevation view)

As can be seen from the figure, a somewhat complex model was created at the pier locations. In these areas, the master-slave relationship was reversed from the relationship that was used for every other location along the length of the bridge, and the nodes of the girder centerline (nodes D and F) became the master of the Tie connection. Without this complex modeling strategy, node B of the girder (which would have been modeled as part of the slave surface without the master-slave reversal) was controlled by two contrary boundary conditions: (1) its master element was located in the deck, which forced node B to deflect downward under the effect of gravity; (2) the roller support underneath node B, which resisted the downward deflection of node B. This phenomenon is called “overclosure” in ABAQUS and causes failure of the model. The model in Figure 6-4 (wherein node-to-node contact having a girder master and deck slave was established for nodes D-C and F-E, but not for nodes B-A, and having a pin or roller boundary condition applied to node B) not only eliminated the “overclosure” problem, but also released the vertical degree of freedom of node A, which was a much more realistic condition for the continuous deck.

The shortcoming of this support model is that the response in these locations was distorted, due to such a complex simulation. However, since the area involved with this advanced interaction scheme was very small (8 in. in length) compared with the width of the whole deck (350 ft), it was deemed acceptable.

6.2.2.6 Model Validation

To validate the modeling techniques used in this study, a single girder and its tributary deck width were isolated from the bridge model, without changing any model characteristics (e.g., the TIE contacts representing the interaction between the deck and girder surfaces were preserved), as illustrated in Figure 6-5. This abbreviated model was analyzed with ABAQUS and by hand calculations. In this model, the load is the self-weight of the bridge. The skew effect was ignored in this simple validation model. Figure 6-6 shows the longitudinal stresses produced for both the top and bottom surfaces from ABAQUS.

The effects of composite behavior are obvious in this figure. The neutral axis of the composite section is located in the girder (and thus completely underneath the concrete deck). Thus, at the middle of each span, both the top and the bottom surfaces of the deck are experiencing compressive stress, as expected. At the areas surrounding the interior supports, the entire deck is shown to be in a state of tension. The stress values at the locations just above the supports were abnormal due to the complex modeling of the support locations, described in Section 6.2.2.5 above. Thus, in the present study, these values were ignored.

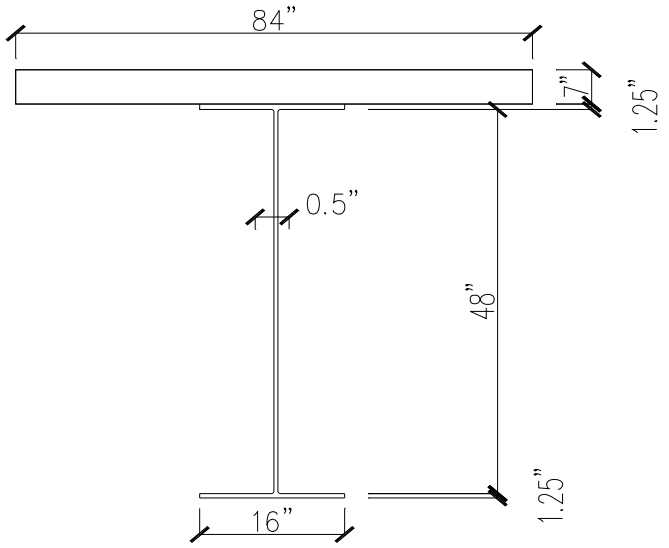

Figure 6-5: Cross section of composite beam validation model (not to scale)

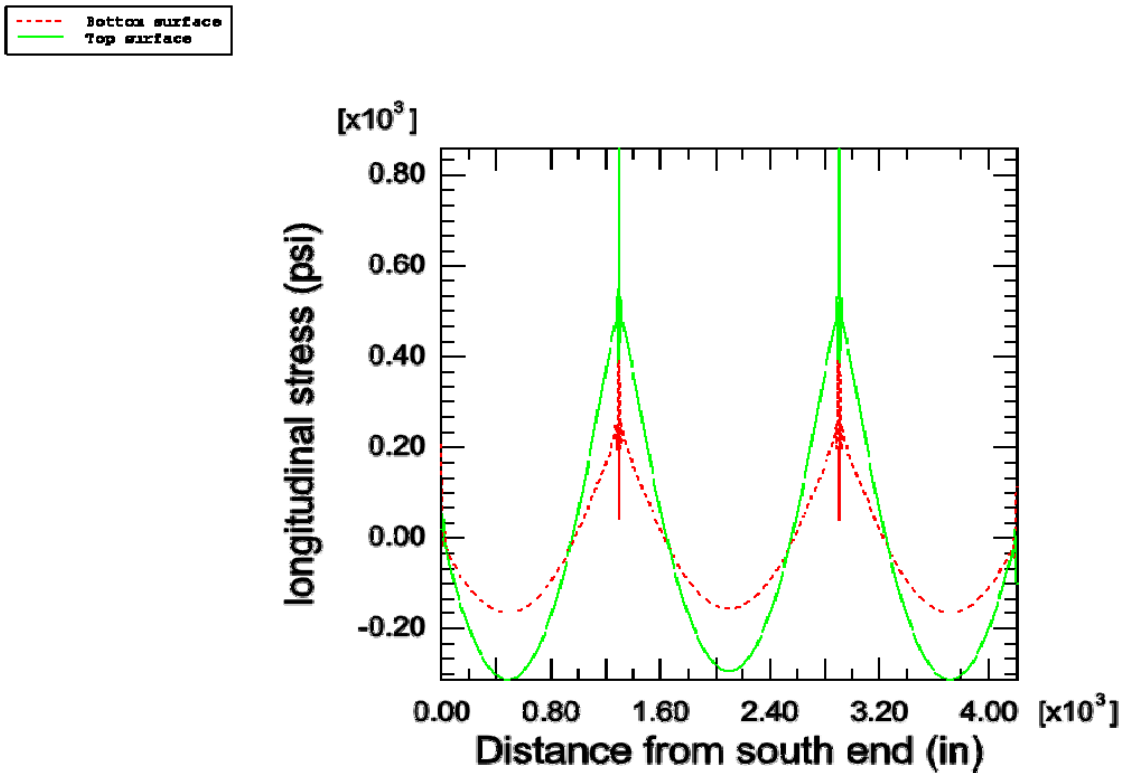

Figure 6-6: Longitudinal stresses from the top and bottom deck surfaces

The results of a hand calculation of the predicted stresses were compared with the FE results; the values are shown for comparison in Table 6-3. The stress was calculated at six locations, considering the symmetry. The maximum compressive stress at the middle of each span was computed for the top and bottom surfaces, as well as the maximum tensile stress at the location of the interior support for both surfaces.

Table 6-3: Validation results for concrete deck stresses

Surface	Location	Stress (psi)		
		Hand Calculation	FE Model	Percent Difference
Top	Interior Span (Midspan)	-291.6	-293.2	0.55%
	End Span (Midspan)	-310.5	-311.7	0.38%
	Support	567.8	564.2	0.63%
Bottom	Interior Span (Midspan)	-163.2	-153.8	5.76%
	End Span (Midspan)	-173.8	-163.0	6.21%
	Support	317.8	253.8	20.1%

The results given above show that the FE prediction of longitudinal stresses agrees very well with the results calculated by hand, especially at the top surface where the effect of the interaction with the girder stresses is not as prominent. This comparison served to confirm that the modeling techniques employed for the study were valid, since no field stresses were available for comparison. (The somewhat larger percent difference noted for the bottom surface at the support location is attributed to the artificial complexity of the stress pattern created there by the complex interaction-modeling scheme used.)

6.2.3 Results and Analysis of Results

6.2.3.1 Deformation and Stress Distribution

Since the main objective of the investigation was to study the cracking behavior of the bridge deck, the results of the model were focused on the response of the deck, despite the fact that the girders and diaphragms were also accurately represented. The deformed shape of the RC deck under external loading is shown in Figure 6-7.

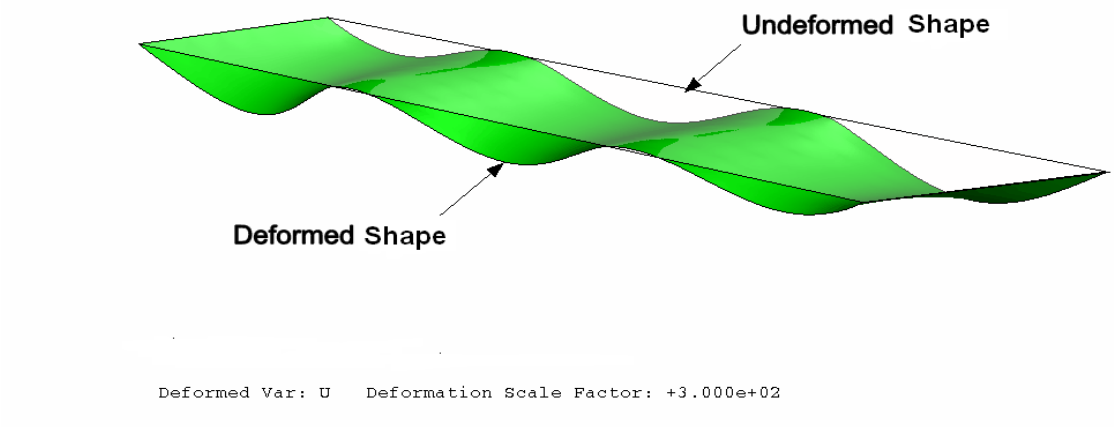

Figure 6-7: Deformed shape of the US 331 bridge deck under external loading

For the deck only, without the steel girders, the bottom deck surface at the midspan locations, and the top deck surface at the supports, would be in tension, based on the deformed shape shown. However, because of the contribution of composite bridge behavior, both the top and bottom surfaces of the deck were in compression at the midspan locations. For the same reason, the deck at the intermediate supports became the most likely areas to experience the maximum tensile stress and the most extensive cracking. Thus, the simulation results for the deck at the locations of the intermediate supports were carefully analyzed, including both the top and bottom surfaces. Figures 6-8 to 6-11 show the distribution of maximum principal stress for the RC deck at the supports.

Because the complex interaction model at the intermediate supports (shown previously in Figure 6-4) caused some unrealistic stresses, these unusually high stresses were ignored during the analysis of the results, and they are not displayed in Figures 6-8 to 6-11 (for the two narrow-width strips just above the interior supports).

As expected, both the top and the bottom of the deck at the intermediate supports are shown to be in tension, and the top surface experiences the largest tensile stress. From the figures, one can see that the tensile stress decreases from the support area towards the midspan area, finally becoming compressive in the midspan area. This behavior fundamentally matches the theoretical moment diagram for a continuous, one-way slab, as expected. As can be seen, this phenomenon is more obvious at the top surface of the deck than at the bottom surface. That is because the bottom of the deck is closer to the neutral axis of bending. The skew effect is also obvious; in Figure 6-8, one can observe that the edge of the contour has a skew angle similar to that for the bridge deck.

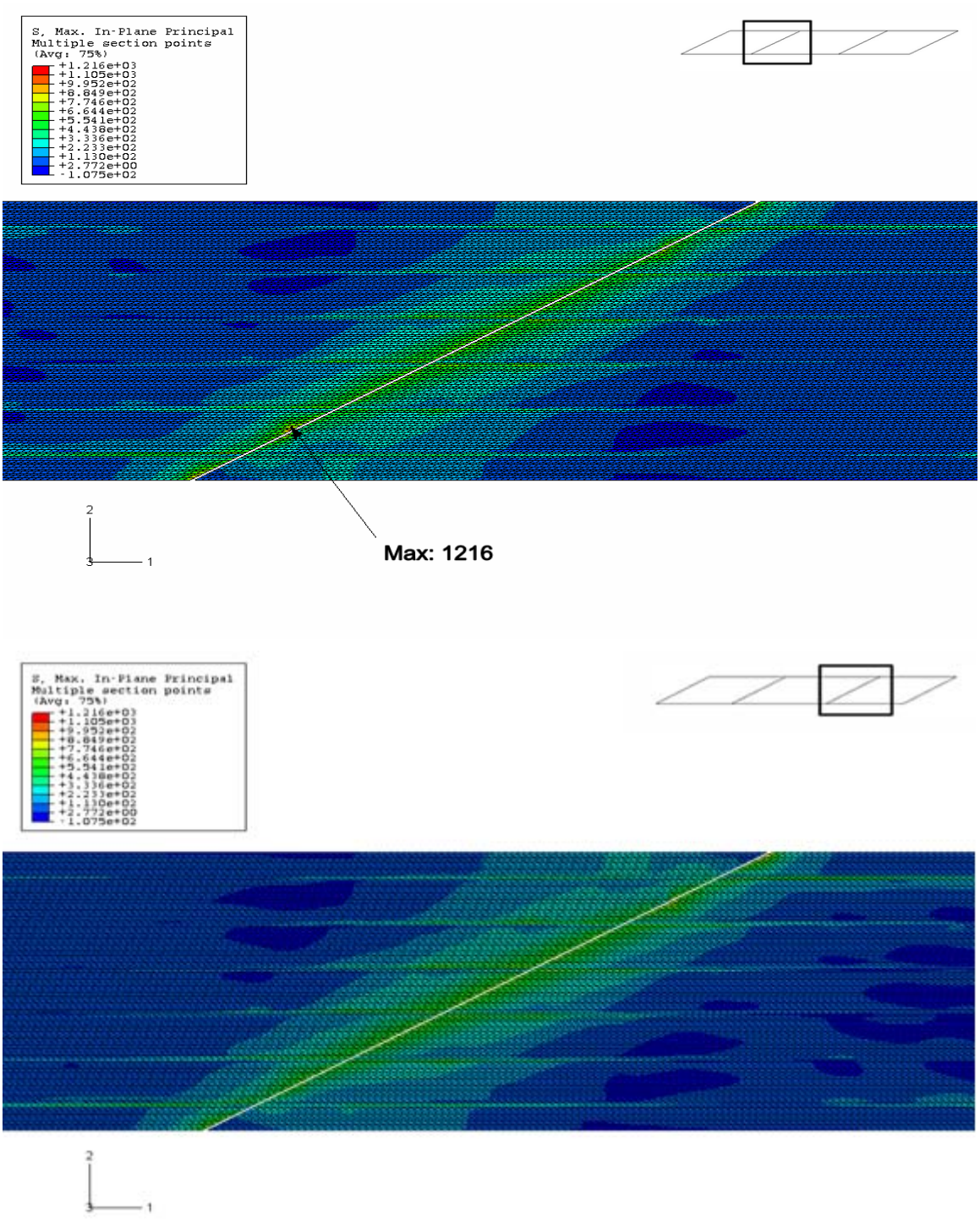

Figure 6-8: Detail view of maximum principal stress distribution at the top of the deck for US 331 bridge, α = 61° (psi)

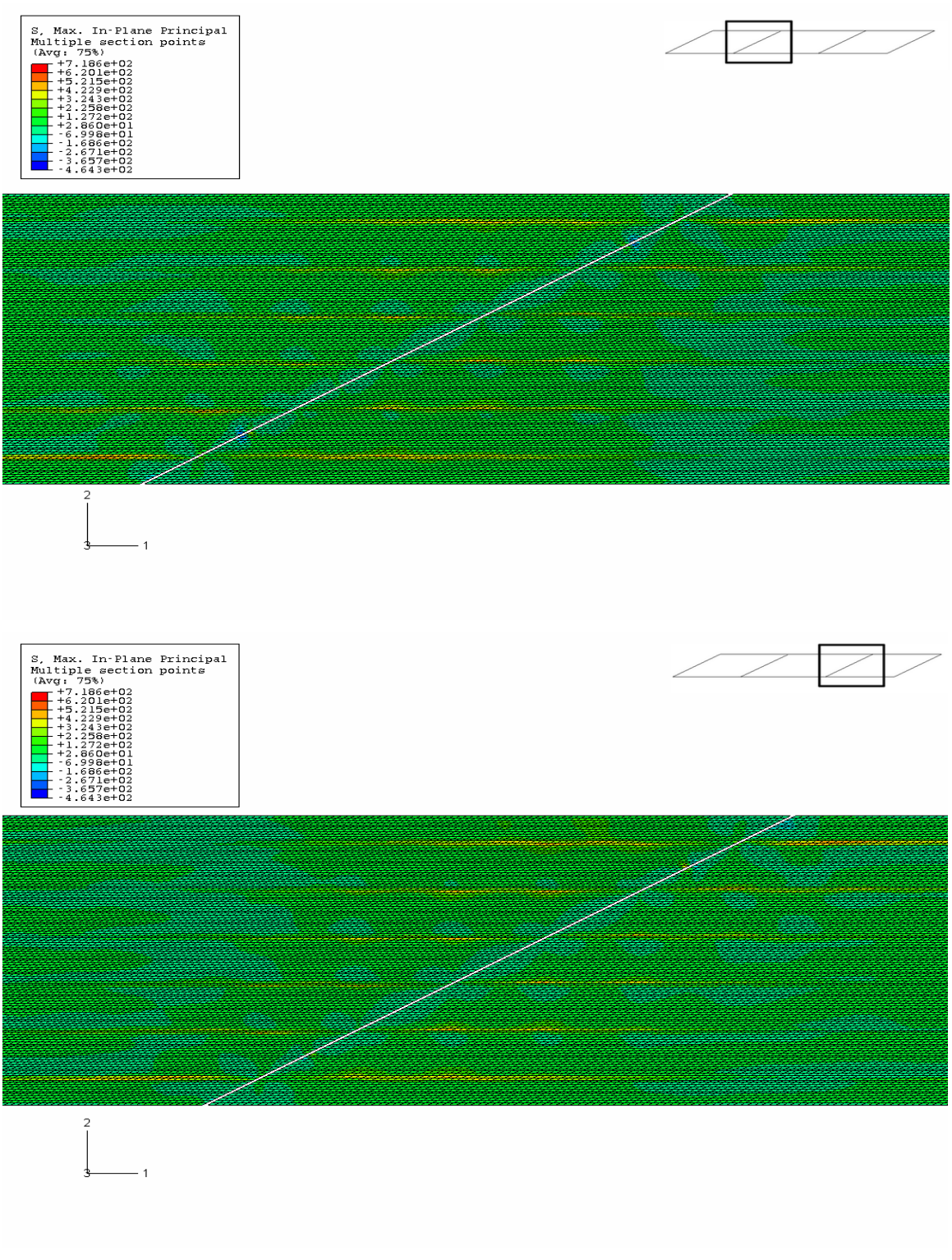

Figure 6-9: Detail view of maximum principal stress distribution at the bottom of the deck for US 331 bridge, α = 61° (psi)

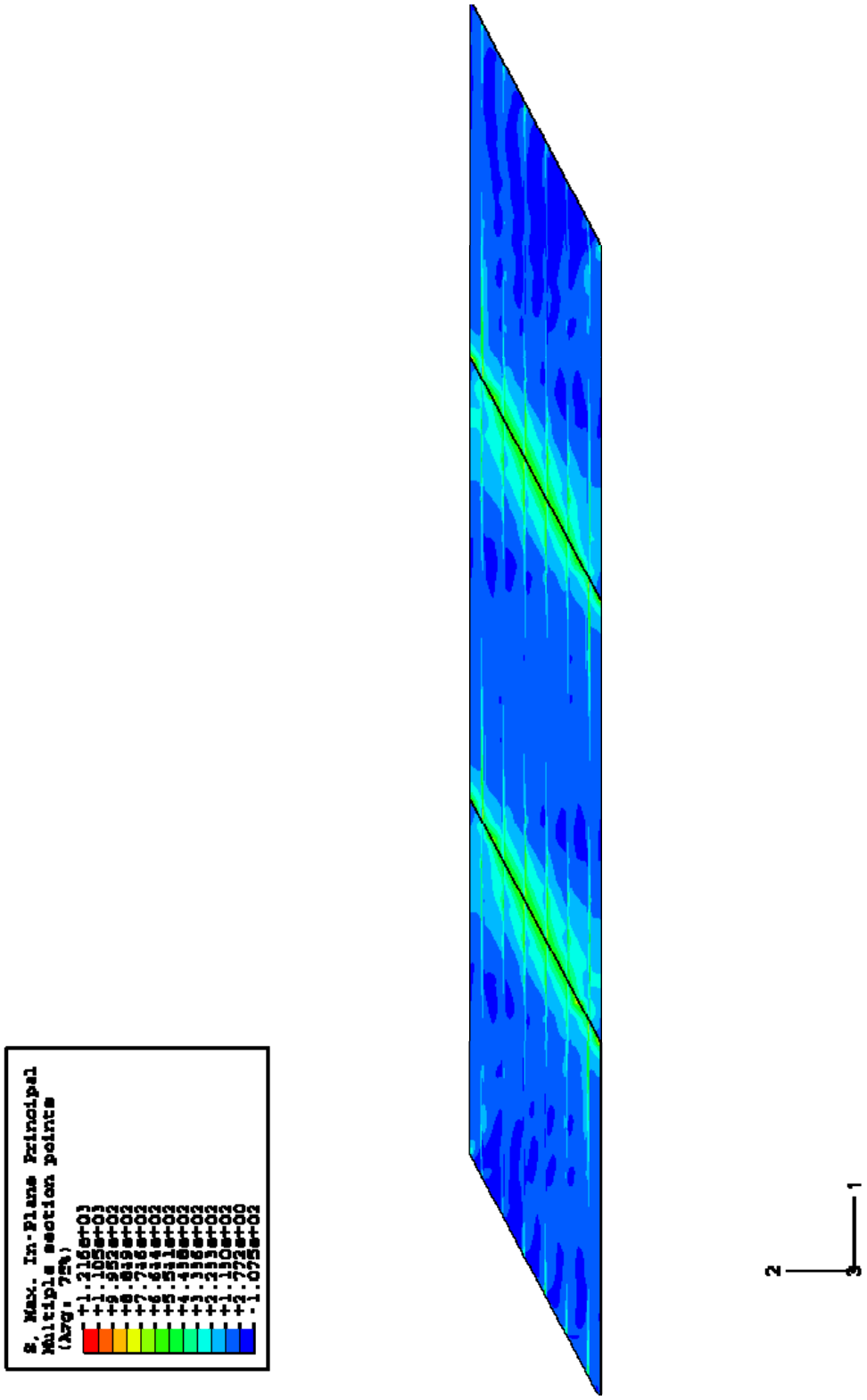

Figure 6-10: Full view of maximum principal stress distribution at the top of the deck for US 331 bridge, α = 61° (psi)

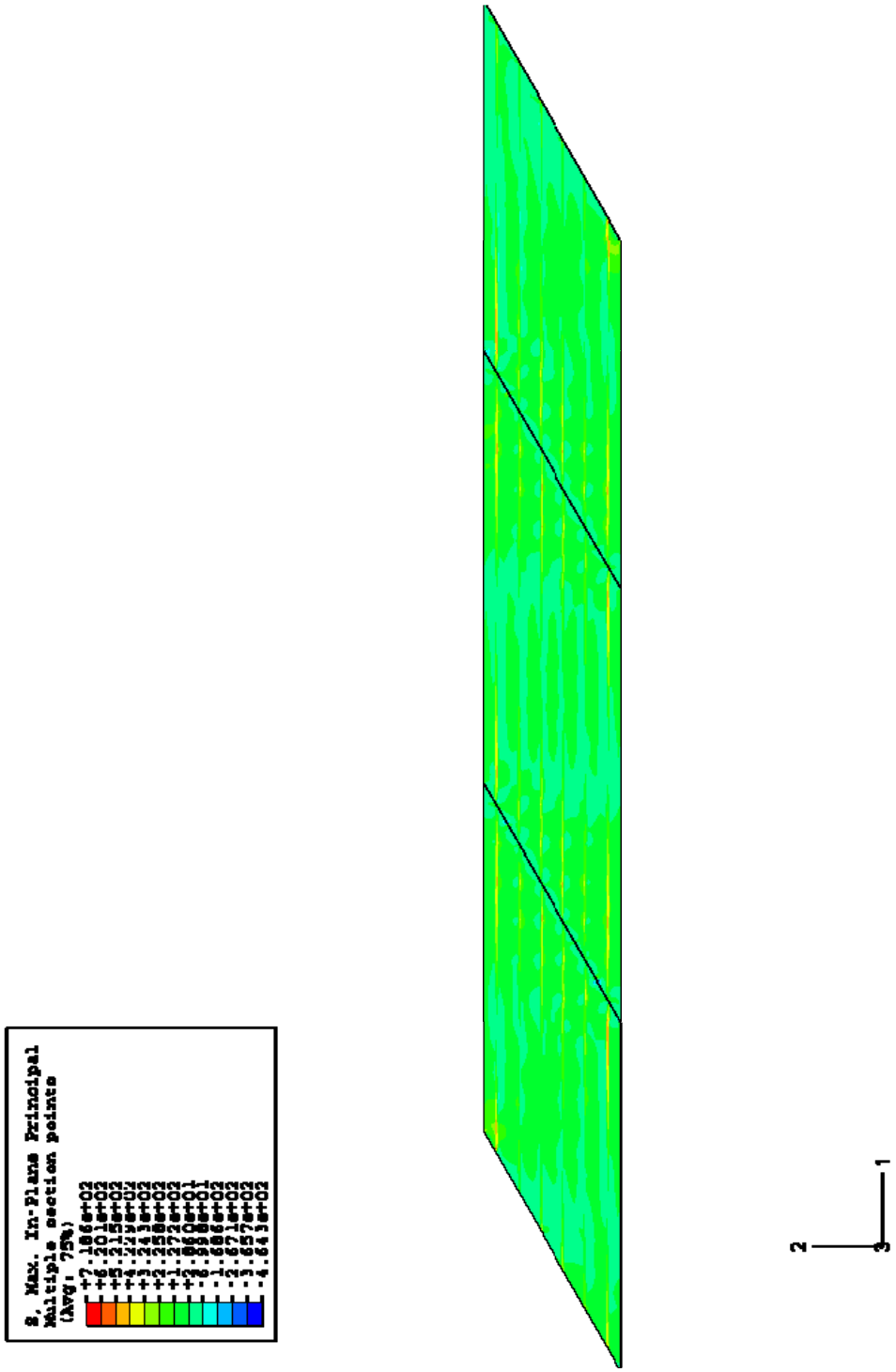

Figure 6-11: Full view of maximum principal stress distribution at the bottom of the deck for US 331 bridge, α = 61° (psi)

6.2.3.2 Detection of Cracking

For this study, in which a linear elastic material model was used to characterize the concrete deck, cracking was assumed to occur when the maximum principal tensile stress of the concrete reached its tensile strength. The tensile strength was defined as 600 psi, based on early field testing results of the concrete deck material. By studying the contours of the maximum principal stress (Figures 6-8 and 6-9), one can identify the cracked area of the model according to the stress level of the elements. Figures 6-12 and 6-13 highlight the cracking zone of the bridge deck. For these figures, and for similar figures in the remaining sections of this chapter, the red-colored elements are those identified by ABAQUS as possessing maximum principal stresses greater than the cracking stress.

As can be seen, at the top surface, cracking primarily occurs at the areas surrounding the intermediate supports. Additionally, the crack distribution exhibits the same degree of skew as the deck. Several strip areas in the longitudinal direction are cracked at the top surface. It is believed that this cracking is due to the contribution of the girder stiffness, which increases the bending stress relative to areas that are further removed from the girders.

At the bottom of the deck, the tensile stress produced was not very large, because this surface is much nearer to the neutral axis of the composite section than is the top surface. The remaining deck area that is not shown in these figures (surrounding the midpoint of each span) only exhibited a few minor cracks in the model results, and was therefore not presented in the figures here. These areas experienced either compressive stress, or very small amounts of tensile stress.

The direction of the maximum principal tensile stress can indicate the orientation of the crack for each cracked element. Using the SYMBOLS function of ABAQUS, symbols (headless arrows here) can be plotted that display the relative magnitude of the stress through varying symbol lengths (the greater the length of the headless arrow, the greater the magnitude of stress), while the orientation of the symbol corresponds to the axis normal to the crack. In Figure 6-14, these symbols are shown as the black lines for the top deck surface.

From these results, it can be observed that cracking is somewhat extensive on the top surface of the deck near the intermediate supports. Additionally, almost all of the cracks are oriented parallel to the bent, which possessed the same degree of skew as the bridge deck. The remaining few cracks are located near the edge of the deck at the support.

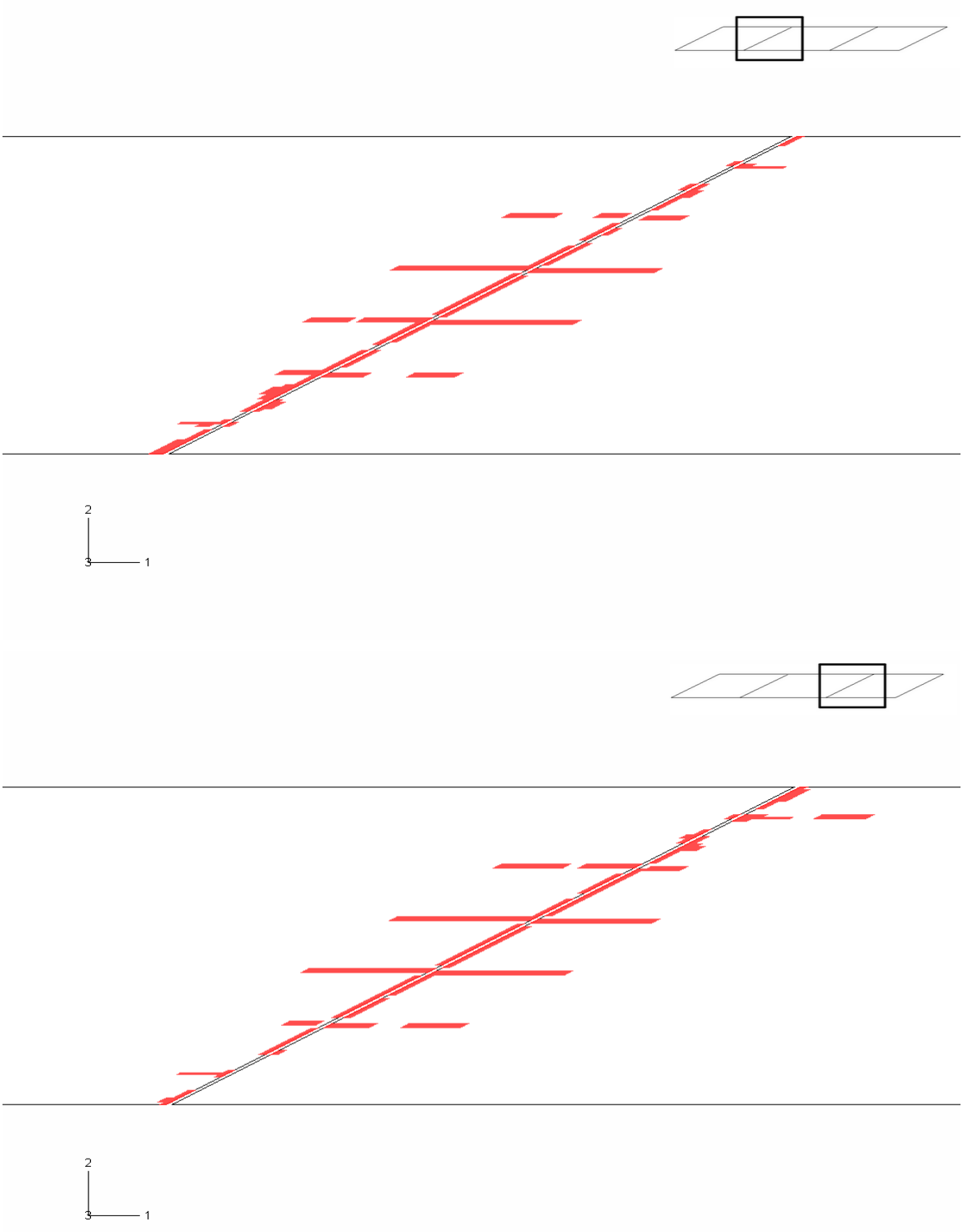

Figure 6-12: Cracked zone at the top of the deck for the US 331 bridge, α = 61°

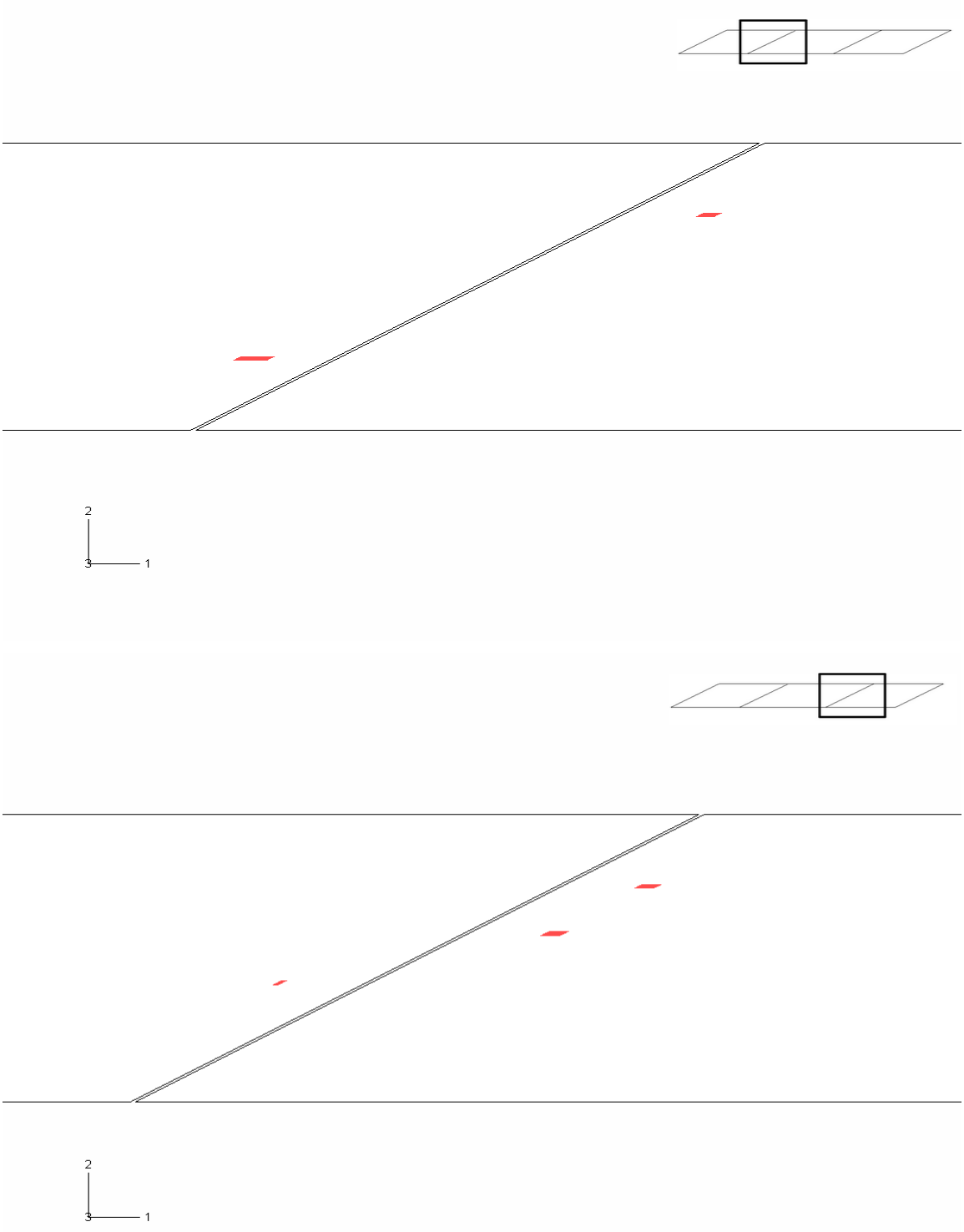

Figure 6-13: Cracked zone at the bottom of the deck for the US 331 bridge, α = 61°

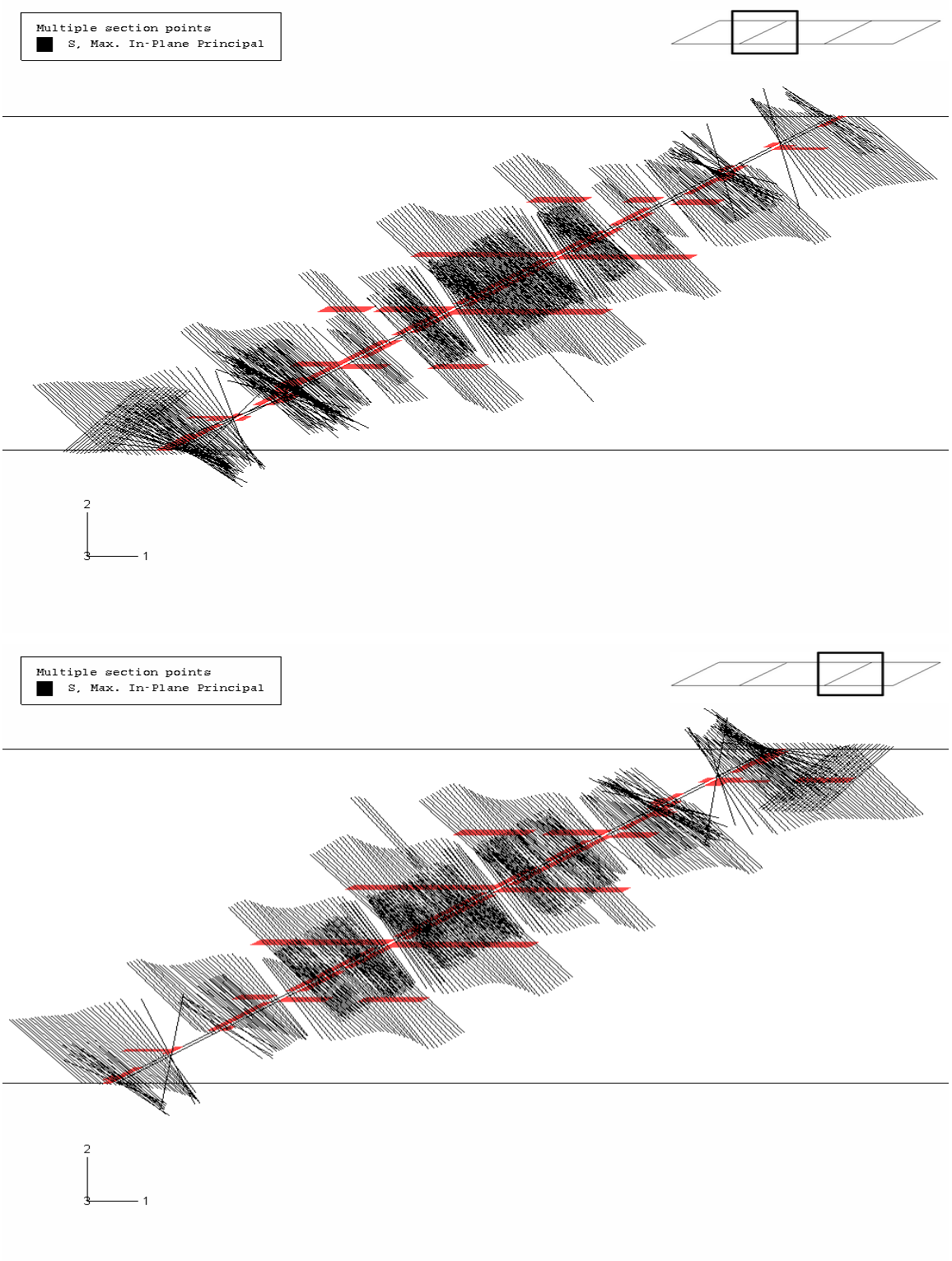

Figure 6-14: Normal direction of cracks (black lines) at top of deck, US 331 bridge, α = 61°

At the bottom surface of the deck, despite the fact that a very small number of cracked elements were observed, as shown in Figure 6-13, no black lines were indicated by ABAQUS. This is because the black lines represent the stress level at the finite-element integration points, while the highlighted cracked zone is determined by the element nodal values of stress. There is a difference between these two values because ABAQUS employs an algorithm to interpolate nodal values from calculated values at the integration points. Due to this difference, at the bottom surface of the deck, the stress at the integration points has not reached the cracking stress, so there are no black lines, but one or more interpolated nodal values have reached the cracking stress, so elements with those nodes have been highlighted as cracked elements.

The crack illustration sequence employed above (plot of maximum principal stress, followed by a plot of cracked elements, followed by a display of the normals to the crack direction) will be utilized again in the next section, in which a parametric study of bridge deck behavior is described.

6.3 PARAMETRIC STUDY

6.3.1 Effect of Skew

Skewed bridges like the bridge on US 331 are often necessary because of the alignment of the roadway and the obstruction that needs to be crossed. However, when the skew angle is larger than 30 degrees, it is quite possible that the effect of the skew becomes significant to the behavior of the bridge. Previous researchers have found that skewed bridges are at risk of experiencing greater vertical defections and bending moments than similar, non-skewed bridges (Choo et al. 2005).

Figures 6-15 to 6-22 show the results obtained from the finite-element model of the US 331 bridge, modified to include 0°-, 30°-, and 45°-skew angles, instead of the actual skew angle of 61°. Each of these models possessed the same characteristics, and the same load, as the base model discussed in Section 6.2; only the skew angle was changed. From the results presented in the previous section, it was evident that most cracking occurred at the top surface of the deck near the intermediate supports, where large tensile stresses were experienced. Therefore, for the parametric study, only the results for the top surface of the deck were monitored. The deck areas which are not shown in the following figures (far removed from the interior bents) only exhibited a very few cracked elements.

Again, because of the nature of the complex modeling utilized for the very narrow areas just over the intermediate supports (detailed in Figure 6-4), some unrealistic stresses were produced at these locations. As was the case for the model with the actual bridge skew angle, these abnormal stress results were ignored during the analysis of the results of the parametric

study, and they are not displayed in the two narrow strip areas above the interior supports in the following figures.

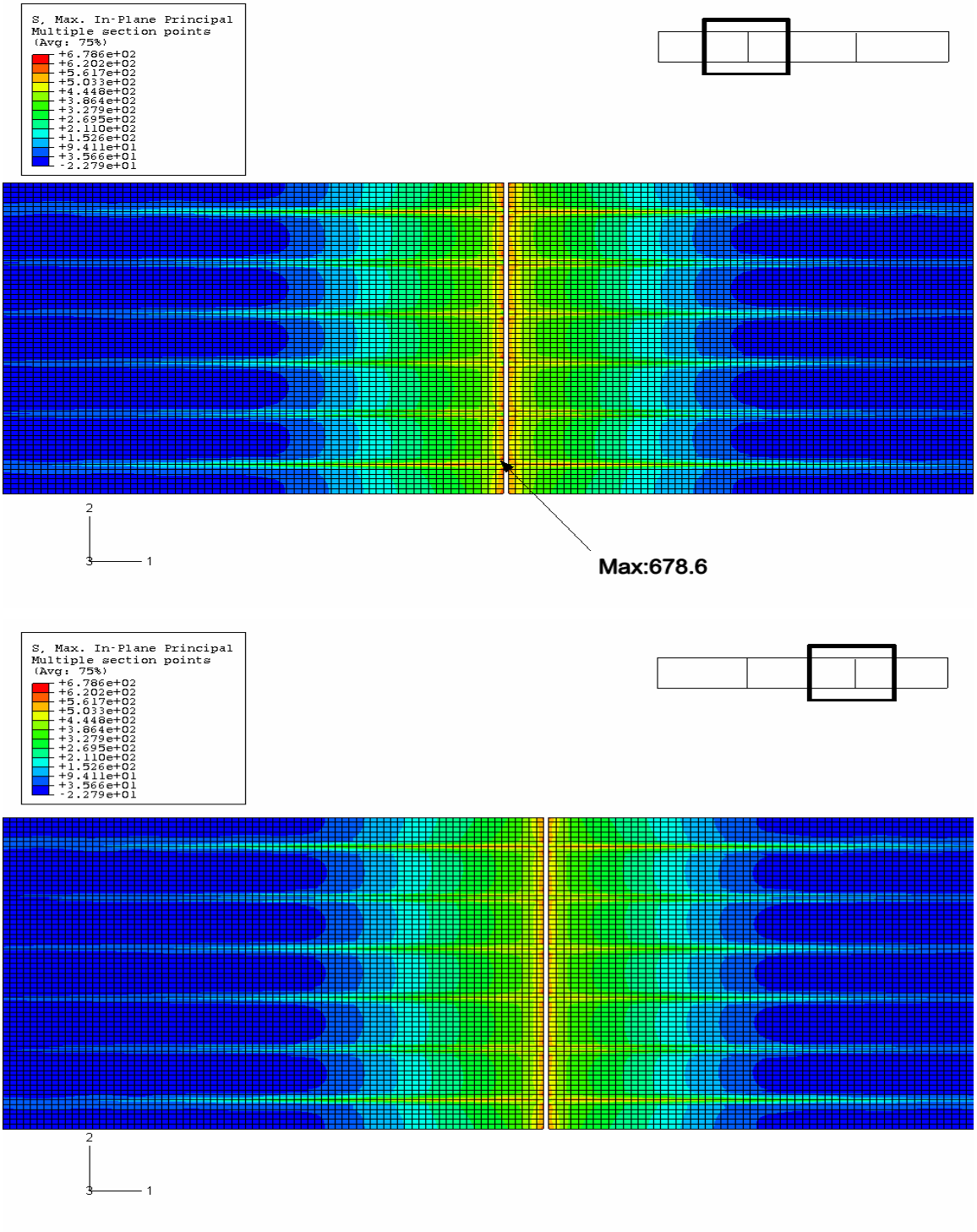

Figure 6-15: Maximum principal stress distribution at top of 0°-skewed deck (psi)

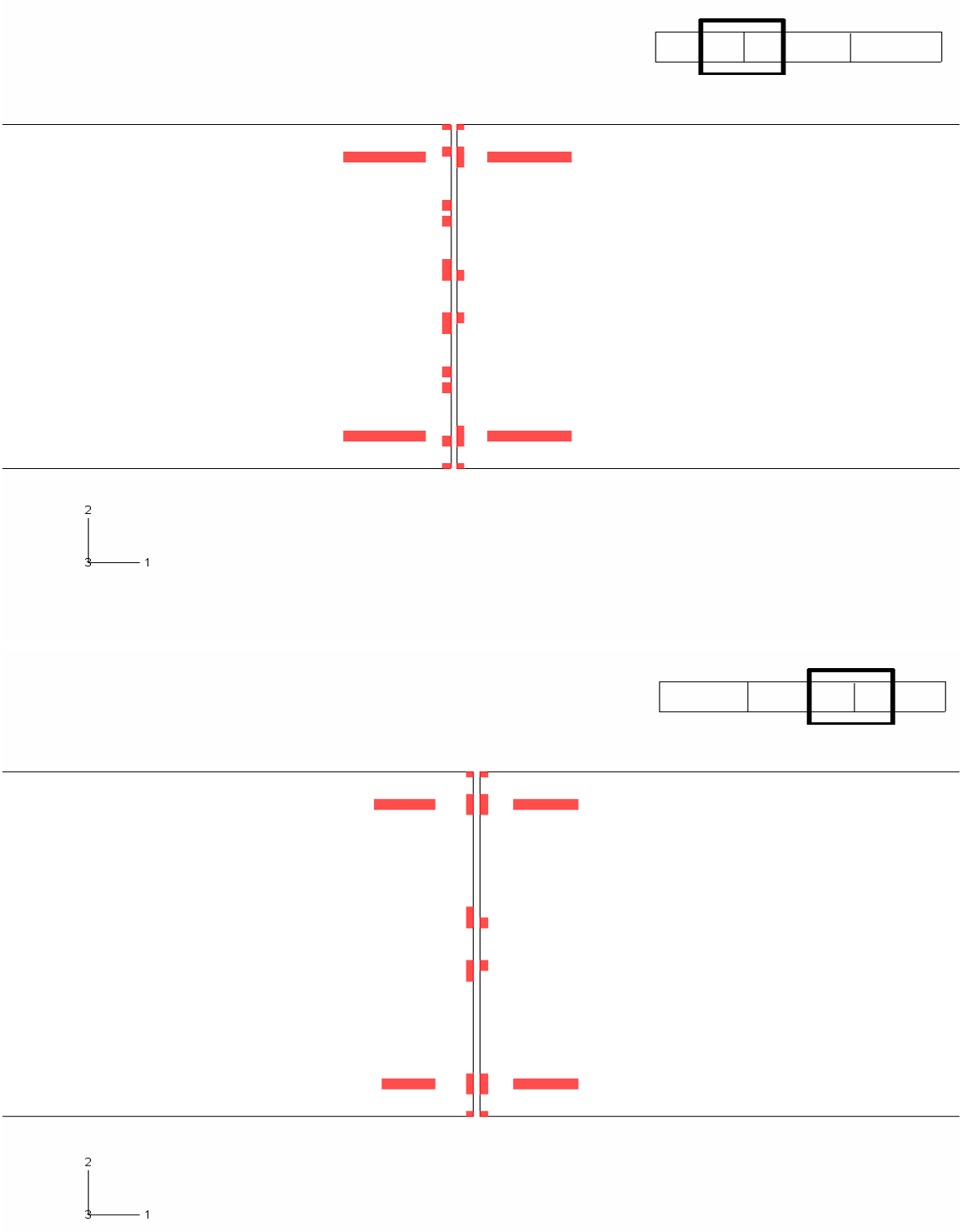

Figure 6-16: Cracking zone at top of 0°-skewed deck

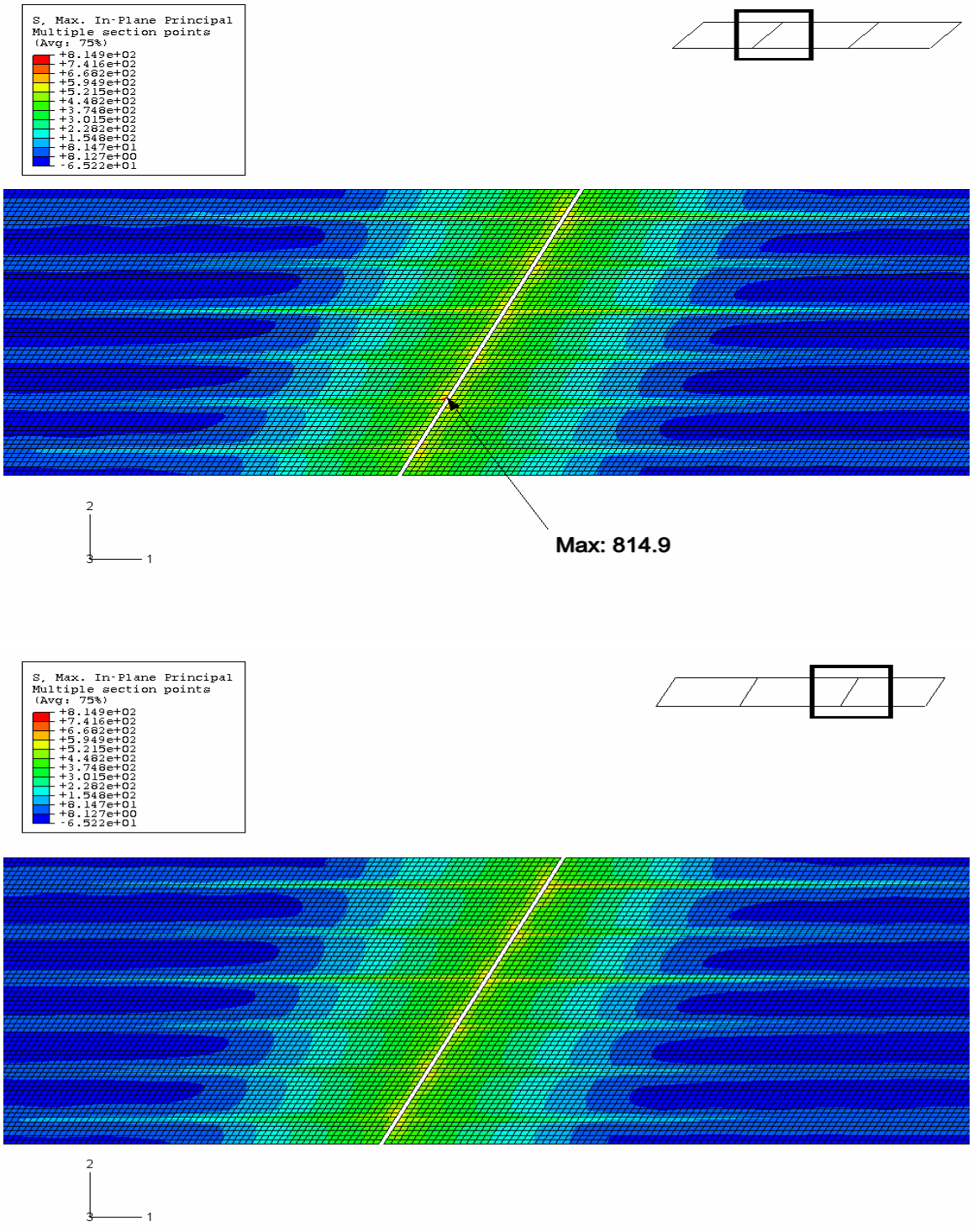

Figure 6-17: Maximum principal stress distribution at top of 30°-skewed deck (psi)

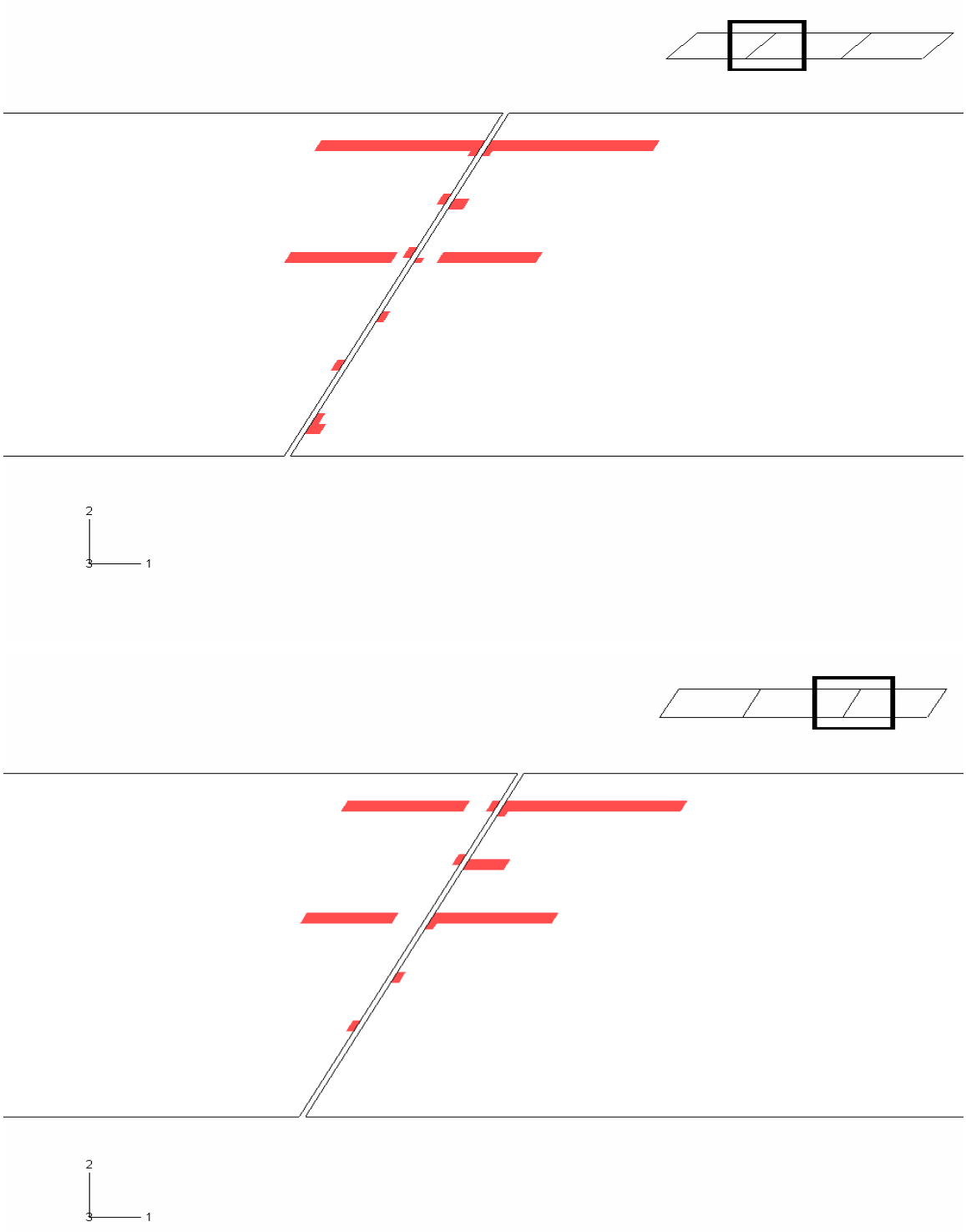

Figure 6-18: Cracking zone at top of 30°-skewed deck

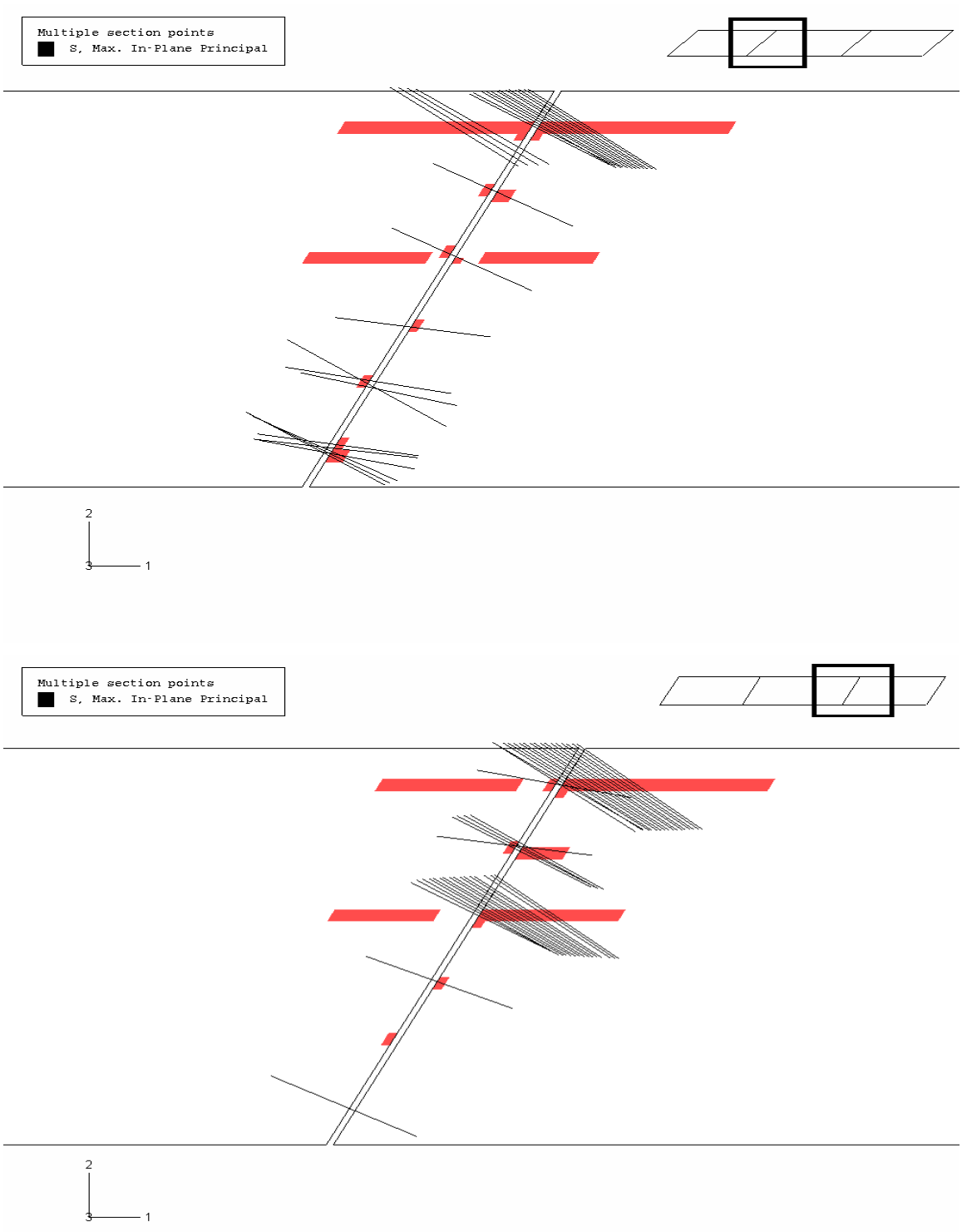

Figure 6-19: Normal direction of cracking (black lines) at top of 30°-skewed deck

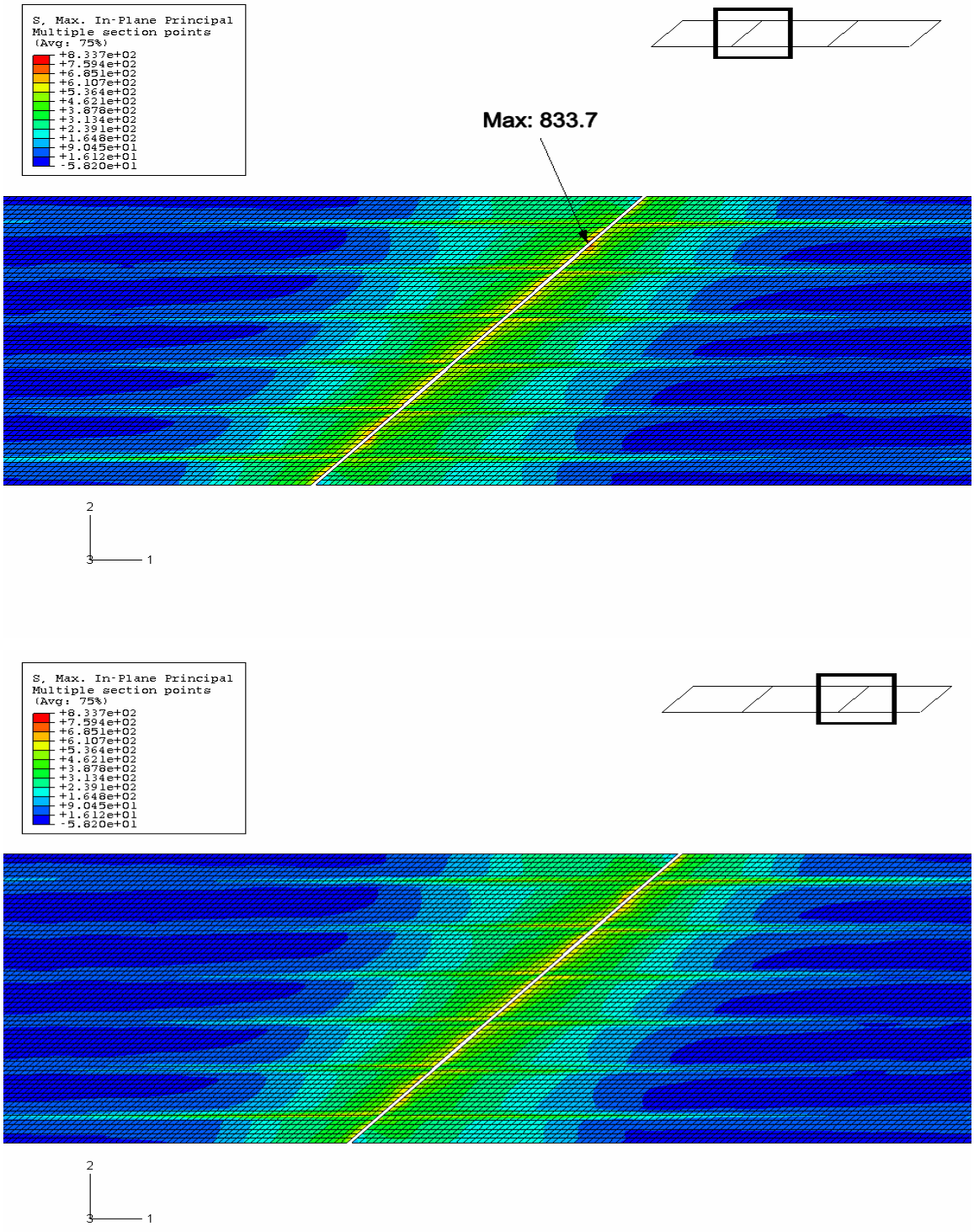

Figure 6-20: Maximum principal stress distribution at top of 45°-skewed deck (psi)

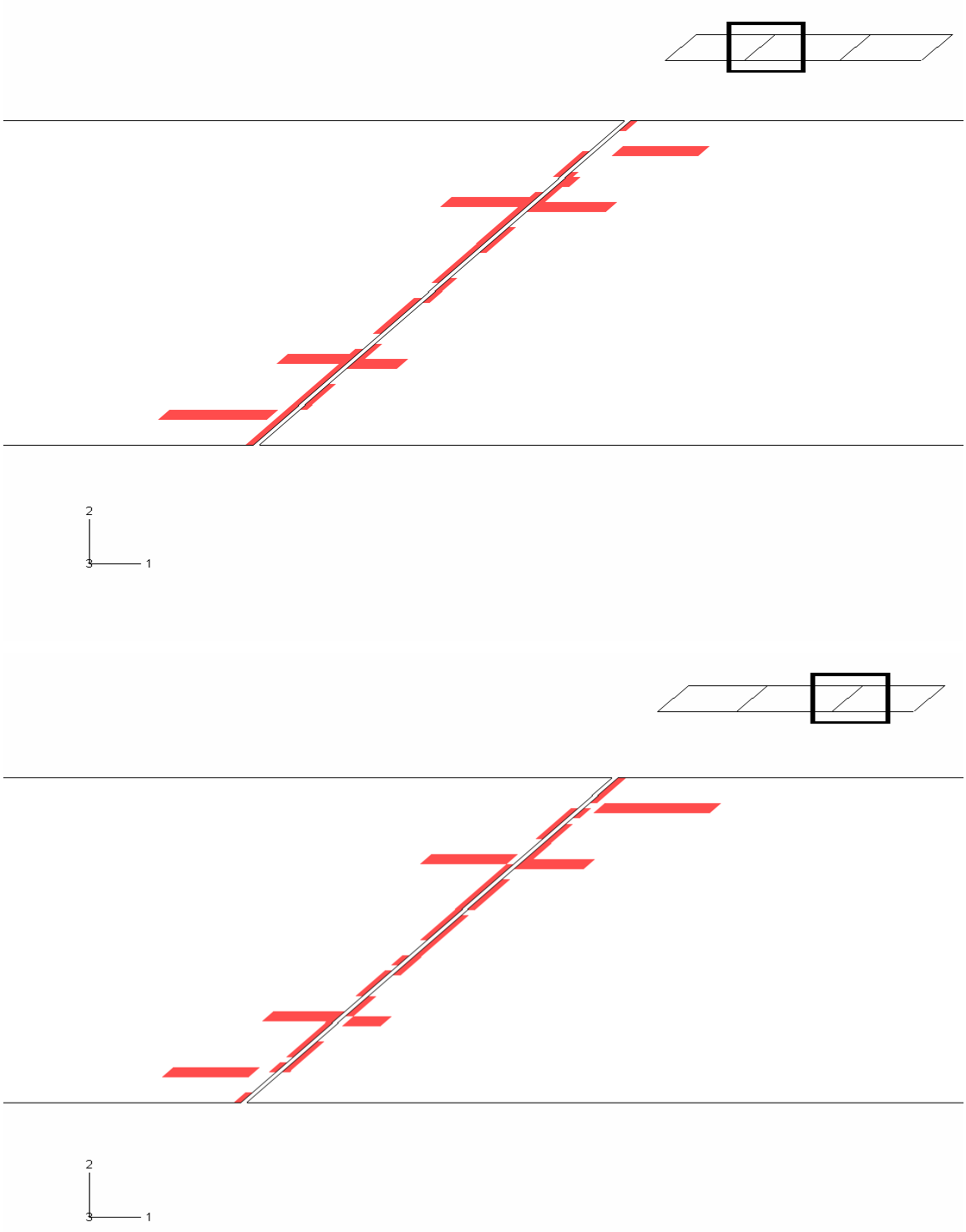

Figure 6-21: Cracking zone at top of 45°-skewed deck

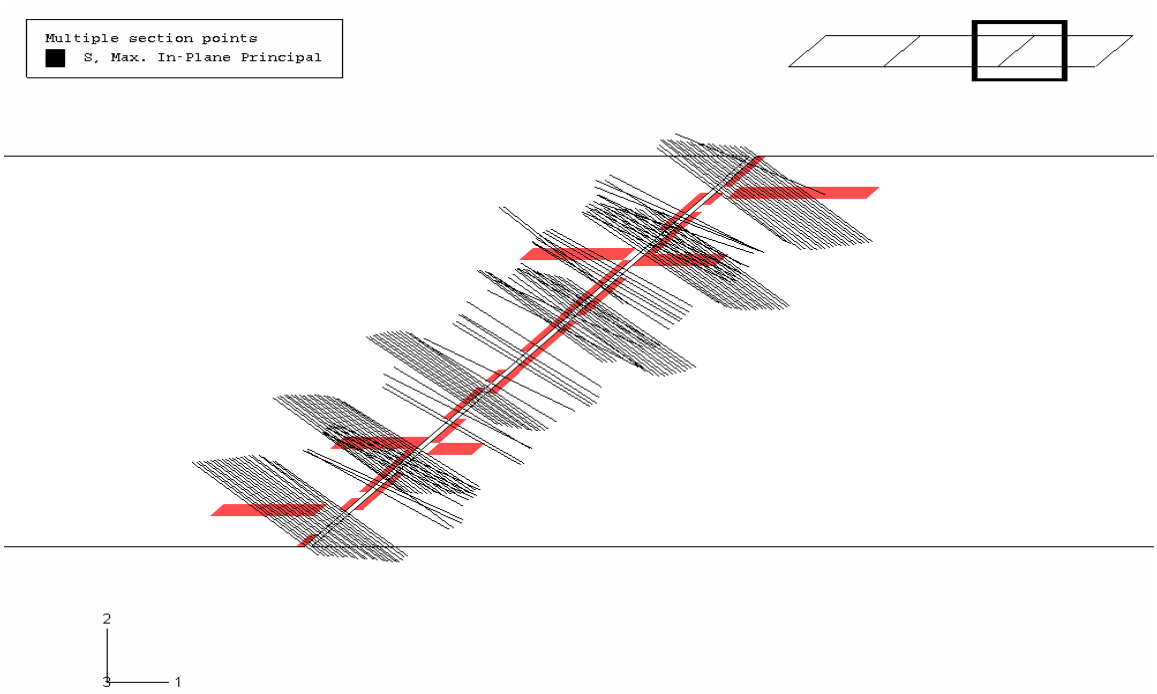

Figure 6-22: Normal direction of cracking (black lines) at top of 45°-skewed deck

Comparing these figures with the results obtained for the 61°-skewed deck model of Section 6.2, one can clearly see that the skew angle does indeed have an effect on the cracking behavior of the deck. Figure 6-23 shows a summary of the cracking information for the deck at the southern-most intermediate support of the bridge, as the skew angle is varied.

From the figure, it is readily evident that the value of the maximum principal stress within a skewed deck is notably higher than that for a similar, non-skewed deck. This phenomenon becomes somewhat extreme when the skew angle is as severe as 60 degrees, as was the case for the actual US 331 bridge deck. The black lines in the figures are the symbols representing the maximum principal stresses in elements, which have reached cracking level. (It is observed that there are cracked elements indicated for the 0° skew case, but no black lines are present. This is again due to the slight difference between integration point stress values and nodal point stress values.) Additionally, as was mentioned earlier, the direction of the black lines represents the normal to the axis of cracking.

From these figures, one can see that the black lines become longer and more densely populated as the skew angle increases. Their direction also varies as the skew angle varies. These results indicate that a more highly skewed deck not only results in higher tensile stresses and more cracking at the top surface, but also that the distribution and direction of cracking is affected. The larger the skewed angle is, the greater the number of cracks and presumably, the wider the cracks will be as many of the individual cracks will likely coalesce into wider cracks. It

is also interesting to note that the cracking zone exhibits a similar skew angle as the deck in each model.

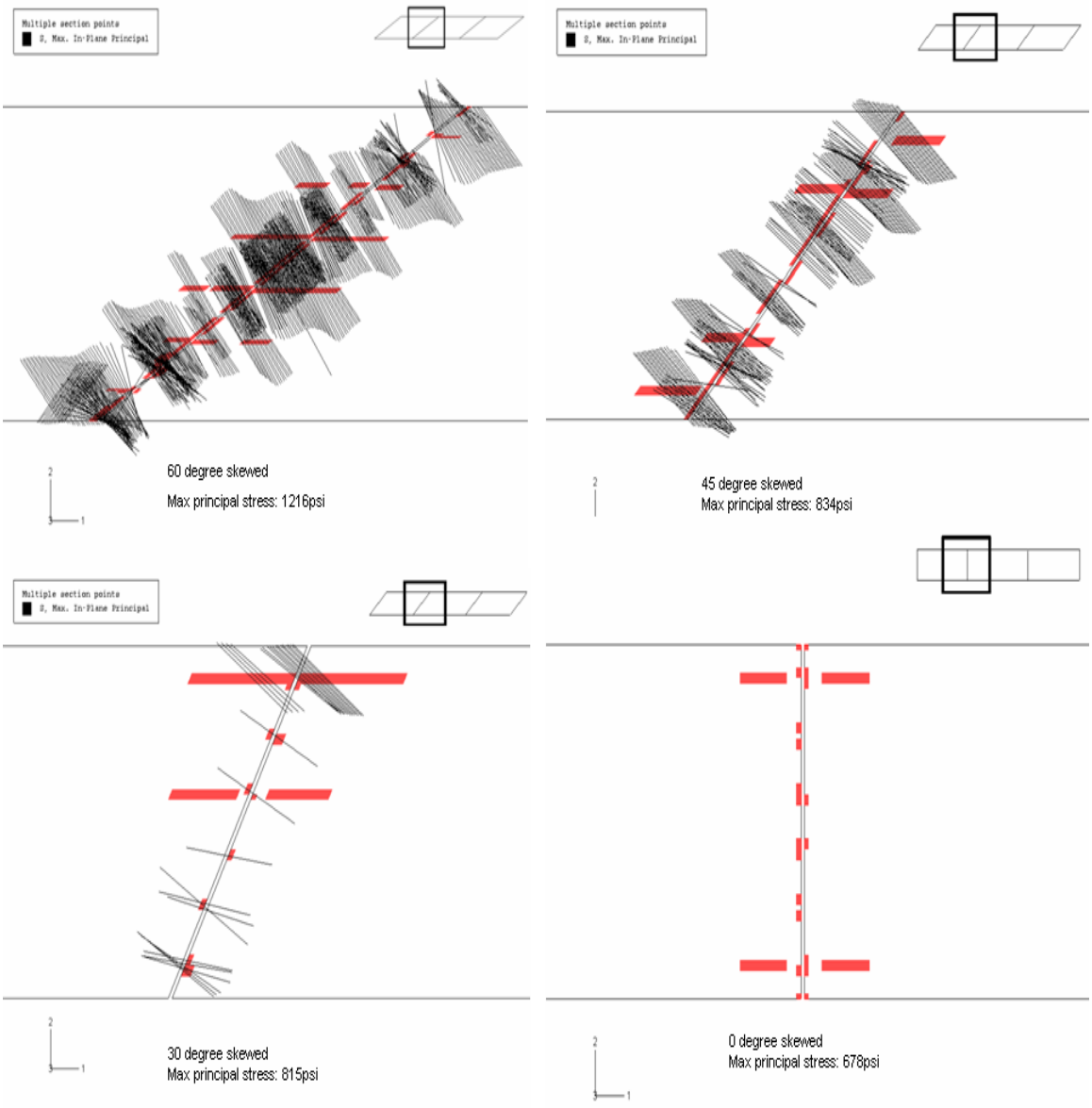

Figure 6-23: Deck cracking information at the southern-most intermediate support for various skew angles

6.3.2 Effect of Differential Support Settlement

Differential settlement of the supports was another possible influential factor affecting the cracking observed on the US 331 bridge deck. The effect of support settlement was examined numerically through the incorporation of changes in the boundary conditions for the US 331

bridge model (discussed in Section 6.2). As shown in Table 6-4 below, four combinations of the settlement of supports A, B, C and D (see Figure 6-24 for their locations) were imposed on the model to study their effect. A unit settlement (1 inch) was used in each of the four cases. Rrsults for the deformation, stress distribution, and cracking information at the top of the deck for all settlement combinations are shown in Figures 6-25 to 6-40. These models possessed the same characteristics, and the same load, as the base model discussed in Section 6.2.

Table 6-4: Combinations of support settlement conditions for parametric study

Case	Support A	Support B	Support C	Support D
Case 1	0	0	0	↓
Case 2	0	0	↓	0
Case 3	↓	0	0	↓
Case 4	0	↓	↓	0

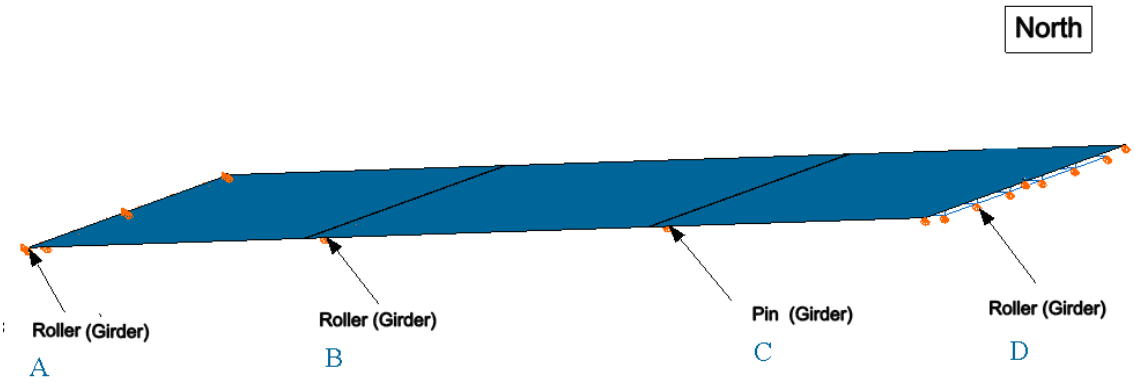

Figure 6-24: Locations of supports A, B, C, and D

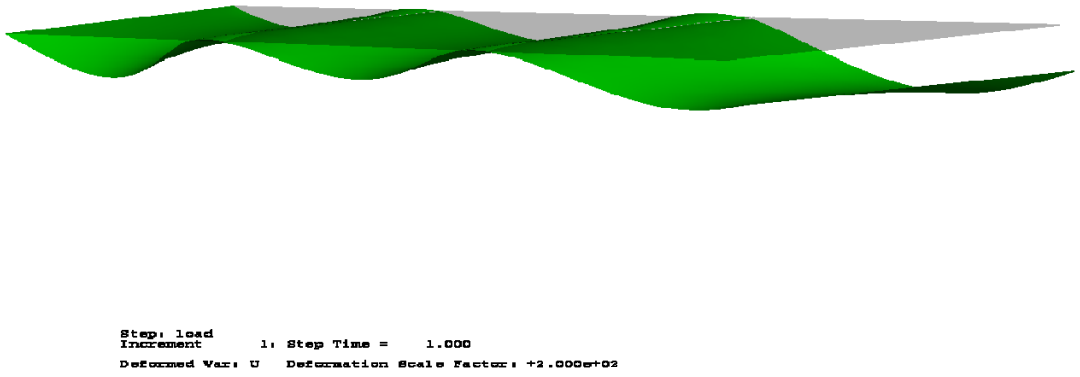

Figure 6-25: Deformed shape for Case 1
(Green: Deformed shape and Gray: Undeformed shape)

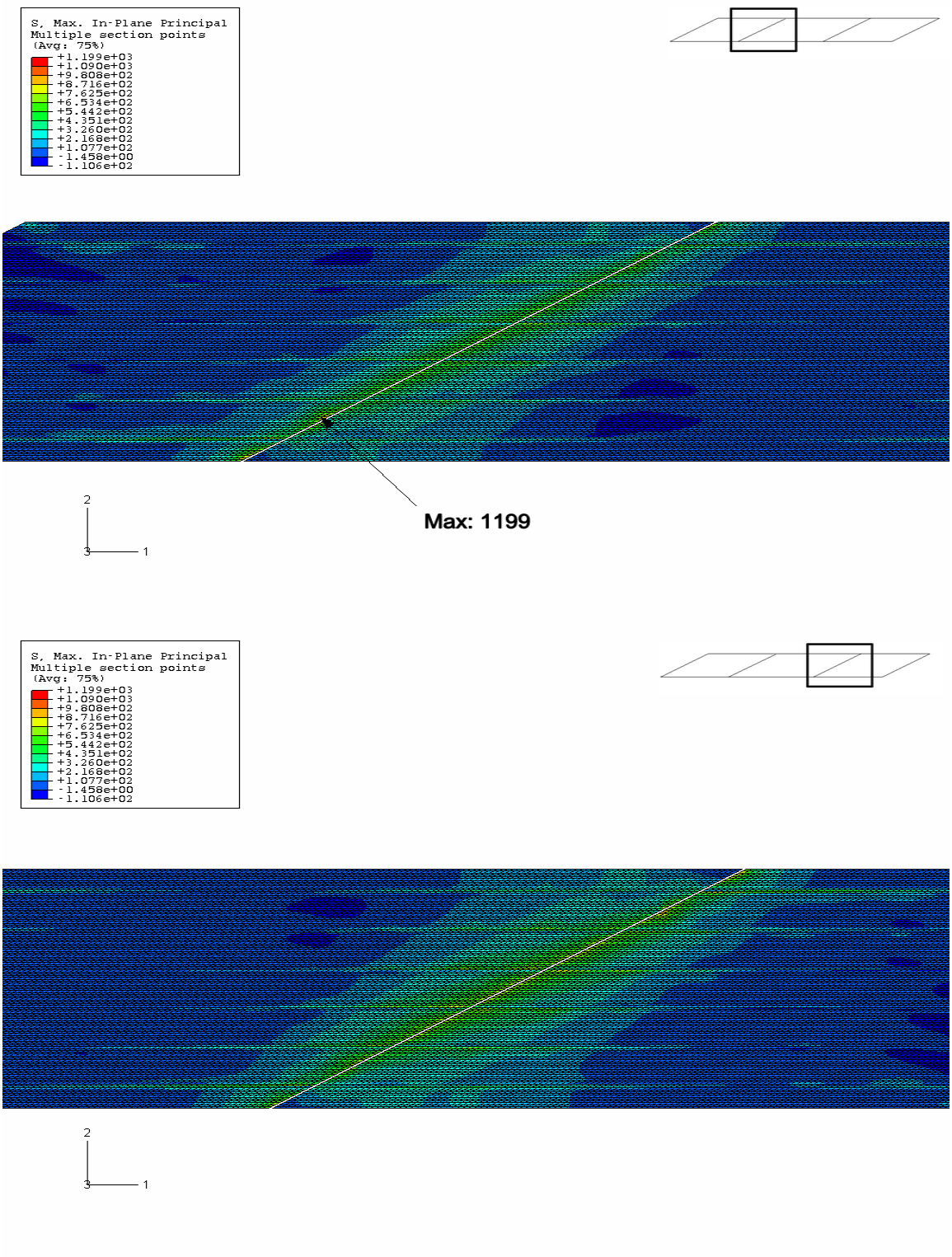

Figure 6-26: Maximum principal stress distribution at top of deck for Case 1 (psi), α = 61°

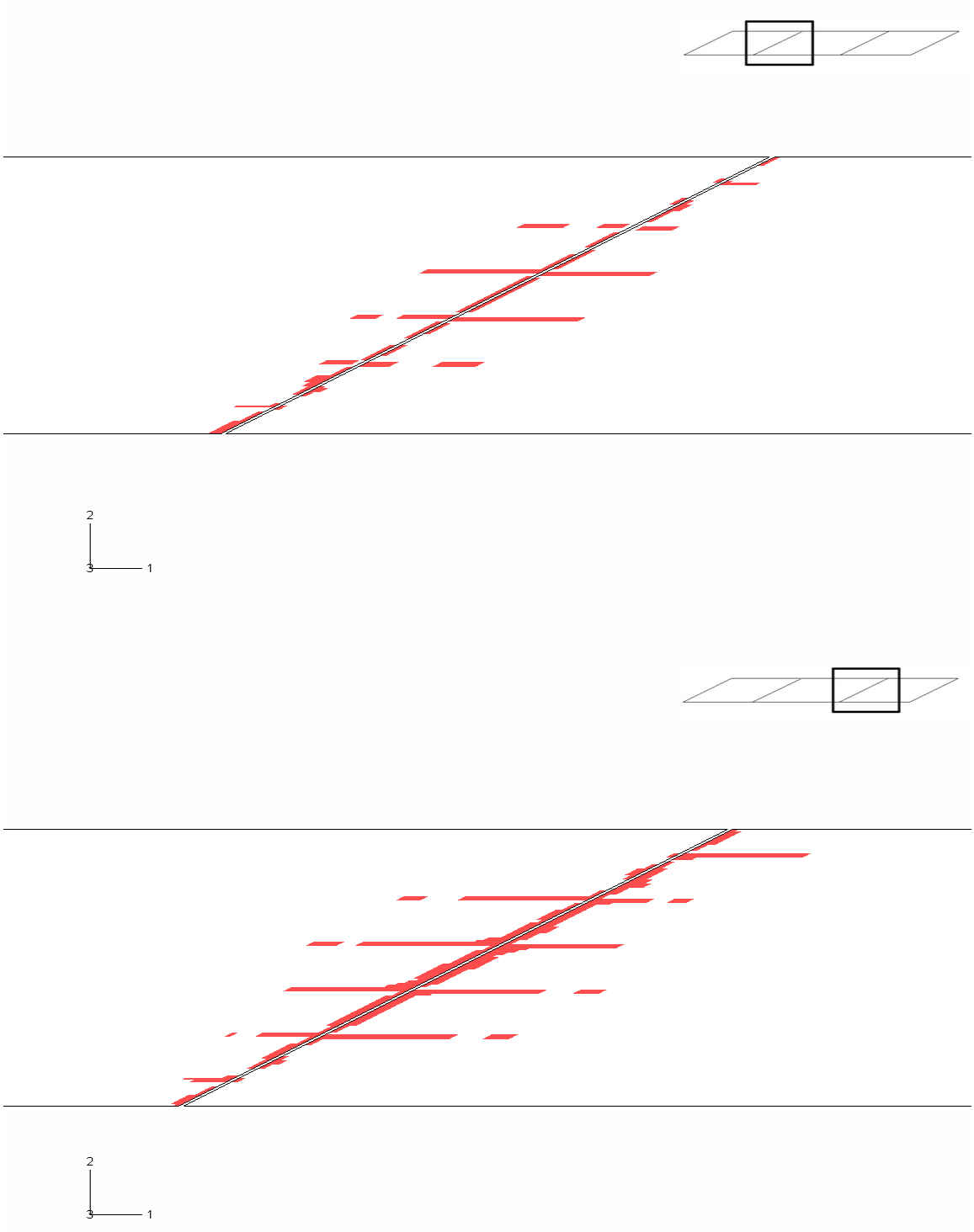

Figure 6-27: Cracking zone at top of deck for Case 1, α = 61°

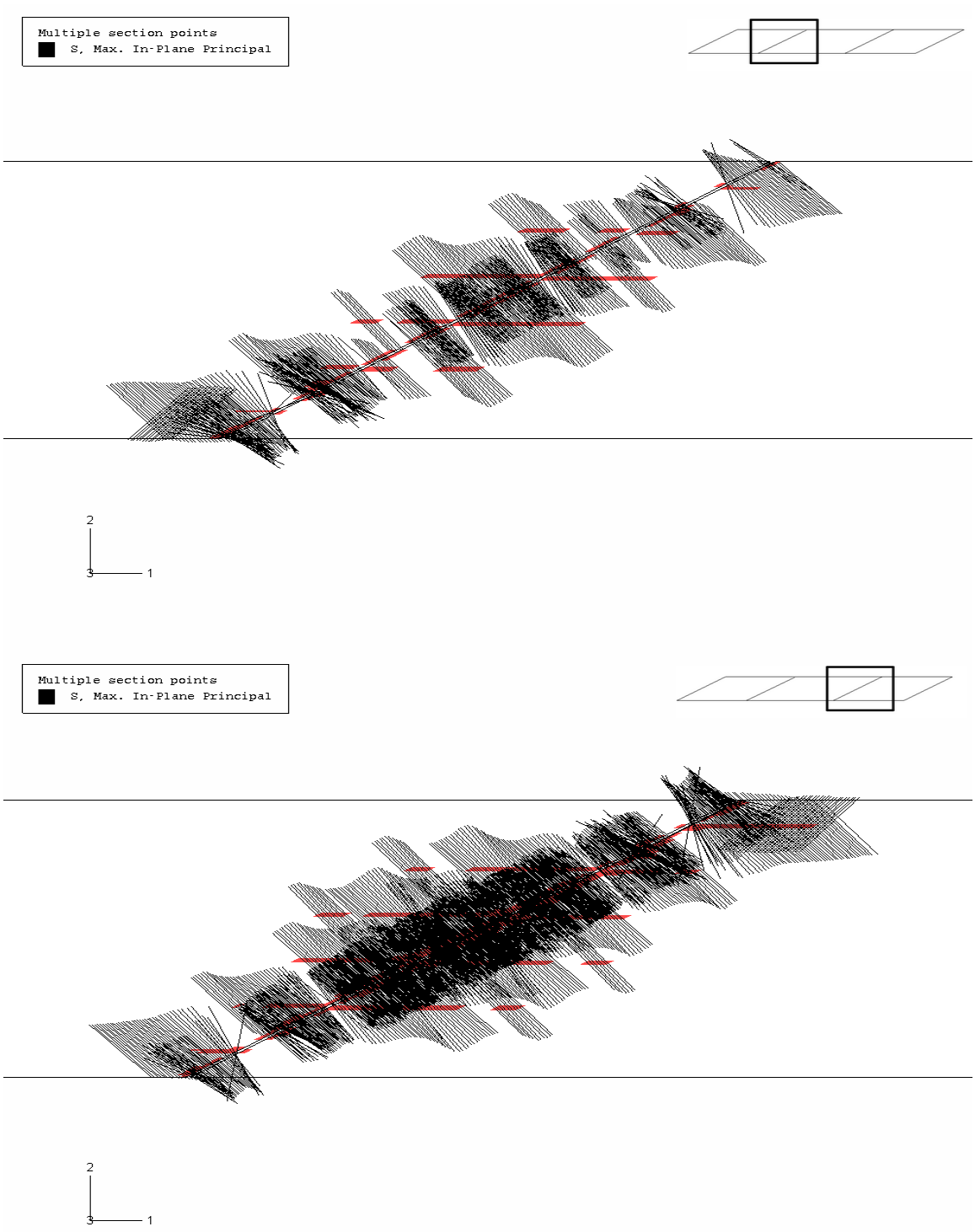

Figure 6-28: Normal direction of cracking (black lines) at top of deck for Case 1, α = 61°

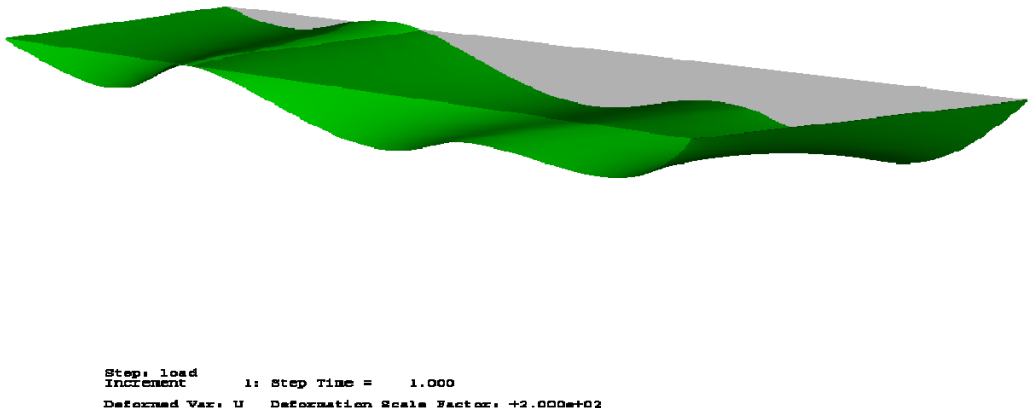

Figure 6-29: Deformed shape for Case 2
(Green: Deformed shape, Gray: Undeformed shape)

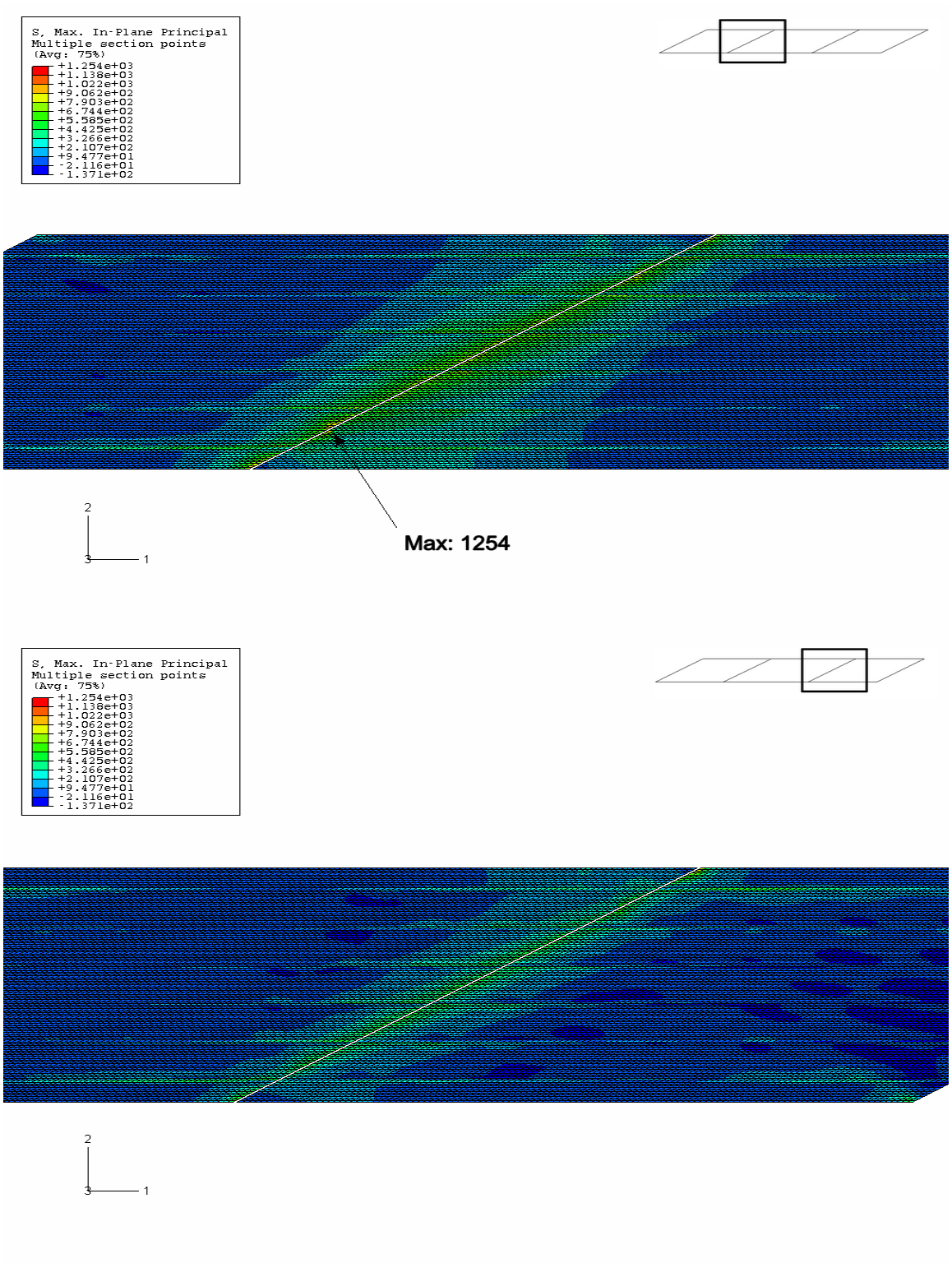

Figure 6-30: Maximum principal stress distribution at top of deck for Case 2 (psi), α = 61°

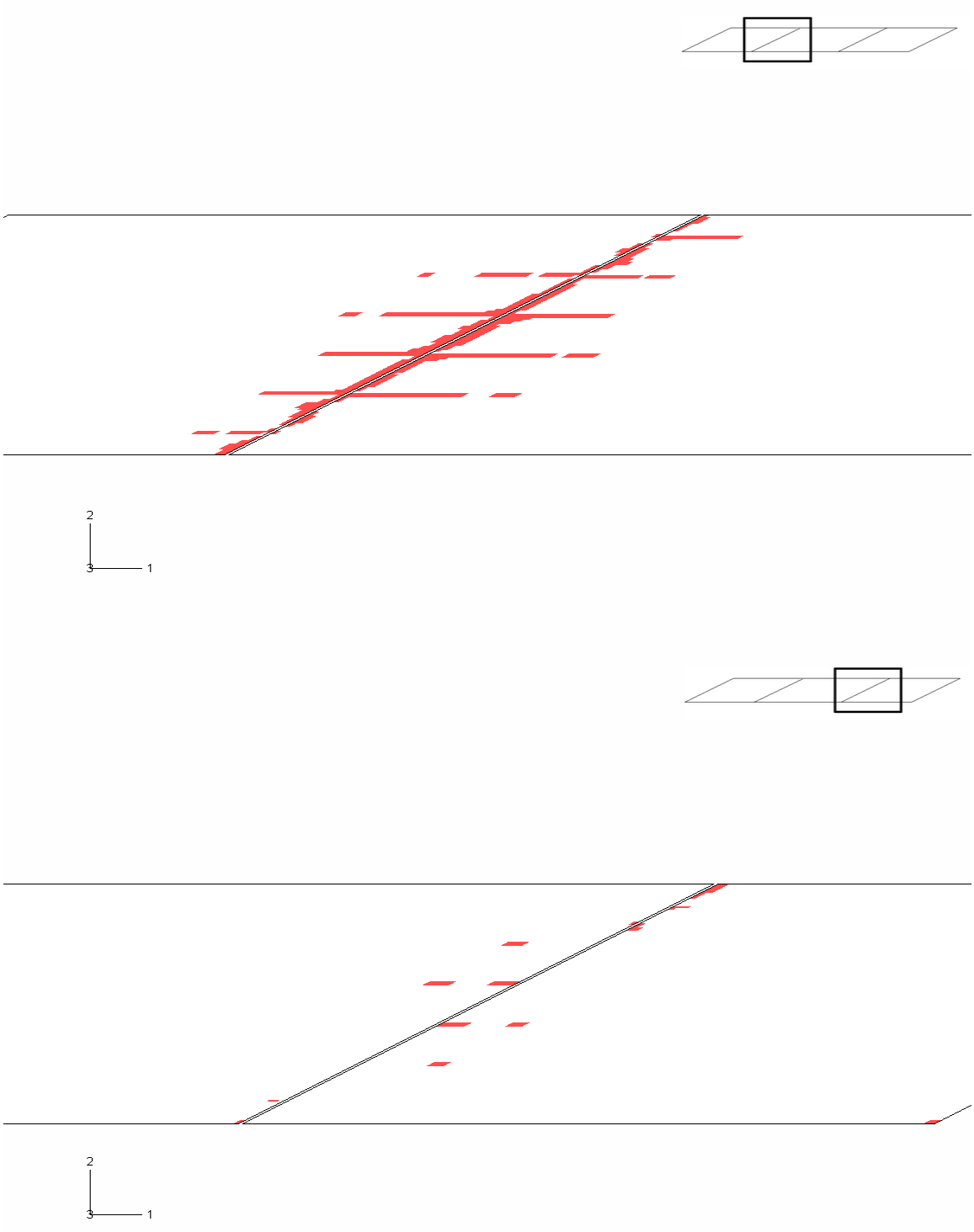

Figure 6-31: Cracking zone at top of deck for Case 2, α = 61°

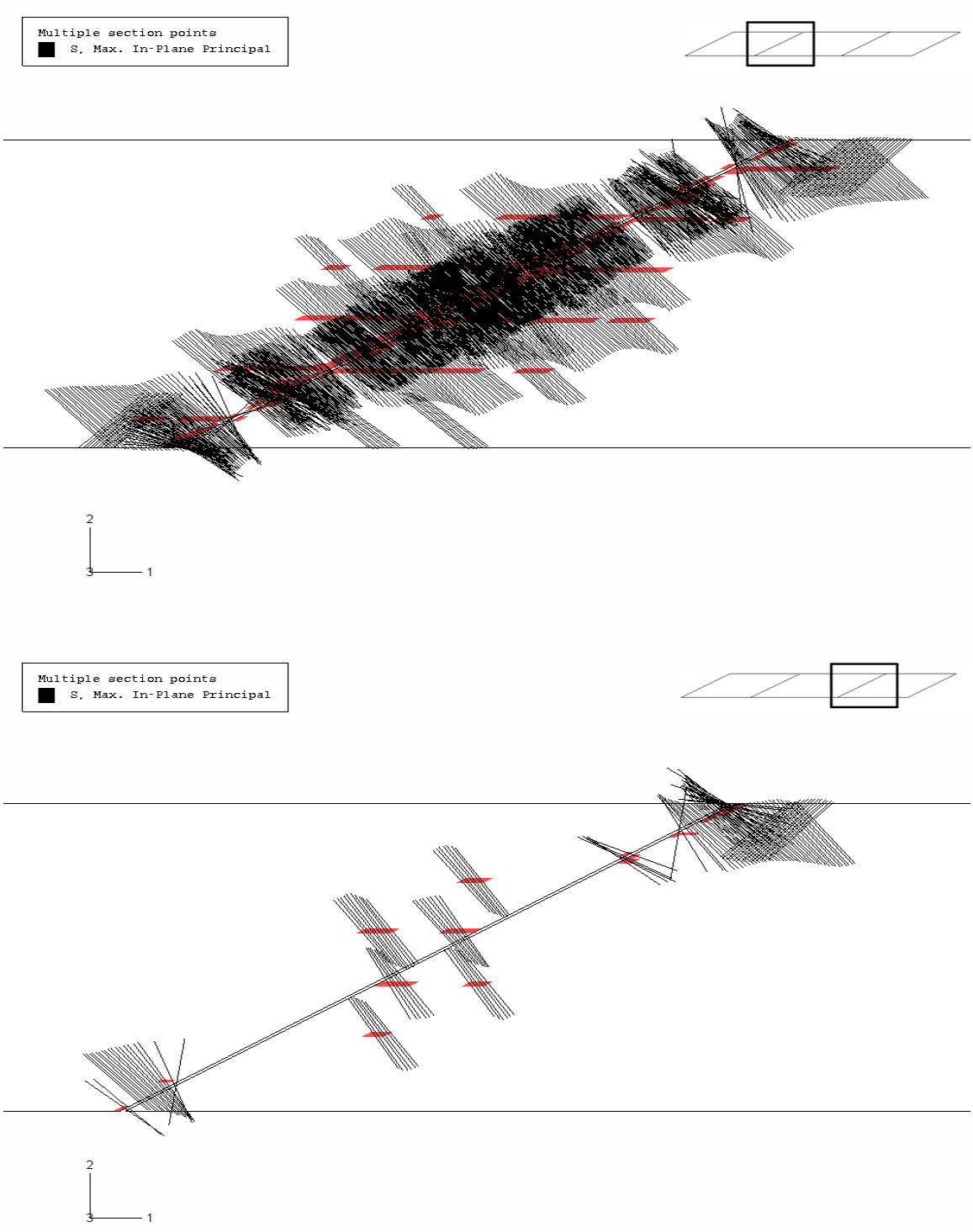

Figure 6-32: Normal direction of cracking (black lines) at top deck for Case 2, α = 61°

Figure 6-33: Deformed shape for Case3
(Green: Deformed shape, Gray: Undeformed shape)

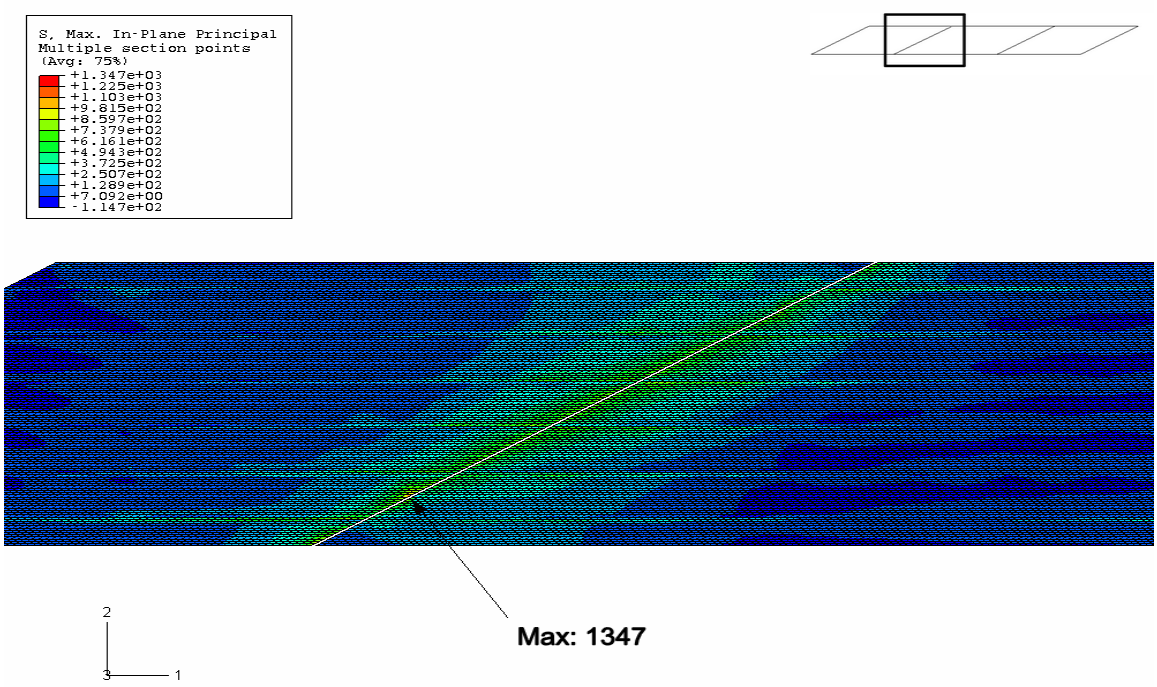

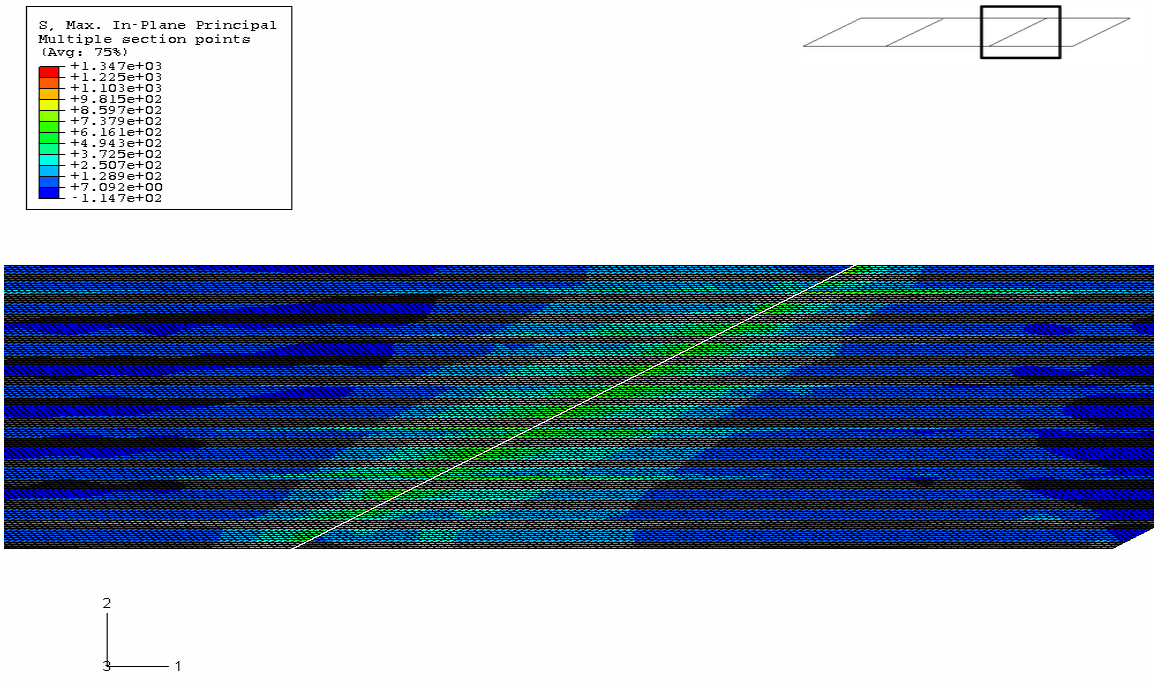

Figure 6-34: Maximum principal stress distribution at top of deck for Case 3 (psi), α = 61°

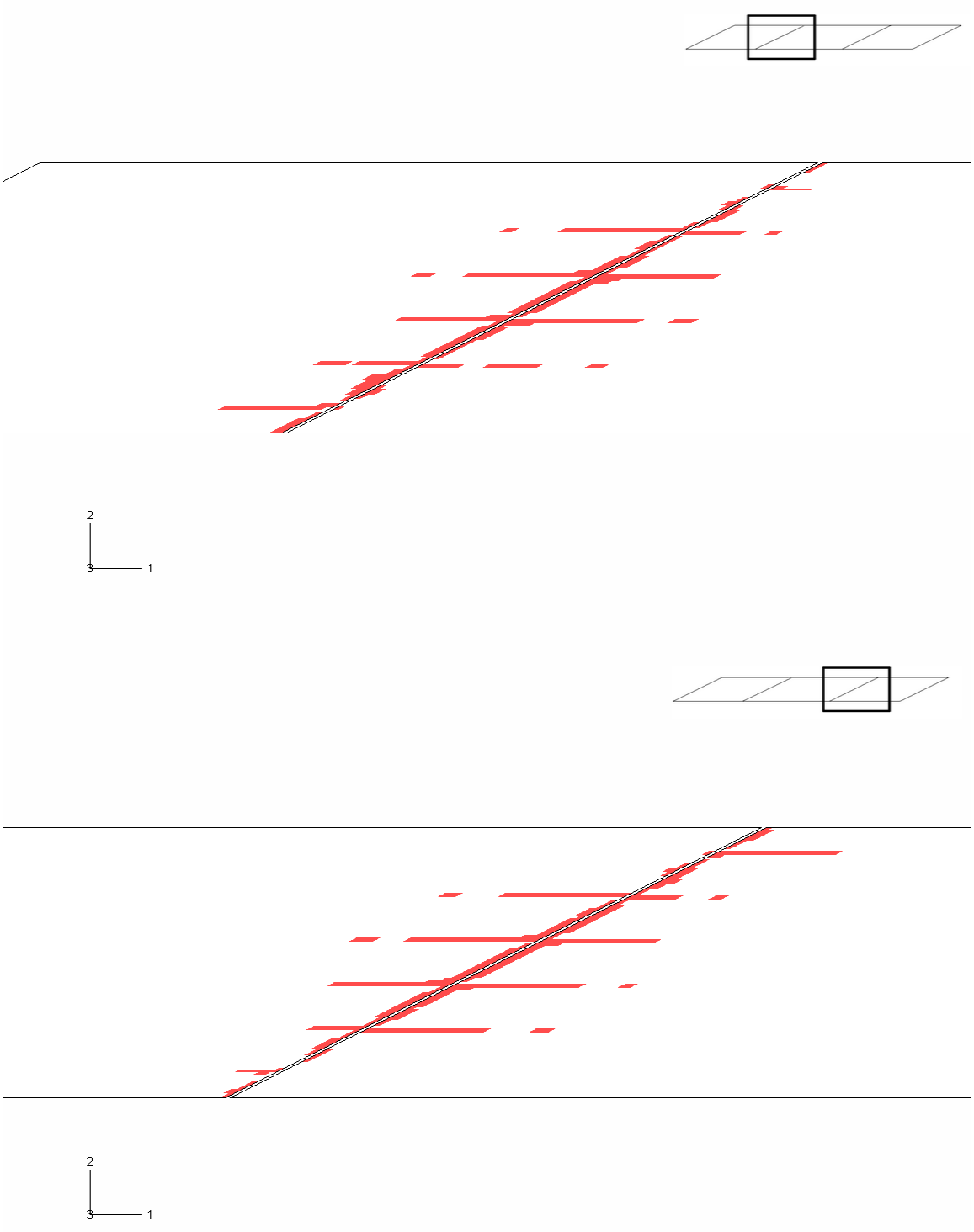

Figure 6-35: Cracking zone at top of deck for Case 3, α = 61°

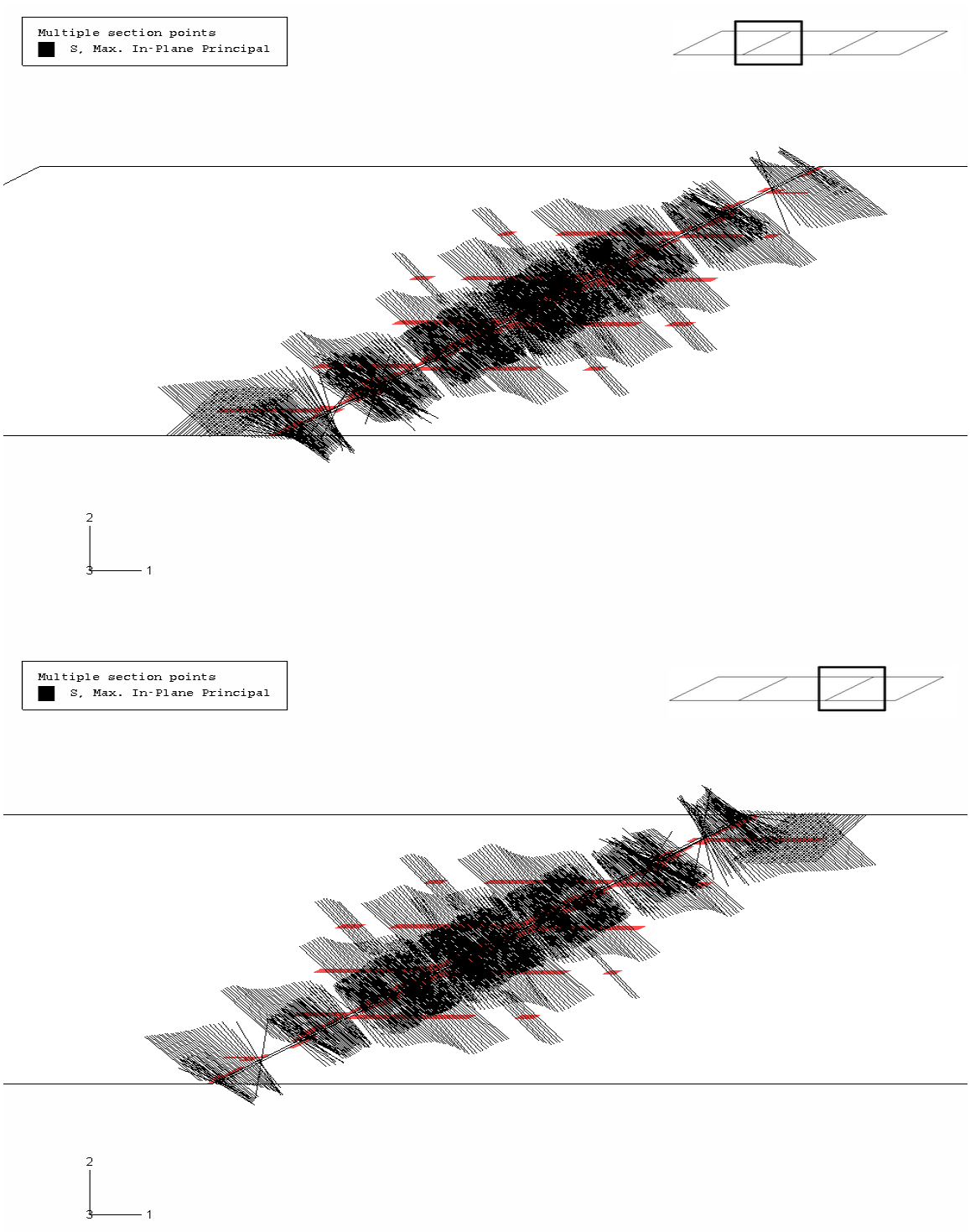

Figure 6-36: Normal direction of cracking (black lines) at top deck for Case 3, α = 61°

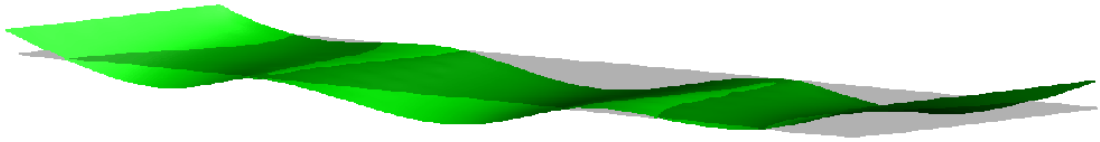

Figure 6-37: Deformed shape for Case 4
(Green: Deformed shape, Gray: Undeformed shape)

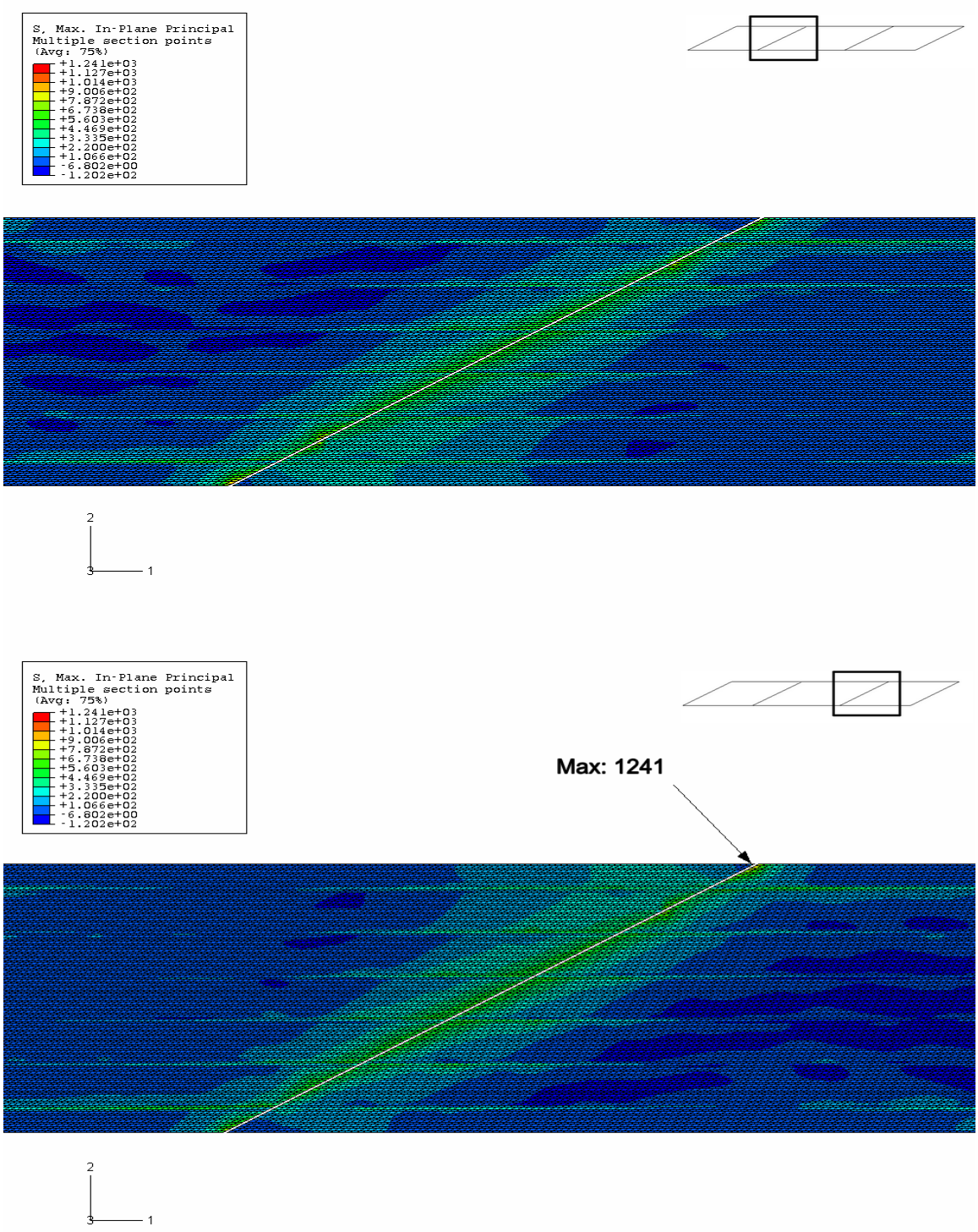

Figure 6-38: Maximum principal stress distribution at top of deck for Case 4 (psi), α = 61°

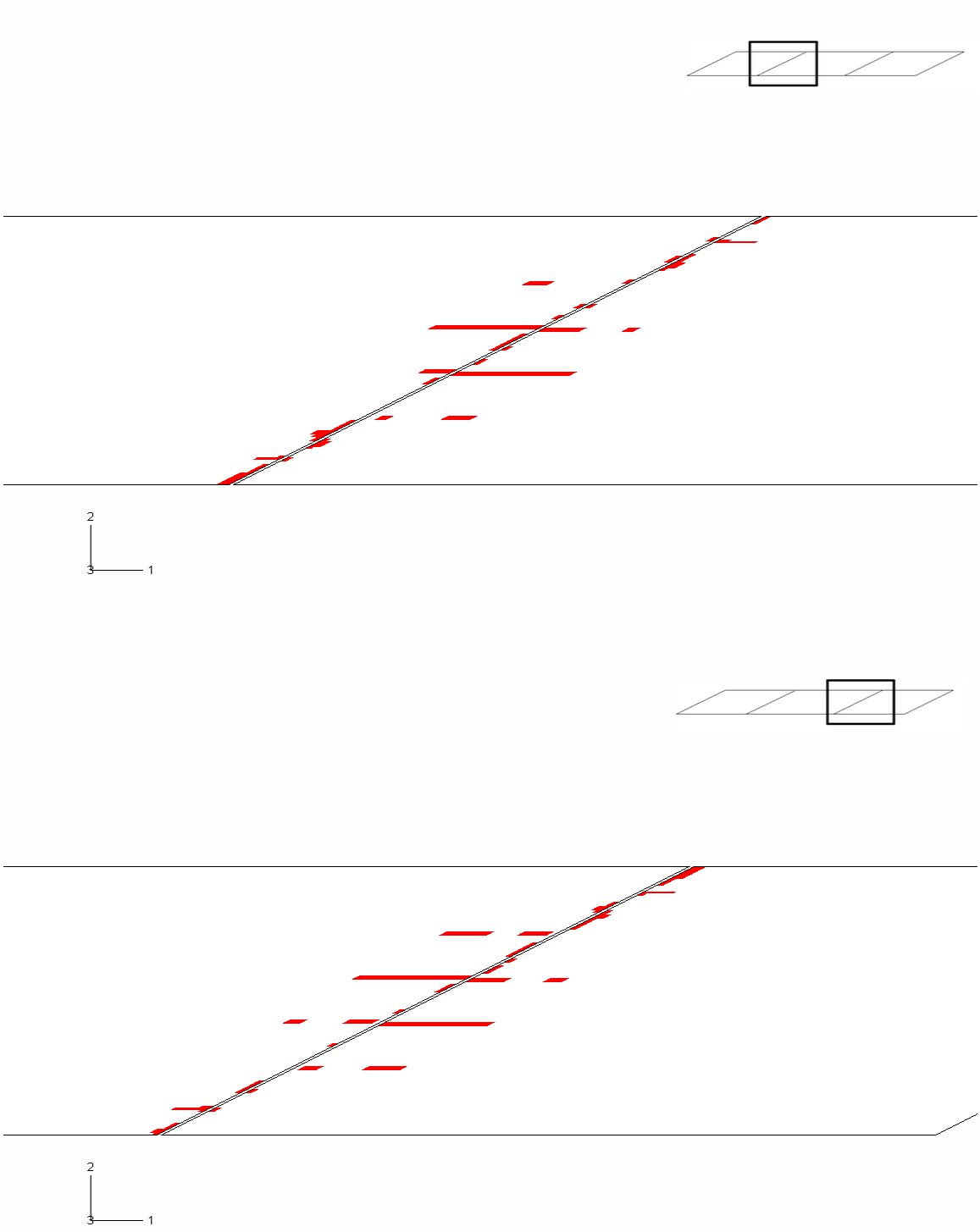

Figure 6-39: Cracking zone at top of deck for Case 4, α = 61°

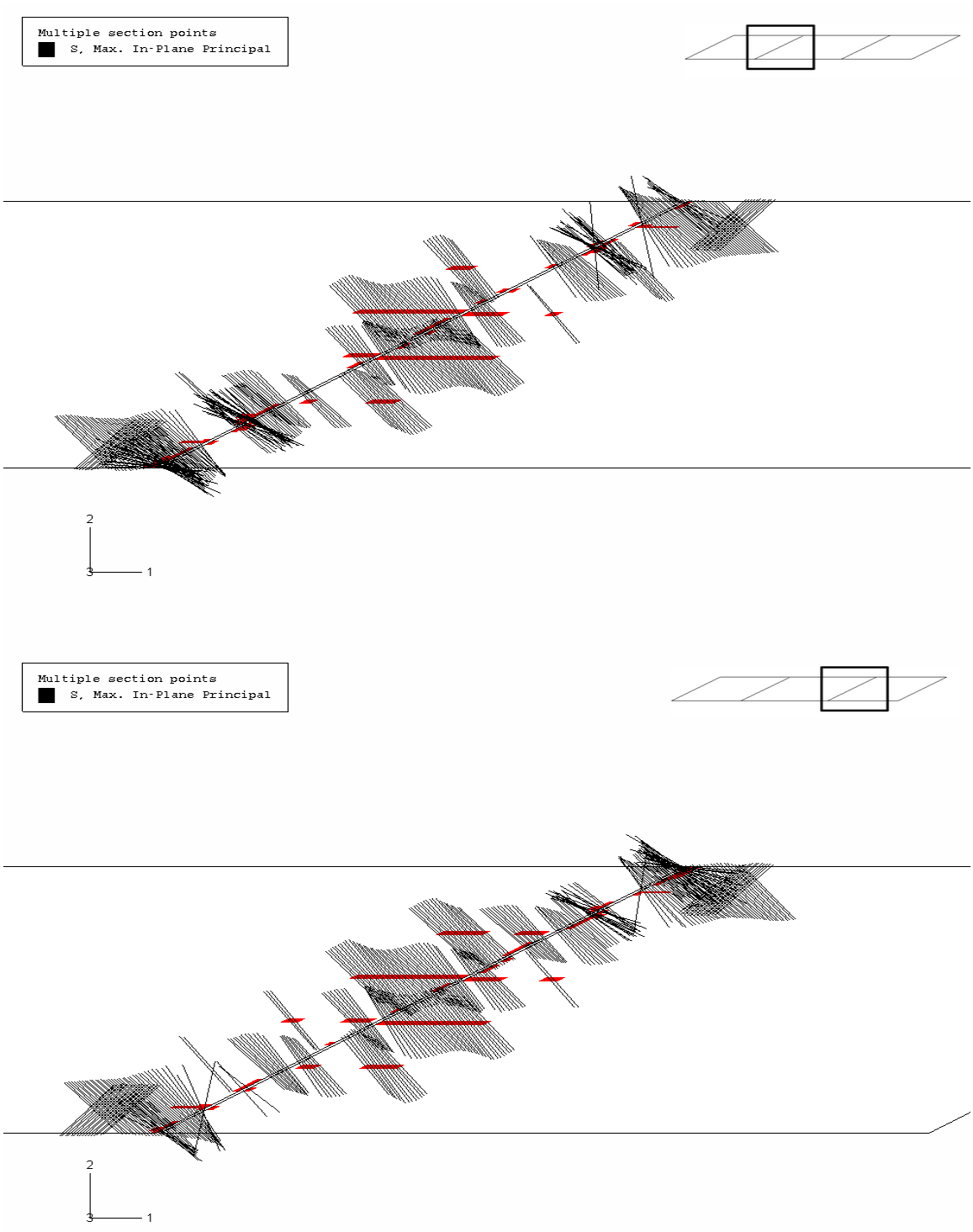

Figure 6-40: Normal direction of cracking (black lines) at top deck for Case 4, α = 61°

Analysis of the figures above shows that the unit support settlement combinations did have some effect on the level of stress and cracking behavior of the deck, but did not seem to produce a very considerable variation in the magnitude of tensile stress. Increasing the settlement's magnitude would certainly increase the magnitudes of the stress levels on the deck. One can also observe that the stress contours and the cracking distribution did not change very much with the different settlements imposed in Cases 1 and 3. However, in Cases 2 and 4, the crack distribution was more noticeably different from the other cases. This is because, in Case 2, the deck did not undergo equal deformations at two intermediate supports, producing the "uneven" nature of the settlement (shown graphically in Figure 6-29). As a result, the deck portion experiencing less deformation carried less tensile stress, and exhibited less cracking.

As for Case 4, it is noticed that the number of cracks produced was much less than that for Cases 1 and 3. That is because, for Case 4, both intermediate supports experienced less deformation than in Cases 1 and 3, and consequently carried less tensile stress under this settlement combination, as shown in Figure 6-38.

These phenomena seem to indicate that if differential settlement occurred at critical areas of the deck, such as at the intermediate support locations, where the deck is in tension under gravity loading, the tensile stress distribution on the deck would be altered (from the results for the case with no differential settlement) and would result in a modified cracking behavior. For this particular type of multi-span, continuous deck bridge, the settlement at the intermediate supports appears to be helpful in reducing the cracking of the deck. Furthermore, the results indicate that single intermediate support settlement (Case 2) is good, and double support settlement (Case 4) is better. However, it is not suggested to use different intermediate supports settlement to avoid cracking because it may cause other effects in the bridge that could adversely affect the service quality of the bridge.

6.4 SMEARED CRACK CONCRETE MODEL

A further advancement was made to the baseline US 331 bridge model detailed earlier in this chapter. The concrete material properties were modified, to utilize the smeared crack concrete model of ABAQUS. Use of this material model includes the capability not only of incorporating nonlinear material properties for a nonlinear numerical analysis, but also of predicting the crack distribution and crack directions automatically.

6.4.1 Smeared Crack Description

The following is the description of the smeared crack concrete model provided in the ABAQUS Manual:

> "The smeared crack concrete model in ABAQUS provides a general capability for modeling concrete in all types of structures. As a ‘smeared’ model, it does not track

individual 'macro' cracks. Constitutive calculations are performed independently at each integration point of the finite-element model. The presence of cracks enters into these calculations by the way in which the cracks affect the stress and material stiffness associated with the integration point. Cracking is assumed to occur when the stress of the element reaches the “crack detection surface” which is a linear relationship between the equivalent pressure stress and the Mises equivalent deviatoric stress. As soon as the crack detection surface has been activated, the crack direction is taken to be the direction of that part of the maximum principal plastic strain. Following the crack detection, the crack affects the response of the model because a damage elasticity model is used (ABAQUS 2006b)."

6.4.2 Concrete Material Modeling

As stated above, nonlinear concrete material properties were considered for the bridge model in this portion of the study. The tensile stress-strain relationship used for the bridge deck concrete is shown in Figure 6-41. The tensile behavior is defined as a linear elastic material until the stress reaches f_{tu}, the cracking stress of the concrete. Then, a linear softening model is used to represent post-cracking behavior using the "tension stiffening" option of ABAQUS. This option allows the user to define the strain-softening behavior for cracked concrete, and allows for the effects of the reinforcement's interaction with concrete (bond behavior) to be simulated. Details of the parameters that were specified for concrete material properties as input for ABAQUS are given in Table 6-5.

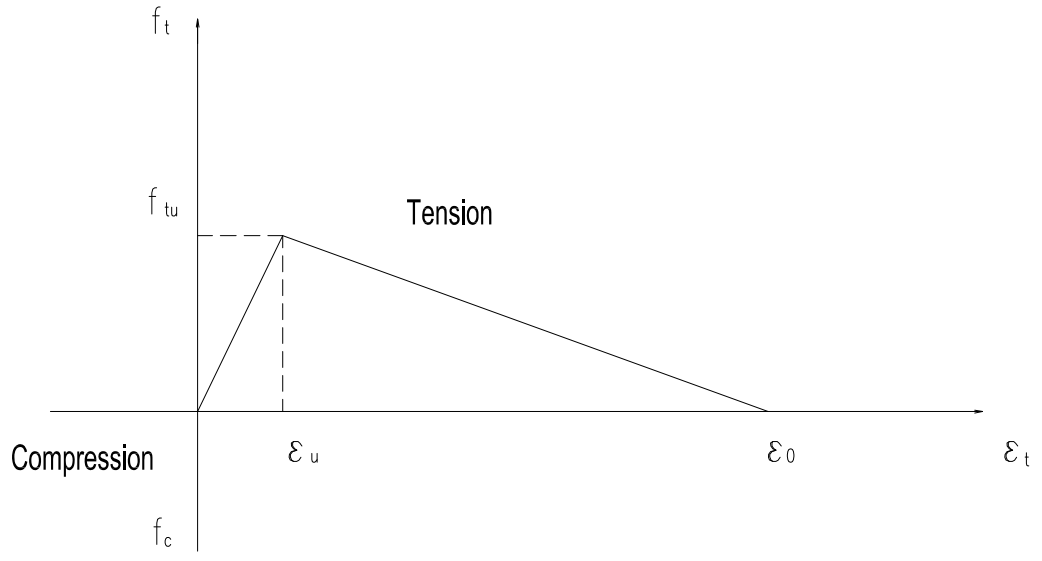

Figure 6-41: Tensile stress-strain relationship for concrete in ABAQUS (adapted from ABAQUS 2006b)

Table 6-5: Concrete material properties

Property	Value
Young's modulus	4.42 x 10^6 psi
Density	0.086 lb/in^3
Poisson's ratio	0.15
Yield stress (compression)	3000 lb/in^2
Failure stress (compression)	6000 lb/in^2
Plastic strain at failure (compression)	1.5 × 10^{-3} in./in.

ABAQUS uses a Rankine criterion to detect crack initiation and to define a crack detection surface, and then computes the value of f_{tu} in Figure 6-43 above from that crack detection surface. Based on that value of f_{tu}, and the modulus of elasticity, the value for ε_u is determined. A value is also supplied to ABAQUS to specify the amount of strain between ε_u and ε_0; for the model herein, this "span" of strain for the descending portion of the curve was defined to be 0.002. Finally, a user-defined value of the ratio of remaining stress to current cracking stress is provided to ABAQUS as input for the point at the apex of the triangle in Figure 6-41, and at the point where the descending branch of the curve meets the horizontal axis. For the present model, that ratio was defined as 1 for the apex, and 0 for the rightmost point of the triangle.

6.4.3 Results and Analysis of Results for Smeared Crack Bridge Model

As stated above, the smeared crack material model was used to replace the previous linear elastic concrete material utilized for the bridge model detailed in Section 6.2, for the same loading. The resulting maximum principal stress distribution is presented in Figure 6-42, and the maximum principal strain contour is presented in Figure 6-43. The maximum principal strain contour was plotted for this model because for the smeared crack model, a certain value of stress could occur either in the pre-cracking or post-cracking stage, and there is no way to distinguish which is reported in the stress contour at each location. Therefore, strain was deemed more indicative of the deck behavior for this model. (However, maximum principal stress values are provided for "completeness," so that the same information is provided for this model as was provided for the previous models.)

A relatively coarse mesh was used for this model to avoid the mesh sensitivity mentioned in the ABAQUS manual associated with smeared cracking concrete models that utilize very fine meshes. The manual states that the finite-element predictions have difficulty converging to a unique solution because increasing mesh refinement leads to narrower crack bands, which

presents a problem since "specification of strain softening behavior in reinforced concrete generally means specifying the post-failure stress as a function of strain across the crack" (ABAQUS 2006b).

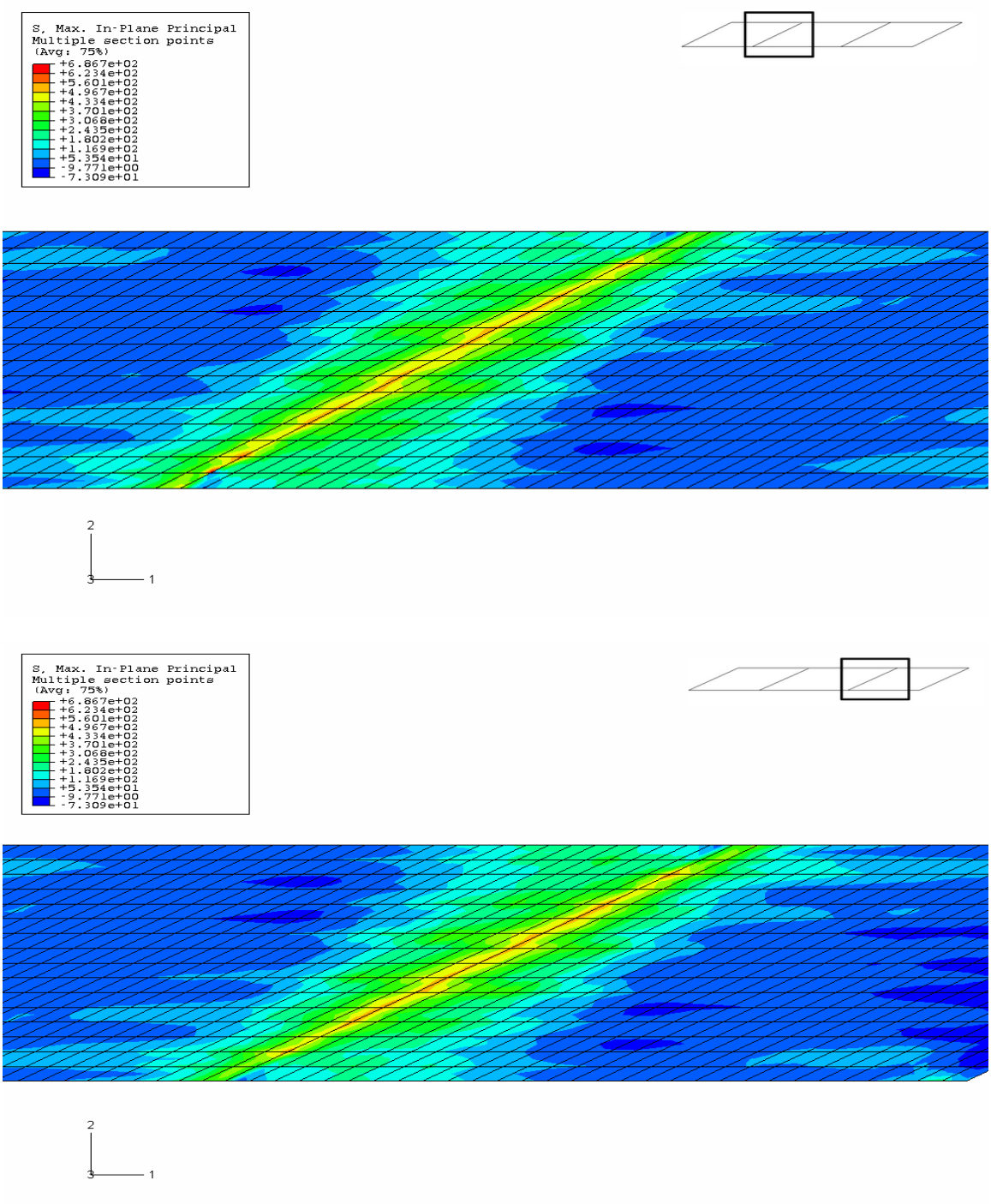

Figure 6-42: Maximum principal stress distribution at top of deck for smeared crack concrete model of US 331 bridge, α = 61°

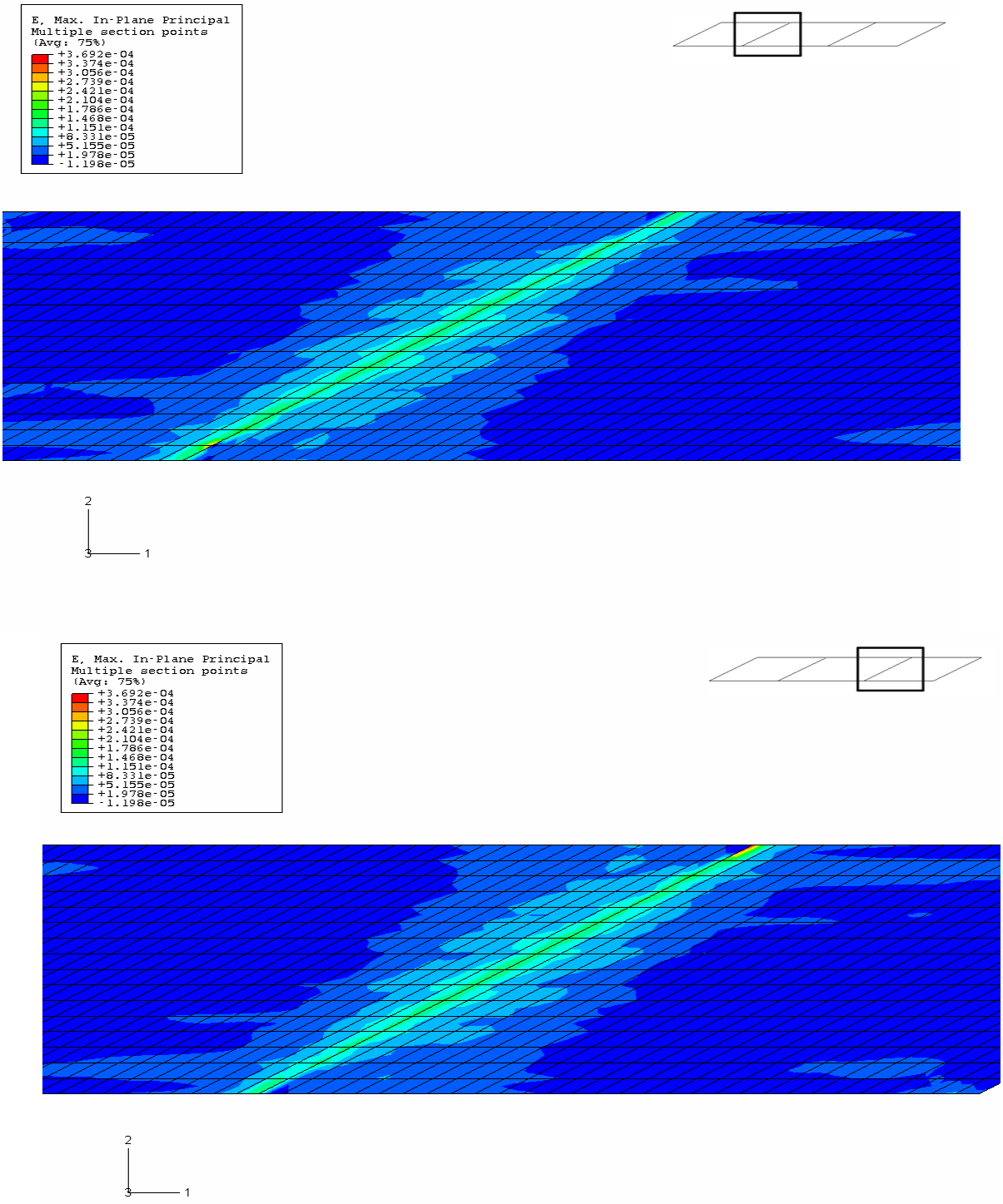

Figure 6-43: Maximum principal strain distribution at top of deck for smeared crack concrete model of US 331 bridge, α = 61°

For this smeared cracking model, the length of the deck was divided into 100 transverse strips, giving a length of approximately 42 in. for each element in the longitudinal direction. Each transverse strip of the deck, then, was divided into 16 elements, giving a width of approximately 30 inches in the transverse direction for each element. Incidentally, the much finer mesh of the previous models was tried first, but was too costly in running time to be practical, and was questionable as to whether it would ever finally converge. Subsequently, the coarser mesh was defined and used for this study.

As can be seen in the figure, the general shape of the strain and stress contours is very similar to the stress contour results shown in Section 6-2 for the model with the linear elastic concrete material. The shape of the strain contour again follows the bridge's angle of skew, and the largest tensile strains are noted to lie exclusively in the areas surrounding the interior bents. The maximum stress achieved was approximately 687 psi, much lower than the maximum stress of 1,216 psi for the corresponding linear elastic model. It is believed that the reason for this reduced stress level is that for the smeared crack model, the stress of the concrete elements was relieved after a crack was detected (i.e., after reaching the cracking surface), and began to follow the degraded portion of the curve in Figure 6-41. However, for the linear elastic concrete model used for the analysis described in the last two chapters, the tensile stress was allowed to increase, even after the cracking stress had been reached (since there was no descending portion of the tensile stress-strain curve defined for that model). It seems that the stress values obtained from this smeared crack concrete model may be more realistic, since it is known that cracking does relieve stress in concrete materials.

When the smeared crack model is incorporated, ABAQUS also generates a large amount of information related to cracking in its output data file. Among other information, the identity of each of the cracked elements is provided in this data file, as well as the Cartesian coordinates of the normal direction of the cracks, given at each integration point. For this model, all cracking was identified for "section point 5" (depicted in Figure 6-44), which indicates that all the cracks for this model occurred at the top of the deck.

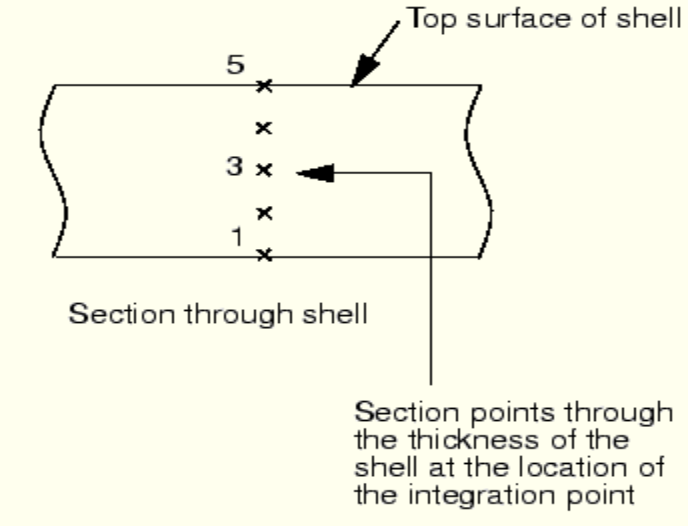

Figure 6-44: Configuration of section points

Based on the cracking information given in the program output, the cracked zone on the top of the deck was identified, and is highlighted in Figure 6-45. From this figure, one can discern that this distribution is similar to the crack distribution shown in Figure 6-12, generated as a result of using an elastic material (linear) analysis, though the effects of the girder's influence are not as prominent for the smeared crack model. This general good agreement serves to indicate that the modeling techniques employed for the complex interaction between the deck and the girders, even when using a linear elastic concrete model, were at least qualitatively valid for simulating the cracking behavior for the nonlinear concrete deck material.

Use of the smeared cracking concrete model provides an alternative method for analyzing the cracking behavior of concrete structures. It is a more realistic representation, compared to use of a linear elastic model, since post-cracking behavior is considered. The capability of detecting cracks automatically (through the list provided in the output data file) is another plus. However, this modeling technique also brings the potential for large numerical difficulties in convergence, due to its complex material properties. As evidence of this phenomenon, Barth and Wu (2006), and Baskar et al. (2002), in their investigations, were unable to achieve convergence with a smeared cracking model.

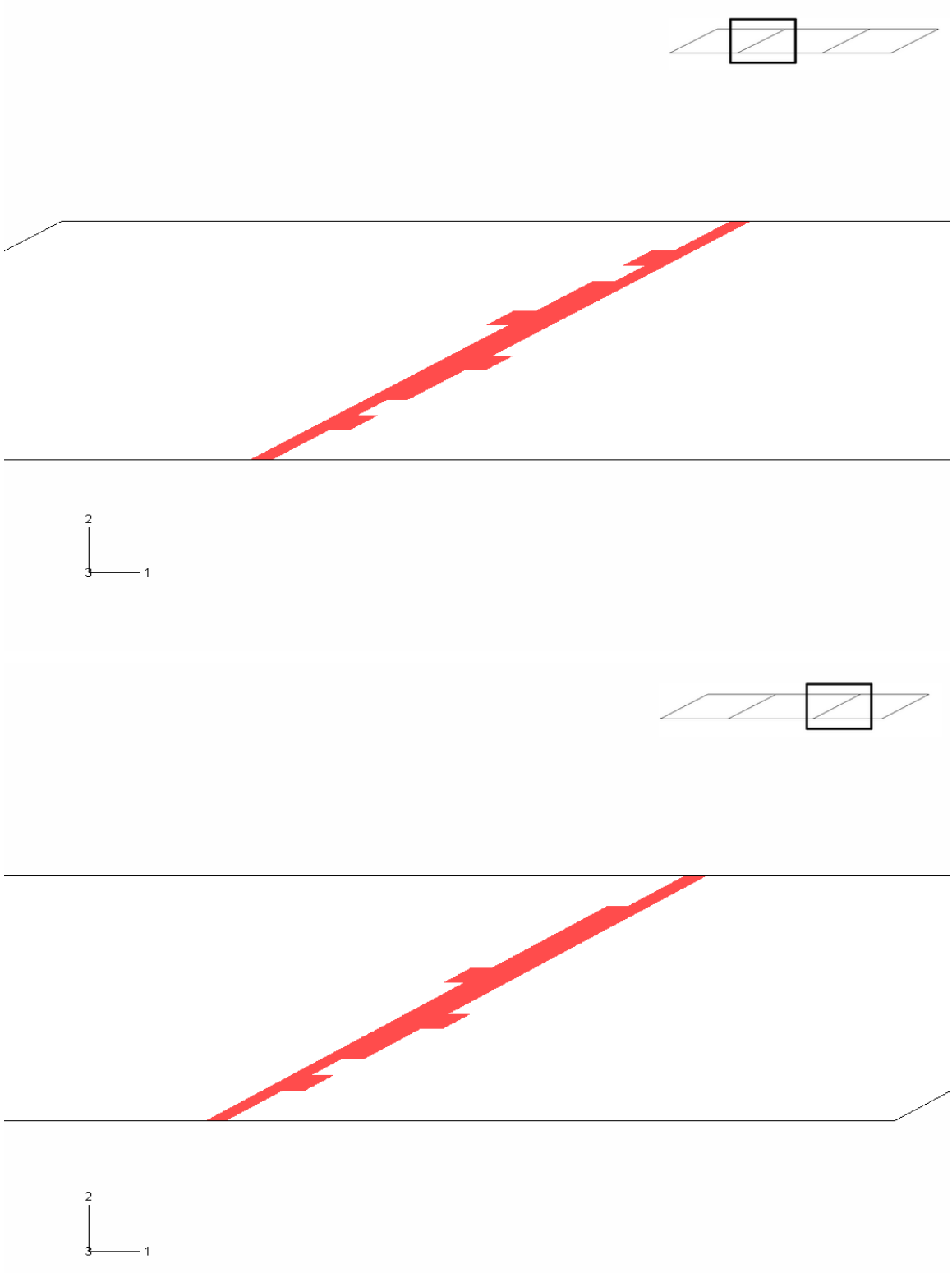

Figure 6-45: Cracking zone at top of deck for smeared crack concrete model of US 331 bridge, α = 61° (psi)

6.5 SUMMARY AND CONCLUSIONS

6.5.1 Summary

A refined finite-element model of this continuous, skewed, composite bridge was developed in detail to predict the stress distribution and cracking behavior of the deck on US 331. The commercially available finite-element software ABAQUS was employed for the analysis. The maximum principal stress contours, the cracking zone, and the direction of cracking were obtained from the finite-element analysis. The suggested modeling technique has been shown to capture the composite bridge's behavior.

To investigate the possible causes of the cracking, a parametric study, which incorporated a skew angle effect and a differential support settlement effect, was conducted using this finite-element bridge model. In addition, an advanced smeared cracking concrete model was introduced to provide an alternative to linear elastic material modeling for simulating RC structures.

6.5.2 Conclusions

Conclusions drawn from the results of the modeling study are as follows:

- A finite-element model of an entire bridge is able to realistic predictions of the stress distribution in the deck. The magnitude and direction of the maximum principal tensile stresses are an important indicator of the crack distribution and direction of cracking.
- For a continuous, skewed bridge, most cracking occurs at the top of the deck near the location of the intermediate supports.
- The skew angle of the deck has a large effect on the stress levels exhibited, and the cracking behavior of the deck. Increasing the skew angle of the deck increases the tensile stresses experienced in the deck. As a result, the deck is more prone to cracking if the skew angle is severe. Cracking for a skewed deck will be parallel to the bridge skew. Since the observed cracking on US 331 occurred perpendicular to the girders and not parallel to the bridge skew, the large skew of this bridge is not a likely cause for the severe cracking encountered on the US 331 deck.
- Differential settlement at the supports is of importance to the cracking distribution of the deck when it occurs at the intermediate supports of a continuous deck. However, the pattern of cracking encountered on the US 331 deck does not match the pattern characteristic of differential support settlement.
- The smeared cracking concrete model of ABAQUS considers post-cracking concrete behavior, and is able to detect the cracking automatically (i.e., without making inferences based solely on a "cutoff" cracking stress). It is believed to be very efficient in reinforced

concrete structure modeling, if a well-configured model can be constructed that will allow for numerical convergence.

Chapter 7

Conclusions and Recommendations

7.1 SUMMARY OF WORK

The focus of this investigation was a three-span, continuous, skewed bridge that was constructed in the summer of 2003 as the northbound roadway bridge over the CSXT railroad on US 331 between Legrand and Montgomery at Station 946 + 40.7085 in Montgomery County, Alabama. The bridge deck was cast in five placements, with the last two pours covering the sections above the interior bents as shown in Figure 3-5. Cracking in the bridge deck was severe although it was never opened to traffic, and in May 2005 the deck was removed and replaced. Excessive amounts of wide surface cracks were initially observed; in addition, horizontal cracks were discovered when cores were extracted from the deck. The horizontal cracks were generally present at the level of the top reinforcement mat; however, in some cases these cracks developed between the top reinforcement mat and the top concrete surface. The extent of the horizontal cracking remains unknown; however, of the 26 cores extracted from the deck, 11 contained horizontal cracks. ALDOT personnel were unfamiliar with these horizontal cracks and were interested in determining the possible cause(s) for the observed distresses.

The location of surface cracks was surveyed, and the results are shown in Figure 1-2. Construction records of the bridge deck were obtained and reviewed. Many cores were extracted from the deck to evaluate the in-place mechanical properties and the vertical distribution of splitting tensile strength present in the deck. The concrete's coefficient of thermal expansion was determined in accordance with AASHTO TP-60 (2004). A petrographic evaluation was performed on core samples. Ground penetrating radar was used to determine the as-built deck thickness and the location of the steel reinforcement.

With the assistance of ALDOT personnel, five other bridges in Alabama were visited in November and December of 2007. Cores were extracted adjacent to transverse cracks present in the decks in an attempt to find horizontal cracks similar to those found in the US 331 bridge.

The effects of constituent materials on the cracking tendency and early-age behavior of bridge deck concretes made with Alabama materials were experimentally evaluated by rigid cracking frame testing techniques. The effect of supplementary cementing materials, water-cement ratio, and placement temperature conditions on the early-age cracking tendency of bridge deck concrete was evaluated.

The coefficient of thermal expansion values of Alabama concretes made with various coarse aggregate types and volumes, water-cement ratios, and sand-aggregate ratios were assessed.

Finite-element analysis techniques were used to gain an understanding of the cracking mechanisms that may have caused excessive cracks in the US 331 bridge deck. A finite-element model of the US 331 bridge was created and used to numerically predict the stress distribution and cracking behavior of the deck. A parametric study was performed to evaluate the effect of bridge skew angle and differential support settlement on the predicted crack patterns.

7.2 CONCLUSIONS

The conclusions from the work document in this report are as follows:

1. The surface crack survey (shown in Figure 1-2) reveals that the majority of the surface cracking is perpendicular to the orientation of the steel girders. This indicates that this cracking maybe caused by the girders' restraint of concrete volume change effects.
2. The ground penetrating radar results indicated that the average deck thickness and the top cover depth exceeded the design values by 1.25 in.
3. The concrete satisfied all standard slump, total air content, and compressive strength requirements. Tests of deck core revealed adequate in-place compressive and splitting tensile strengths.
4. No reduction in tensile strength was evident at the top of the deck when compared to the middle and bottom of the deck. An average splitting tensile strength of 600 psi was obtained. The bond between the aggregates and the paste was as anticipated for most concretes made with this compressive strength. These results indicate that the cracking is probably not attributable to inadequate curing.
5. No horizontal cracking was found in cores of five bridge decks that had structural configurations similar to that of the US 331 bridge.
6. The results of the cracking sensitivity study show that the use of fly ash or slag cement improves the concrete's resistance to cracking when placed under hot weather conditions. Bridge deck concrete is much more prone to cracking when placed under summer construction conditions.
7. The average coefficient of thermal expansion (CTE) for Alabama concretes made with river gravel, granite, and dolomitic limestone are 6.95, 5.60, and 5.52 x 10^{-6} /^{o}F, respectively. Changes to the sand-aggregate ratio and water-cement ratio do not have much of an effect of the concrete's CTE.
8. Finite-element analysis results indicate that increasing the skew of the deck increases the tensile stresses experienced in the deck. As a result, a bridge deck is more prone to cracking if the skew angle is severe. The cracking for a skewed deck will be parallel to the bridge skew. However, four of the five in-place bridges surveyed had skew angles that varied from 39° to 60° and no horizontal cracks were found in these decks. Since the observed cracking on the US 331 deck occurred perpendicular to the girders and not

parallel to the bridge skew, the large skew of this bridge is not a likely cause for the severe cracking encountered in the US 331 deck.

9. Differential settlement at the supports is of importance to the cracking distribution of the deck when it occurs at the intermediate supports of a continuous deck. However, the pattern of cracking encountered on the US 331 deck does not match the pattern characteristic of differential support settlement.
10. The US 331 bridge was constructed during the summer months, which can produce high early-age thermal stresses. The bridge deck was supported by steel girders and was continuous over three spans, which is a condition that generates a high degree of restraint to any volume change effects. The concrete in the US 331 deck had a high coefficient of thermal expansion and high modulus of elasticity, which made it crack-prone when subjected to significant early-age volume change effects and a high degree of restraint. The majority of the surface cracking on the US 331 bridge deck is perpendicular to the orientation of the steel girders, whichs supports the conclusion that these cracks are related to the restraint provided by the steel girders. It is thus finally concluded that horizontal cracking in the US 331 bridge deck was most likely caused by excessive early-age temperature gradients combined with drying shrinkage gradients that produced large shear and normal stresses at the top reinforcement mat location in a concrete with a high coefficient of thermal expansion and high modulus of elasticity.

7.3 RECOMMENDATIONS

The following recommendations are offered based on the work documented in this report:

1. The use of fly ash or slag cement improves the concrete's resistance to cracking when placed under hot weather conditions. Bridge deck concrete is much more prone to cracking when placed under summer construction conditions. It is thus recommended to require the use of a partial cement replacement of 20% Class F fly ash, 30% Class C fly ash, or more than 30% slag cement in bridge decks constructed from May 15 to September 15 each year.
2. The use of concrete with a low coefficient of thermal expansion will reduce thermal stresses in decks placed under hot weather conditions (Krauss and Rogalla 1996). It is recommended to avoid the use of river gravel coarse aggregate in *continuous* bridge decks constructed from May 15 to September 15 each year.
3. Some hot weather concreting problems, which include the development of large thermal stresses during early hydration, can be controlled by limiting the concrete temperature at placement (Krauss and Rogalla 1996). ALDOT has no specified limit on the fresh concrete placement temperature. Krauss and Rogalla (1996) report that most transportation agencies use a limit of 90 °F, but some have lower limits. It is

recommended to limit the maximum concrete temperature at placement to 85 °F for bridge deck construction.

4. No horizontal cracking was found in cores of five bridge decks that had a structural configuration similar to that of the US 331 bridge. If the primary failure mechanism involves the use of a cracking-sensitive mixture, large thermal and moisture gradients, and a high degree of restraint in the deck, then this type of cracking should be present in other bridge decks in Alabama. It is recommended to visit more bridges in search of additional decks with horizontal cracking.

REFERENCES

AASHTO TP 60. 2004. *Standard Method of Test for Coefficient of Thermal Expansion of Hydraulic Cement Concrete*. Washington D.C: American Association of State Highway and Transportation Officials.

AASHTO. 2007. *AASHTO LRFD Bridge Design Specifications*. Customary U.S. Units 4th ed. Washington D.C: American Association of State Highway and Transportation Officials.

ABAQUS. 2006a. *Benchmark Manual*. Version 6.6-1. ABAQUS, Inc., Providence, Rhode Island.

ABAQUS. 2006b. *User's Manual*. Version 6.6-1. ABAQUS, Inc., Providence, Rhode Island.

ACI 116R-12. 1997. *Cement and Concrete Terminology*. American Concrete Institute. Farmington Hills, Michigan.

ACI 201.1. 1997. *Guide for Making a Condition Survey of Concrete in Service*. American Concrete Institute. Farmington Hills, Michigan.

ACI 207.1R. 1996. *Mass Concrete.* American Concrete Institute, Farmington Hills, Michigan.

ACI 209R. 1997. *Prediction of Creep, Shrinkage, and Temperature Effects in Concrete Structures*. American Concrete Institute, Farmington Hills, Michigan.

ACI 232.2R. 1997. *Use of Fly Ash in Concrete, American Concrete Institute*. Farmington Hills, Michigan.

ACI 233.R. 1997. *Ground Granulated Blast-Furnace Slag as a Cementitious Constituent in Concrete*. American Concrete Institute, Farmington Hills, Michigan.

ACI 318. 2008. *Building Code Requirements for Structural Concrete and Commentary*. American Concrete Institute, Farmington Hills, Michigan.

Barth, K. E., and H. Wu. 2006. Efficient Nonlinear Finite Element Modeling of Slab on Steel Stringer Bridges. *Finite Elements in Analysis and Design,* Vol. 42, pp. 1304-1313.

Baźant, Z.P., and L.J. Najjar. 1972. Nonlinear Water Diffusion in Nonsaturated Concrete. *Materials and Structures*, Vol. 5, No. 25, pp. 3-20.

Bjøntegaard, Ø. 1999. *Thermal Dilation and Autogenous Deformation as Driving Forces to Self-Induced Stresses in High Performance Concrete*. Doctoral Thesis. Norwegian University of Science and Technology, Division of Structural Engineering.

Bogue, R.H. 1929. Calculations of the Compounds in Portland Cement. *Industrial and Engineering Chemistry*, Vol. 1, No. 4, pp. 192-197.

Breitenbücher, R. 1990. Investigation of Thermal Cracking with the Cracking-Frame. Materials and Structures, Vol. 23, No. 135, pp. 172-177.

Breitenbücher, R., and M. Mangold, 1994, Minimization of thermal cracking in concrete at early ages. In RILEM Proceedings 25, *Thermal cracking in concrete at early ages*, ed. R. Springenschmid, London: E & FN Spon, pp. 205-212.

Choo, T., D.G. Linzell, J. Lee, and J.A. Swanson. 2005. Response of a Continuous, Skewed, Steel Bridge During Deck Placement. *Journal of Constructional Steel Research,* Vol. 61, pp. 567-586.

Dakhil, F.H., P.D. Cady, and R.E. Carrier. 1975. Cracking of Fresh Concrete as Related to Reinforcement. *Journal of the American Concrete Institute*, Vol. 72, No. 8, pp. 421-428.

Darwin, D., and J. Browning. 2008. Construction of Low Cracking High Performance Concrete (LC-HPC) Bridge Decks: Field Experience. *Proceedings of the Concrete Bridge Conference*, May 4-7, St. Louis, MO, CD-Rom.

Dobson, V. 1994. Time of Setting. In *Significance of Tests and Properties of Concrete and Concrete-Making Materials*, STP 169C, ed. P. Klieger and J.F. Lamond, Philadelphia, Pennsylvania, ASTM International, pp. 77-87.

Emanuel, J.H., and L. Hulsey. 1977. Prediction of the Thermal Coefficient of Expansion of Concrete. *Journal of the American Concrete Institute*, Vol. 74, No. 4, pp. 149-155.

Emborg, M. 1989. *Thermal Stresses in Concrete Structures at Early Ages*. Doctoral Thesis. Luleå University of Technology, Division of Structural Engineering.

FHWA. 2005. *Cast-in-Place High Performance Concrete*. Federal Highway Administration High Performance Concrete Website, http://knowledge.fhwa.dot.gov/cops/hpcx.nsf/home?openform&Group=HPC%20Cast-in-Place%20Construction&tab=WIP, accessed 2008.

Holt, E. 2001. *Early Age Autogenous Shrinkage of Concrete*. Doctoral Thesis. The University of Washington in Seattle.

Issa, M.A. 1999. Investigation of Cracking in Concrete Bridge Decks at Early Ages. *Journal of Bridge Engineering*, Vol. 4, No. 2, pp. 116-124.

Japan Concrete Institute. 1998. Technical Committee Report on Autogenous Shrinkage of Concrete. In *Autogenous Shrinkage of Concrete*, ed. Ei-ichi Tazawa, London, E & FN Spon, pp. 3-67.

Jenkins, R.S., and J.F. Lane. 2004. *Petrographic Evaluation of Cores from ALDOT Project MGF-009(500)*. MACTEC Project No. 6136-05-0037, MACTEC Engineering and Consulting, Atlanta, Georgia.

Kim, S.K., and M.C. Won. 2004. Horizontal Cracking in Continuously Reinforced Concrete Pavements. *ACI Structures Journal*, Vol. 101, No. 6, pp. 784-791.

Kosmatka, S.H., B. Kerkhoff, and W.C. Panarese. 2002. *Design and Control of Concrete Mixtures*. 14th Edition. Portland Cement Association, Skokie, Illinois.

Krauss, P.D., and E.A. Rogalla. 1996. *Transverse Cracking in Newly Constructed Bridge Decks*. NCHRP Report 380, Transportation Research Board, National Research Council, Washington, D.C.

Lange, D.A., and S.A. Altoubat. 2002. Early Thermal Changes. In RILEM Report 25, *Thermal Cracking in Concrete at Early Ages*, ed. A. Bentur, RILEM Publications S.A.R.L., pp. 37-38.

Mangold, M. 1998. Methods for Experimental Determination of Thermal Stresses and Crack Sensitivity in the Laboratory. In RILEM Report 15, *Prevention of Thermal Cracking in Concrete at Early Ages*, ed. R. Springenschmid, E & FN Spon, London, UK, pp. 26-29.

Meadows, J.L. 2007. *Early-Age Cracking of Mass Concrete Structures*. Master's Thesis, Auburn University, Alabama.

Mehta, P. K., and P.J.M. Monterio. 2006. *Concrete: Microstructure, Properties, and Materials*. 3rd Edition. McGraw-Hill, Inc., New York, NY.

Mindess, S., J. Young, and D. Darwin. 2002. *Concrete*. 2nd Edition. Prentice Hall, Upper Saddle River, NJ.

Neville, A.M., and J.J. Brooks. 1987. *Concrete Technology*. Essex, UK: Longman Scientific and Technical.

Nilsson, M. 2003. *Restraint Factors and Partial Coefficients for Crack Risk Analyses of Early Age Concrete Structures*. Doctoral Thesis, Luleå University of Technology, Division of Structural Engineering.

Poole, J.L, K.A. Riding, R.A. Browne, and A.K. Schindler. 2006. Temperature Management of Mass Concrete Structures, *Concrete Construction Magazine*.

RILEM Technical Committee 119-TCE, 1998, Testing of the Cracking Tendency of Concrete at Early Ages in the Cracking Frame Test. In Rilem Report 15, *Prevention of Thermal Cracking in Concrete at Early Ages*, ed. by R. Springenschmid, E & FN Spon, London, UK, pp. 339-346.

Schindler, A.K., and B.F. McCullough. 2002. The Importance of Concrete Temperature Control During Concrete Pavement Construction in Hot Weather Conditions. *Journal of the Transportation Research Board*, TRR No. 1813: 3-10.

Schindler, A.K., and K.J. Folliard. 2005. Heat of Hydration Models for Cementitious Materials. *ACI Materials Journal*, Vol. 102, No. 1, pp. 24-33.

Sioulas, B., and J.G. Sanjayan. 2000. Hydration Temperatures in Large High-Strength Concrete Columns Incorporating Slag. *Cement and Concrete Research*, Vol. 30, No.11, pp. 1791-1799.

Springenschmid, R., and R. Breitenbücher. 1998. Influence of Constituents, Mix Proportions and Temperature on Cracking Sensitivity of Concrete. In RILEM Report 15, *Prevention of Thermal Cracking in Concrete at Early Ages*, ed. R. Springenschmid, E & FN Spon, London, pp. 40-50.

Townsend, C.L. 1965. *Control of Cracking in Mass Concrete Structures*. Engineering Monograph No. 34. Water Resources Technical Publication. U.S. Department of the Interior, Bureau of Reclamation.

Westman, G. 1999. *Concrete Creep and Thermal Stresses: New Creep Models and their Effects on Stress Development*. Doctoral Thesis. Luleå University of Technology, Division of Structural Engineering.